AN EXPERIMENTAL STUDY OF NONEQUILIBRIUM SUPERCONDUCTIVITY

Thesis by

Ming Lun Yu

In Partial Fulfillment of the Requirements

for the Degree of

Doctor of Philosophy

California Institute of Technology

Pasadena, California

1974

(Submitted December 27, 1973)

ACKNOWLEDGMENTS

I would like to thank my advisor, Professor J. E. Mercereau, for his support, inspiring guidance, insight, and deep interest in this research through its duration. I also wish to express my sincere gratitude to Dr. H. A. Notarys for his advice, humor and company through many evenings in the laboratory, besides all his essential help.

I am also grateful to Dr. G. J. Dick, my first teacher in experimental low temperature physics, and Dr. R. K. Kirschman for his friendship, advice and pioneering work in Time Dependent Superconductivity. Special thanks go to Edward Boud, Sandy Santantonio, and Donald Lawson for their indispensable technical assistance, and to Miss G. Kusudo for her general assistance and pleasant help.

I am indebted to all my graduate student colleagues who made life in the "Bosonics" Laboratory so enjoyable and enlightening--in particular to S. Decker, T. Ganz, W. Lai, D. Palmer and R. H. Wang of the "time dependent" group for many valuable suggestions and discussions, and to H. C. Yen and T. Yogi for their extensive help and good meals.

I would like to thank the Earle C. Anthony Foundation, the Schlumberger Foundation, and the California Institute of Technology for their financial assistance.

The fine typing work in this thesis is due to Mrs. Ruth Stratton whose help and patience I greatly appreciate.

Finally, I would like to thank the American Physical Society for permission to use Figures 3.3, 3.4, 3.6 and 5.3 which appeared in Physical Review Letters, Vol. 28 and 30.

ABSTRACT

Experimental investigations were made on the transport properties of several superconducting systems in which the superconducting state was out of thermodynamic equilibrium. In such systems, the dynamics of the pairing processes governs the restoration of equilibrium. Systematic investigations into the nonequilibrium dynamics were made possible by creating a steady state depairing region at a supernormal interface with a transport current. Information was obtained by direct probing of the potential profiles in the depairing region. Measurements were made with superconducting microcircuits with high spatial resolution extending to the scale of the wavelength of light which limits our fabrication system.

It was found that at the depairing region, the experimental results can be described by the existence of two distinct potentials, one for the single electron excitations and one for the electron pairs. A theory for the dynamics of the nonequilibrium process was proposed and succeeded in accounting for most of the experimental observations. The relaxation time associated with this dynamics is found to be longer than the usual equilibrium relaxation time for the condensed electron pairs.

Similar measurements were extended to nonequilibrium regions close to current carrying interfaces between two different superconductors. In this case it was found that the two-potential measurements performed within the nonequilibrium region can be described in terms of a time dependent boundary condition at the interface.

To study the nonequilibrium superconductivity associated with this time dependent boundary condition in a controlled way, two such superconducting boundaries were brought very close to each other, creating a well defined boundary region less than one micron in length. It was found that the boundary region showed Josephson-like effects as well as a unique phenomenon in which electromagnetic radiation increases the apparent superconducting transition temperature. A model for this situation was proposed in which two complex wavefunctions with independent phase angles interfere quantum mechanically inside the boundary region. This model successfully explains most of the observed phenomena associated with the boundary region in the voltage sustaining nonequilibrium state.

TABLE OF CONTENTS

Chapter 1

INTRODUCTION

Superconductivity is a manifestation of a quantum mechanical phenomenon on a macroscopic scale. In this state approximately 10^{22} per cm^3 of conduction electrons in a metal condense in momentum space to form a giant coherent quantum mechanical state. This huge condensate accounts for most of the spectacular properties of superconductors, one of which is their infinite conductivity for electric current. Once they are cooled below their respective transition temperatures, usually a few degrees above absolute zero, common metals such as tin, lead and aluminum are superconductors. In 1957, Bardeen, Cooper and Schrieffer (abbreviated as BCS) put forth a successful microscopic model. They proposed that conduction electrons pair up through an electron-phonon interaction to form a quasi-Bose system which condenses in momentum space. Electrons no longer act alone, but coherently. Many electric and magnetic properties can readily be explained by the coherency of this condensed state. In thermodynamic and chemical equilibrium with the condensate is also an electronic gas of thermally excited quasiparticle excitations. They represent the depaired superconducting electrons and behave similarly to ordinary electrons.

Such an equilibrium model gives a satisfactory description at low frequencies even when an electric field is present which produces time dependent phenomena in superconductors. These phenomena include microwave surface impedance (Mattis and Bardeen 1958), flux motion (Anderson and Kim 1964) and weak superconductivity within a Josephson

tunneling barrier (Josephson 1962). However, as more systems have been examined and more information sought, equilibrium superconductivity within the scheme of BCS model has proved to be inadequate. The BCS model provides an excellent description of equilibrium superconductivity in most cases; however, it does not consider how equilibrium is established by means of nonequilibrium mechanisms.

Nonequilibrium phenomena inside a superconductor are not yet well understood. Recently much attention and interest have been focused on these problems such as the structure of fluxoid (Thompson and Hu 1971), the depairing at a super-normal interface (Pippard, Shephard and Tindall 1971) and the existence of weak superconductivity with time dependent Josephson-like behavior in metallic systems (Notarys and Mercereau 1971). All these narrow down to the fundamental question of nonequilibrium superconductivity.

Both the condensate and the gas of quasiparticles may be out of thermodynamic equilibrium with the background lattice and with themselves, and the chemical equilibrium between the two entities can also be disturbed. Recent progress in technology has permitted us to begin to probe these nonequilibrium processes under controlled conditions. Such experiments usually involve time scales of 10^{-6} to 10^{-13} sec or less and dimensions of a few microns to a hundred Å or less. It has been the purpose of this research to explore experimentally these newly opened areas, trying to shed some light on our understanding of these fundamental phenomena in nonequilibrium superconductivity. Experimental investigations were done on two nonequilibrium current-carrying dynamic systems. The pairing or depairing nonequilibrium

process is accompanied or induced by a nonzero center of mass momentum of the Cooper pairs.

The first system to be discussed is the depairing region at a single current carrying superconducting-normal (S/N) boundary. This research originated from a theory proposed by Rieger, Scalapino and Mercereau (RSM1) in 1971 where they studied the new idea of using a two potential concept to explain the puzzling problem of nonequilibrium superconductivity. This theoretical breakthrough inspired our research into the potential distribution at the S/N interface. The experiment described in Chapter 3 is the first successful attempt to verify experimentally this new two potential concept. This verification was further extended to the highly dynamic case where N is a superconductor but driven dynamically normal with a large current. Further new boundary potentials were discovered at these various supernormal interfaces and they are reported in Chapter 4.

Our knowledge on nonequilibrium superconductivity thus acquired was applied to further our understanding in time dependent nonequilibrium superconductivity. The second system investigated is the time dependent phase slippage inside a submicron region bound by two superconducting boundaries. We believe the latter system, which we shall refer to as the proximity effect bridge, is a situation where two superconducting wavefunctions are allowed to interfere quantum mechanically, resulting in an oscillation in the strength of superconductivity inside the submicron region. A two phase model presented in Chapter 5 was proposed to explain the phase slippage

phenomenon in these proximity effect bridges. Experimental investigation on the enhancement of critical current by external radiation in these bridges supports the proposed model. To reach for a better insight into the working of these bridges, we sought to have direct access to the phase slippage region with voltage probes. Many fascinating facts hence revealed suggest new insights into the phase slippage process and still have to be understood. The periodic pairing and depairing of the transport current in these bridges provides a test ground and a new source for our knowledge of nonequilibrium superconductivity.

Chapter 2

THE PHYSICAL BASIS OF EQUILIBRIUM AND NONEQUILIBRIUM SUPERCONDUCTIVITY

2.1 The Phenomenon of Superconductivity

Superconductivity was first observed by Kamerlingh-Onnes in 1911 when he cooled mercury with liquid helium. The electrical resistance of mercury abruptly vanished when it was cooled below $4.15^{\circ}K$, the superconducting transition temperature of mercury. Thereafter many superconductors were found. For example, tin goes superconducting at $3.72^{\circ}K$, niobium at $9.46^{\circ}K$, tantalum at $4.48^{\circ}K$. On the other hand in many other metals, for example gold and copper, superconductivity has never been observed. They are normal metals. Normal metals, or superconductors at temperatures above their respective transition temperatures, have a finite electrical resistance towards electric current. They are all in the normal resistive state. The coherent superconducting state of the conduction electrons has a lower free energy than the electron gas would have if it remained in the normal state. This free energy difference is the condensation energy and has been determined from the specific heat studies of superconductors.

The superconducting state has two prominent electrical characteristics:

a) infinite electrical conductivity,

b) perfect diamagnetism (Meissner effect).

The ability for a nondissipative transport of electric current inside of a superconductor in thermodynamic equilibrium is the result of the macroscopic coherence. The 10^{22} electrons form a quantum mechanical state whose de Broglie wavelength is orders of magnitude longer than the interatomic distances ($\sim$ Å) such that usual scattering mechanisms for normal electrons are negligible. Current densities as high as 10^7 amp/cm^2 have often been observed, for example in niobium at 4°K. When the kinetic energy associated with the transport current exceeds the condensation energy superconductivity is quenched, and the superconductor goes into the normal state. This determines the critical current. For thin superconducting strips in which the current distribution is uniform, the critical current density j_c varies with temperature T in the following way:

$$j_c \propto (T_c - T)^{3/2} \quad \text{when } T \text{ is near } T_c. \tag{2.1}$$

This geometric situation was very often encountered in most of the experiments to be described in this thesis.

The ability of a superconductor to expel magnetic flux was first observed by Meissner and Ochsenfeld (1933). This phenomenon is a consequence of the rigidity of the coherent macroscopic wavefunction against external magnetic field perturbation (Lynton 1969). Physically, the superconductor responds by generating a nondissipative surface current shielding the inside of the superconductor from external magnetic fields. As the external field goes up, perfect diamagnetism holds until the energy required to expel the external field exceeds

the condensation energy, and superconductivity is then quenched. The critical magnetic field H_c is temperature dependent in the following general way:

$$H_c(T) \simeq H_{co} \{1 - (T/T_c)^2\} \tag{2.2}$$

Typical values for H_{co} are 309 gauss for tin, 803 gauss for lead.

2.2 The Microscopic Theory

Although the macroscopic coherent nature of superconductivity was recognized very early by F. London (1950) and Ginzburg and Landau (1950), a successful microscopic model did not appear until 1957 when Bardeen, Cooper and Schrieffer (BCS 1957) put forth the idea that electrons with opposite linear momentum and spin ($\vec{k}\uparrow$, $-\vec{k}\downarrow$) pair up through a phonon mediated attractive electron-electron interaction and form a quasi-Bose system. Electron-electron attractive interaction through the exchange of virtual phonons was first proposed by Frölich in 1950 (Frölich 1950). Motion of the conduction electrons excites phonons and the polarization of the lattice associated with the phonons in turn acts on other conduction electrons and establishes indirect electron-electron interaction. This idea was later verified by the isotopic effect. For a single element with more than one isotope, the transition temperature is found to be inversely proportional to the square root of the nuclear mass of the isotope, just like the Debye frequency of the lattice.

Then in 1956, Cooper (Cooper 1956) put forth a theoretical argument that the ground state of a free electron gas is unstable in the presence of an attractive interaction. Each electron will group with another with opposite linear momentum and spin to form a two-electron bound state of energy $E < 0$.

Taking up the electron phonon interaction and the Cooper phenomenon, in 1957, Bardeen, Cooper and Schrieffer proposed a microscopic model for superconductivity. Starting by treating all conduction electrons on the same footing--with the electron-phonon interaction--electrons group themselves to form Cooper pairs, giving up energy to the external world. Although the exclusion principle still restricts the occupation of states by the constituent electrons, the collection of Cooper pairs form a quasi-Bose system readied for condensation in momentum space.

The size of the Cooper pair, which is roughly the range of the attractive interaction, is expressed by the coherence length ξ of the superconductor. ξ at $0^{o}K$ ranges from 10^{-4}cm for aluminum to 900Å for lead and is in general at least two orders of magnitude longer than the interatomic distance ($\sim$ Å). A sphere of diameter ξ can contain centers of mass of some 10^{6} Cooper pairs. The resulting strong overlap of these large number of electron pair wavefunctions extends through individual spheres of diameter ξ and establishes long range order throughout the whole piece of superconductor. In actual fact all the Cooper pairs condense in momentum space into a single coherent macroscopic quantum state. The ground state of this

condensate is the state in which all the center of mass linear momenta of the pairs equal zero, similar to a boson condensate. As was remarked before, the coherent nature is manifested in the collective motion of these pairs. The pairs all have the same center of mass momentum when the superconductor is in the current carrying dynamic equilibrium state. As the velocity ($\sim$ cm/sec) of the pairs is far less than the Fermi velocity ($\sim 10^8$ cm/sec) of the electrons, the associated de Broglie wavelength of the pairs is at most the order of the coherence length ξ which is macroscopic when compared to interatomic spacing. Hence the Cooper pairs suffer no scattering by the lattice and the current is dissipationless. ξ not only gives a measurement of how rapid superconductivity can vary spatially, it is also a measure of the nonlocality of the response of superconducting electrons to external perturbations, as for example electric and magnetic fields (Pippard 1953). In this way the coherence of the macroscopic system accounts for most of the superconducting properties. Close to the transition temperature T_c, ξ depends on temperature in the following way:

$$\xi(T) = 0.74\ \xi_o \left(\frac{T_c}{T_c - T}\right)^{1/2} \tag{2.3}$$

ξ_o is the BCS coherence length which is related to the Fermi velocity v_F.

$$\xi_o = 0.18\ \frac{\hbar\, v_F}{k_B T_c} \qquad \text{(Tucker and Halperin 1971, Appendix)} \tag{2.4}$$

$2\pi\hbar$ is the Planck's constant and k_B is the Boltzmann's constant.

In the dirty limit where we have a non-perfect lattice or impure material in which the electron mean free path ℓ is much less than ξ_o ,

$$\xi(T) = 0.85 \sqrt{\ell \xi_o} \left(\frac{T_c}{T_c - T}\right)^{1/2} \quad \text{(Tucker and Halperin, 1971)} \tag{2.5}$$

Another significant result of the BCS model is that with the exception of several special cases the Cooper pair formation releases condensation energy and introduces an energy gap Δ right on top of the Fermi sphere of the electron energy spectrum. The energy gap Δ per electron separates the condensate ground state from the first excitation level. Δ is related to the transition temperature T_c . Actually

$$\Delta(0) = 1.74\ k_B T_c \quad \text{at} \quad 0^oK \tag{2.6}$$

and is about 0.7 mev for tin, and for T close to T_c

$$\Delta(T) = \Delta(0) \left(\frac{T_c - T}{T_c}\right)^{1/2} \qquad \text{(Blatt 1964)} \tag{2.7}$$

For a pure metal with a perfect lattice, the BCS coherence length ξ_o is the distance an electron travels at the Fermi velocity during a characteristic time $\hbar/\pi\Delta(0)$, that is,

$$\xi_o = \frac{\hbar V_F}{\pi \Delta(0)} \qquad \text{(de Gennes 1966)} \tag{2.8}$$

consistent with (2.4).

The low lying excitations of the condensed state correspond to the breaking up of Cooper pairs into excited electrons, and 2Δ is the minimum energy for this process to occur. In the quasiparticle

representation of the excitations, the dispersion relationship which connects the excitation energy E to the wave vector k of the quasiparticle is

$$E(k) = \sqrt{(\frac{\hbar^2 k^2}{2m} - \mu)^2 + \Delta^2} \tag{2.9}$$

where μ is the Fermi level or chemical potential of the electron gas, and the corresponding k vector k_F is the Fermi momentum in units of $\hbar$. That is,

$$\mu = \frac{\hbar^2 k_F^2}{2m} \tag{2.10}$$

In general, two values of k, one above k_F and one below k_F, can give the same value of $E(k)$. The electron and hole excitation concept for a normal metal may be loosely carried over to this description of the excitation spectrum. We refer states with $k > k_F$ and $k < k_F$ to the electron-like and hole-like branches of the quasiparticle spectrum respectively.

Besides the gap which forbids occupation, the density of states of the excitations are modified by the nonlinear dispersion relationship (2.9). Actually the densities of states of both the electron-like and hole-like branch go up to infinity right at the gap edge in order to compensate the loss of occupation states within the gap. In actual fact it is given by:

$$\frac{dn}{dE} = \frac{EN(0)}{(E^2 - \Delta^2)^{1/2}} \qquad E > \Delta \qquad \text{(de Gennes 1966)} \tag{2.11}$$

where $N(0)$ = density of state at Fermi level.

Quasiparticle excitations are excited thermally in a superconductor in thermodynamic equilibrium at a temperature T . The quasiparticles obey the Fermi-Dirac statistics and are distributed with the Fermi function:

$$f(E) = \frac{1}{1 + \exp(E/k_B T)} \tag{2.12}$$

Since the quasiparticle excitations are no longer part of the condensate, they are scattered by the lattice and impurities as an ordinary conduction electron. In the ground state the net velocity of the excitations is zero. There is no transport current by the quasiparticle excitations except under the action of an electric field. In the dynamic state only the condensate contributes to charge transport in the field free condition.

2.3 The Two Fluid Model

The condensate and the quasiparticle excitations are in chemical equilibrium with each other through interconversion. Condensed pairs are continually breaking up, forming quasiparticles above the gap, and quasiparticles are recombining to form pairs.

$$2e \rightleftarrows e + e \tag{2.13}$$

But otherwise, treating these two entities as two weakly interacting fluids gives a conceptually useful phenomenological description of many physical properties of a superconductor. The condensate constitutes the superfluid and the quasiparticle excitations constitute the normal fluid. The evolution of the fluids is governed by the chemical

potentials μ_p and μ per electron for the super and normal fluids respectively.

F. London in 1950 recognized the coherent nature of superconductivity which is accompanied by long range order. Ginzburg and Landau (1950) extended this idea and described this coherent system with a complex order parameter ψ which we shall at times refer to as the macroscopic wavefunction for the superconductor. ψ in general can be expressed in the form

$$\psi = \sqrt{\rho_s}\, e^{i\phi} \tag{2.14}$$

where both ρ_s and ϕ are real functions of position and time. In particular, the amplitude squared $\rho_s = |\psi|^2$ is the local density of Cooper pairs. In this phenomenological theory ψ in thermodynamic equilibrium is chosen to minimize the free energy $\mathcal{F}$ of the superconductor. In other words,

$$\frac{\delta \mathcal{F}}{\delta \psi^*} = 0 \tag{2.15}$$

The nondissipative supercurrent carried by the condensate is given by:

$$\vec{j}_s = \frac{ie\hbar}{m} \{\psi^*(\vec{\nabla} - \frac{2e}{c}\vec{A})\psi - \text{complex conjugate}\} \tag{2.16}$$

where $\vec{A}$ is the magnetic vector potential. Substituting in the general form as given in (2.14), the supercurrent $\vec{j}_s$ is expressed by

$$\vec{j}_s = \frac{2e\hbar\rho_s}{m}\vec{\nabla}\phi - \frac{4e^2\rho_s}{mc}\vec{A} \tag{2.17}$$

The dependence on A is a consequence of the Meissner effect discussed above and will be neglected in most cases under consideration since the magnetic field is small in all these cases. Writing j_s as $2\rho_s e v_s$, we see that $(h/m)\nabla\phi$ has the significance of the center of mass velocity of the condensate. The chemical potential μ_p per electron of these condensed pairs is defined by the Josephson relationship (Anderson, Werthamer and Luttinger 1965)

$$\mu_p = \frac{\hbar}{4|\psi|^2}\left(\psi^* \frac{\partial\psi}{\partial t} - \psi \frac{\partial\psi^*}{\partial t}\right) \tag{2.18}$$

and hence determines the time evolution of the condensate.

The density ρ_n of the normal fluid is given by the number of quasiparticles excited thermally from the condensate and

$$\rho_n = \int_{\Delta}^{\infty} \frac{2N(0)E}{(E^2 - \Delta^2)^{1/2}} \frac{1}{1 + \exp(\frac{E}{k_B T})}\, dE \tag{2.19}$$

In the limit of negligible interaction between the two fluids, the normal current j_n carried by the quasiparticle excitations is given by

$$j_n = -\frac{\sigma_{eff}}{e}\nabla\mu \tag{2.20}$$

where σ_{eff} is the electrical conductivity of the quasiparticles (Appendix A) and μ is the chemical potential of the excitations. The total current flowing is given by the sum of the supercurrent j_s and the normal current j_n.

$$j = j_s + j_n \tag{2.21}$$

Most of our understanding of the phenomenon of superconductivity up to the present time is limited to the thermodynamic equilibrium state. Condition for equilibrium requires

$$\mu_p = \mu \tag{2.22}$$

At the time independent steady state, normal fluid does not appear in the picture, as current is being carried completely by the supercurrent without any energy dissipation. In other words, electric field

$$E = -\frac{1}{e}\nabla\mu = 0 \tag{2.23}$$

Electric fields can exist inside a superconductor to cause a normal current flow. Such cases include the nonequilibrium depairing and pairing at an S/N interface and inside a proximity effect bridge, or during acceleration or deceleration of a supercurrent when a superconductor is subjected to an rf field.

2.4 Nonequilibrium Superconductivity

Nonequilibrium superconductivity with its vastly unexplored frontier has received a lot of attention recently. The breakthrough came with the two potential concept which assigns different potentials to quasiparticles and condensate as put forth by Rieger et al. (RSM 1). The experiment reported in Chapter 3 of this thesis gave the first verification of this concept and later was followed by

the experiment of Clarke (1972). Thereafter various nonequilibrium processes involving quasiparticles (Tinkham 1972) and condensate (Owens and Scalapino 1972) were studied theoretically and the following sections will give a summary of the present theoretical picture. Experimental data available for comparison are still scarce. The majority of these were quasiparticle recombination time determinations done before the importance of nonequilibrium processes was realized. The experiments reported in this thesis represent a major portion of the work contributed to the understanding of a perturbed condensate. J. Clarke's experiment on branch mixing (1972) and Parker and Williams' experiment (1972) on effect of photon excited quasiparticles on the superconducting gap also gave support to the present picture of quasiparticles in the nonequilibrium state.

At the present stage, we still have to carry over much of the concepts in equilibrium superconductivity in the description of possible nonequilibrium processes. These include the assumption that it is legitimate to think of a local excitation spectrum and a local energy gap Δ, although with the understanding that superconductivity itself is a nonlocal cooperative phenomenon in which long range order plays the most important part. The concept of chemical potential is also assumed to be useful in most cases, although we may encounter various situations which are no longer within the realm of equilibrium thermodynamics. Then there is the concept of relaxation time. When a superconductor is disturbed from equilibrium, it is always assumed that the system will relax back to the new equilibrium state with a relaxation time characteristic

of the particular nonequilibrium process involved. Again the validity of such approximation still has to be tested. In particular, it is believed that the return of a disturbed condensate with a finite gap fails to be described by a simple relaxation scheme (Gor'kov and Eliashberg 1968)*. Although there is so much reservation as to the validity of all our postulates, these simple models at least allow us to make some progress. For small perturbations of the equilibrium system, the above mentioned assumptions may be able to provide a qualitative description of reality. Experimental facts seemed to give reasonable agreement with theories proposed along these lines and will be summarized below. The experiments reported in this thesis are examples. Within our present limited understanding, major nonequilibrium processes inside a superconductor can loosely be classified into two general categories. They are i) nonequilibrium processes associated with perturbation of the quasiparticle excitation spectrum, and ii) nonequilibrium processes associated with perturbation of the condensate.

---

*All related quantities will have a singularity in their frequency dependence due to the absorption threshold $\hbar\omega_o = 2\Delta$. However, the characteristic time scale encountered in a perturbed superconducting condensate is just of the order of $1/\omega_o$. This singularity is reflected in the time evolution (mathematically through a fourier transform from the frequency domain to the time domain) as an oscillatory behavior, making it difficult to define a relaxation time.

2.5 Perturbation of the Quasiparticles

In the first category, there are several processes with their respective relaxation times, depending on the way the quasiparticle spectrum is perturbed. Usual ways include external injection or extraction of quasiparticles, photon excitation or thermal excitation. Injection may be realized with an electron tunneling junction. Quasiparticle excitations are injected from a piece of normal metal or another piece of superconductor by tunneling through a few tens of Å thick insulating layer (e.g., oxide). Without loss of generality, we consider quasiparticles being injected with $k > k_F$ into the electron-like branch of the excitation spectrum. Three steps have to be taken to establish equilibrium:

i) First is the thermalization of the injected quasiparticles within their own branch ($k > k_F$ in this case) so that the quasiparticles in this branch all settle down to the same temperature T as the lattice, and satisfy the Fermi distribution with a chemical potential $\mu_{e,k>k_F}$. This is achieved through phonon emission. It had been estimated in the approximation of high injection energy (several Δ's above the gap) and a very cold lattice ($T \ll \theta$), time required for the injected particles to cool down to T is

$$\tau_{TH} \simeq \frac{3\tau_\theta}{16} \left(\frac{\theta}{T}\right)^3 \quad * \qquad \text{(Tinkham 1972)} \qquad (2.24)$$

Here θ is the Debye temperature, and τ_θ is the electron-phonon

---

* The factor $(\frac{\theta}{T})^3$ comes in because $(\frac{T}{\theta})^3$ is approximately the fraction of the phase space occupied by the thermal phonons at temperature T.

scattering time at $T = \theta$ which is $\sim 10^{-14}$sec for normal metals. Taking $\theta \sim 200^{\circ}K$ and $T \sim 4^{\circ}K$, $\tau_{TH} \sim 2 \times 10^{-10}$sec .

ii) Another step towards equilibrium is the relaxation of the branch imbalance between the populations of the electron-like and the hole-like branches of the quasiparticle spectrum in a superconductor, or in other words, it has to equalize the chemical potentials $\mu_{e,k>k_F}$, $\mu_{e,k<k_F}$ of these two branches (Tinkham and Clarke 1972). This involves branch crossing of a quasiparticle with $k > k_F$ into the branch with $k < k_F$ or vice versa. This is brought about by both inelastic phonon processes and elastic scattering by gap anisotropy. The first mechanism is believed to dominate. Phonons take care of the momentum balance and cool the excitations at the same time. For temperature $T \to T_c$ such that $\Delta(T)$ is small, and when internal equilibrium of the two branches through thermalization is already achieved, the characteristic relaxation time for branch mixing is given by

$$\tau_Q \simeq 0.068\ \tau_\theta\ (\frac{\theta}{T_c})^3\ \frac{\Delta(0)}{\Delta(T)}$$

$$\sim 2 \times 10^{-10}\text{sec}\,(\frac{\Delta(0)}{\Delta(T)}) \qquad \text{for tin} \tag{2.25}$$

Experimental results (Clarke 1972) gave support to this theoretical prediction.

iii) The above two processes both involve reestablishing equilibrium within the quasiparticle excitations. However, even if such equilibrium is achieved, it may still be out of equilibrium with the condensate, although both the lattice and the electron gas are

characterized by the same temperature T. The excess of quasiparticle excitations as compared to the equilibrium value normally excited from the condensate is reflected by the difference in the two chemical potentials: the chemical potential of the condensate μ_p and the chemical potential of the quasiparticle excitations μ. Such situations are encountered when a superconductor is under an external dynamic pair breaking influence such as strong laser light or short heat pulses (Parker and Williams 1972). The extra unpaired electrons depress the energy gap and raise the free energy of the superconducting state (Owens and Scalapino 1972). To achieve chemical equilibrium between the quasiparticle excitations and the condensate, thermalization is followed by recombination of pairs of quasiparticles with opposite spin, forming Cooper pairs and emitting phonons of energy 2Δ. When the density of injected quasiparticles N is small compared with N_T, the equilibrium number, the recombination process is characterized by a relaxation time τ_R. τ_R increases as temperature goes down through the factor e^{Δ/k_BT}. This has been verified experimentally for a number of cases:

$$\tau_R = \frac{2.8 \times 10^{-8}\, e^{\Delta/k_BT}}{\sqrt{T}} \text{ sec for aluminum} \qquad \text{(Levine and Hsieh 1968)}$$

$$= \frac{2 \times 10^{-9}\, e^{\Delta/k_BT}}{\sqrt{T}} \text{ sec for tin} \qquad \text{(Parker 1973)} \qquad (2.26)$$

This factor arises from the fact that the number of excited electrons available for pairing with a given electron is roughly proportional to $e^{-\Delta/k_BT}$, the Boltzmann factor.

2.6 Perturbation of the Condensate

Perturbation of the condensate constitutes the second category of nonequilibrium phenomena. Although considerable effort has been extended, our present understanding is still very restricted to some theoretical speculations, and experimental work along this line is still scarce. Our experiment reported in this thesis is an attempt to uncover some of the mysteries in several systems in which we think the nonequilibrium behavior of the condensate plays a major role. The majority of the theoretical work had been restricted to $T = 0^{o}K$ so that all dissipative processes may be neglected and also to $T \to T_c$, that is, in the small gap or gapless case, so that we may borrow the elegant formalism of Ginzburg and Landau together with new terms for energy dissipation.

In the nonequilibrium state, the free energy $\mathscr{F}$ no longer must be a minimum. In the above mentioned circumstance, it relaxes towards its equilibrium value with some characteristic time. Abrahams and Tsuneto (1966) proposed a relaxation form of a time dependent Ginzburg-Landau equation (TDGL):

$$\left(\frac{\partial}{\partial t} + \frac{2i\mu}{h}\right)\psi = \frac{1}{\tau_{GL}{}^{a}} \frac{\delta \mathscr{F}}{\delta \psi^{*}}$$

$$= \frac{1}{\tau_{GL}} \left\{1 - \eta|\psi|^{2} + \xi^{2}(T)\left(\nabla - \frac{2ie}{ch} A\right)^{2}\right\}\psi \qquad (2.27)$$

where τ_{GL} is the Ginzburg-Landau relaxation time for the condensate and from the microscopic theory

$$\tau_{GL} = \frac{\hbar\pi}{8k_B|T_c - T|} \tag{2.28}$$

$$\sim 10^{-12}\text{sec} \quad \text{when} \quad T_c - T \simeq 1^{\circ}K$$

a and η are constants (Appendix B).

The chemical potential μ of the system need not coincide with the potential of the pairs defined by the time evolution of the order parameter ψ (equation (2.18)). However, at equilibrium, TDGL reduces to

$$\frac{\delta \mathscr{F}}{\delta \psi^*} = 0$$

and

$$\left(\frac{\partial}{\partial t} + \frac{2i\mu}{\hbar}\right)\psi = 0 \tag{2.29}$$

and the latter implies $\mu = \mu_p$.

That μ_p of the Cooper pairs may differ from the chemical potential of the system μ as a result of a perturbed condensate was first suggested by Rieger, Scalapino and Mercereau (1971) (RSM1). Perturbation of the condensate includes local build up of Cooper pair density by injection, sudden decrease of pair density through evaporation of pairs into quasiparticles, or rapid spatial redistribution of pair density (e.g., density waves). In the experiments to be reported, the first situation was experimentally achieved by a current running through a supernormal interface. The last situation was attained by quantum mechanical interference of two superconducting wavefunctions in a superconducting proximity effect bridge.

2.7 Comparison among the Various Time Scales in Nonequilibrium Superconductivity and Their Characteristic Lengths

Available experimental values for the various time scales are still restricted to only a few materials. However, since all the quasiparticle processes are of similar origin, phonon emission, the qualitative features are not expected to differ very drastically from material to material. The general understanding is that for the various relaxation times:

$$\tau_R > \tau_Q \gtrsim \tau_{TH} > \tau_{GL} \tag{2.30}$$

where τ_R is the recombination time,

τ_Q is the branch mixing time,

τ_{TH} is the thermalization time of quasiparticles,

and τ_{GL} is the Ginzburg-Landau relaxation time of the condensate.

For the first three, each differs from the successive one by about an order of magnitude. But as their respective temperature dependences are different, there may be cross-over points, especially for τ_Q and τ_{TH}. τ_{GL} is in general much shorter than all the others in quasiparticle processes. For example, in the case of tin,

$$\begin{aligned} \tau_R &\sim 10^{-9}\text{sec} \\ \tau_Q &\gtrsim 10^{-10}\text{sec} \\ \tau_{TH} &\lesssim 10^{-10}\text{sec} \\ \tau_{GL} &\sim 10^{-12}\text{sec} \end{aligned} \tag{2.31}$$

As all the electrons involved are close to the Fermi surface, we may define the characteristic length λ over which the particular nonequilibrium process occurs to be the distance traversed with Fermi velocity v_F in one characteristic time τ in the clean limit or the geometric mean with the mean free path ℓ of the electron when ℓ is short with respect to $v_F\tau$ in the dirty limit. So for recombination of quasiparticles:

$$\lambda_R \simeq \sqrt{v_F \tau_R \ell}$$

for branch mixing: (2.32)

$$\lambda_Q \simeq \sqrt{v_F \tau_Q \ell}$$

For a typical τ of 10^{-10}sec, $v_F \sim 10^8$cm/sec, and $\ell \sim 100\text{Å}$ for our films. λ is about 1 micron.

The characteristic length for the condensate itself is just the coherence length introduced before. The microscopic result can be written as

$$\xi(T) = 0.575 \sqrt{v_F \tau_{GL} \ell}$$ (Tucker and Halperin 1971, Appendix) (2.33)

Using the same v_F and ℓ as were used to calculate λ, and with a typical $\tau_{GL} \simeq 10^{-12}$sec, we find that

$$\xi \sim 0.06 \text{ micron}$$

Thus, under these conditions, the coherence length ξ is in general shorter than the characteristic lengths for quasiparticle processes.

The characteristic distance λ indicates the distance such a phenomenon is going to affect the long range order of a superconducting state, or in other words, how far the information of this nonequilibrium process can propagate. As will be seen later, a determination of these characteristic lengths provides a guideline to the understanding of the basic nonequilibrium mechanism behind a certain process. This is exemplified by the experiment on super-normal interfaces. At the initial stage of the research only the relaxation of the condensate was theoretically studied and assumed to be responsible for the nonequilibrium behavior at the interface. τ_{GL} and ξ were supposed to be the controlling parameters. However, the experimental results pointed to a longer τ and λ. Further nonequilibrium effects involving quasiparticles were hence suspected. The consistency of our present picture of nonequilibrium superconductivity can probably be revealed by experiments which provide independent measurements of λ and τ under various circumstances. As an applied aspect, τ and λ also give the time and spatial limitations of devices based on such mechanisms.

Chapter 3

NONEQUILIBRIUM SUPERCONDUCTIVITY AT A S/N INTERFACE

3.1 Introduction to the Problem

When an electric current flows through an interface between a superconductor S and a normal metal N, the interface defines a nonequilibrium region within which the current carriers go from the pairs of the condensate to quasiparticle excitations. The depairing (or pairing) process does not occur abruptly at the boundary. The coherent or nonlocal nature of superconductivity demands the superconducting order parameter ψ to taper off slowly from its full value in the superconductor side to zero in the normal side within a few coherence lengths. At finite temperatures the order parameter decays exponentially in the normal metal. In a clean normal metal whose transition temperature T_{CN} is zero, the decay length ξ_N is

$$hv_F/(6\pi k_B T) \sim 3000\text{Å} \text{ at } 4^\circ\text{K} \quad \text{(Parks 1969)} \tag{3.1}$$

If the normal metal is actually a superconductor above its transition temperature T_{CN}, the decay length is

$$hv_F/\{6\pi k_B T(1 - \frac{T_{CN}}{T})\} \tag{3.2}$$

In the dirty limit the geometric mean with the mean free path has to be taken. This induced order parameter in the normal metal as a

result of the proximity of the superconductor reflects the finite lifetime of the Cooper pairs within the normal metal before they are destroyed by thermal fluctuations. Thus the proximity effect allows the normal metal to support a decaying supercurrent. The S/N interface provides a system with coexisting normal current flow and supercurrent flow. Combining equations (2.20) and (2.21), we have

$$\begin{aligned} \vec{j} &= \vec{j}_s + \vec{j}_n \\ &= \vec{j}_s - \frac{\sigma_{eff}}{e} \nabla\mu \end{aligned} \tag{3.3}$$

However, an inconsistency arises since this implies the existence of an (d.c.) electric field which would accelerate the condensate. If this happens, the supercurrent $\vec{j}_s$ will grow until it exceeds the critical current density at which superconductivity is quenched. But experimentally the S/N interface turns out to be a stable system. The first possible solution to this puzzle was suggested by Rieger, Scalapino and Mercereau (RSM1) in 1971. They put forward the concept of multipotentials for nonequilibrium superconductivity. In the nonequilibrium state the chemical potential of the quasiparticles need not be the same as the potential for the condensate. In actual fact a potential difference is required to drive the nonequilibrium pairing (or depairing) process inside the conversion region. Hence the potential μ_p of the pairs can stay constant so that there is no net thermodynamic force coming from the potential gradient to accelerate the supercurrent even in the presence of an electric field.

3.2 The Electrodynamics of the S/N Interface

Unlike the condensate, the quasiparticles which compose the normal current are believed to be scattered by imperfections of the ionic lattice. Hence a chemical potential gradient is required to drive the normal flow. The Ohm's law for the normal current can be written as

$$\vec{j}_n = - \frac{\sigma_{eff}}{e} \nabla\mu \tag{3.4}$$

where σ_{eff} is the effective conductivity for the quasiparticles. However the effect of the condensate modifies significantly the energy spectrum of the quasiparticles, and as is shown in Appendix A they have extremely small effective mass. This compensates the scarcity of the quasiparticles such that at temperatures not too far away from T_c, σ_{eff} is close to the normal conductivity of the metal at that temperature.

This conclusion is strongly supported by the evidences obtained from proximity effect bridges in which it is believed to have a simultaneous existence of normal and superflow. Experimentally, the resistance of the proximity effect bridge in the phase coherent state is very close to the resistance when the bridge is normal, implying that the normal flow is essentially subjected to the normal resistivity. So for an order of magnitude estimation, the normal conductivity σ will be assumed. As we would expect, the extent of the potential difference $\mu_p - \mu$ depends on the rapidness of the pairing or depairing. This is measured by the divergence of the supercurrent,

$\vec{j}_s$. We have

$$\begin{aligned} \nabla\cdot\vec{j} &= \nabla\cdot\vec{j}_s + \nabla\cdot\vec{j}_n \\ &= \nabla\cdot\vec{j}_s - \frac{\sigma}{e}\nabla^2\mu \end{aligned} \tag{3.5}$$

In the steady state, charge conservation requires $\nabla\cdot\vec{j} = 0$.

Hence

$$\nabla\cdot\vec{j}_s = \frac{\sigma}{e}\nabla^2\mu \tag{3.6}$$

and

$$\mu = \mu_o + \frac{2}{3}\mu_o\frac{\delta\rho}{\rho} + eV \tag{3.7}$$

where $\delta\rho$ represents a deviation in the electron density from equilibrium and V is the scalar electric potential. The second term comes from the fact that the chemical potential is a function of electron density:

$$\mu_o = \frac{\hbar^2}{2m}(3\pi^2\rho)^{2/3} \qquad \text{(Kittel 1968)} \tag{3.8}$$

hence

$$\frac{\delta\mu_o}{\mu_o} \simeq \frac{2}{3}\frac{\delta\rho}{\rho} \tag{3.9}$$

It was shown that (RSM1,1971) this term may be neglected with respect to the electrostatic term. Thus using Poisson's equation,

$$\nabla\cdot\vec{j}_s = -4\pi\sigma\,\delta\rho \tag{3.10}$$

$$\delta\rho = -\frac{1}{4\pi\sigma}\nabla\cdot\vec{j}_s \tag{3.11}$$

Hence depairing is accompanied by an electric field and charge build-up. Since the process starts within the superconductor side of the interface, this model predicts a d.c. electric field inside the superconductor as a result of the nonequilibrium depairing.

This description is a result of the two fluid model and the two potential concept only and is independent of the detailed mechanism by which the two potentials split from each other. Rieger et al, who first suggested the two potential concept also suggested describing the nonequilibrium state with the time dependent Ginzburg-Landau formalism.

3.3 Description of the Nonequilibrium State

In the absence of transport current, interconversion of pairs and quasiparticles establishes a chemical equilibrium. With a transport current the unidirectional conversion upsets the chemical equilibrium at the interface region. The condensate is perturbed as a result of the pair injection or extraction. Rieger et al (RSM1 1971) suggested describing this nonequilibrium superconducting state with the time dependent Ginzburg-Landau differential equation (2.27) with a nonequilibrium chemical potential μ. Here the quasiparticles are assumed to be already at equilibrium with the lattice vibration and have attained the same chemical potential μ as the system. They also used equation (2.18) to define a potential μ_p usually referred to as the potential of the pairs. As was discussed in §2.6, μ_p is the chemical potential of the system if it were in equilibrium.

It governs the time evolution of the phase of the superconducting wave function (equation (2.18)). The force on the pairs and hence the acceleration of the supercurrent is proportional to the gradient of μ_p (equation (2.17)). According to their analysis, there is a charge build up as a result of the depairing of the superfluid and there is a potential difference between the pairs and the quasi-particles. Actually,

$$\mu_p - \mu = \frac{m\xi^2(T)}{4|e|\tau_{GL}} \frac{\nabla\cdot\vec{j}_s}{|\psi|^2} \tag{3.12}$$

where $\vec{j}_s$ is given by equation (2.16).

Equation (3.10) states that a difference in potentials $\mu_p - \mu$ exists only when $\nabla.\vec{j}_s \neq 0$, and it is in the neighborhood of the S/N interface that such a regime exists. Now with μ_p staying constant spatially so that there is no acceleration of the supercurrent, the dilemma about the stability of the supercurrent is then solved. That the two potentials may differ allows a nonzero gradient of μ to drive the normal flow. Hence using the fact that

$$\nabla\cdot\vec{j}_s = -\nabla\cdot\vec{j}_n = \frac{\sigma}{e}\nabla^2\mu$$

and (3.13)

$$\nabla\mu_p = 0$$

the spatial extension of this effect is governed by

$$\nabla^2(\mu_p - \mu) - \frac{4e^2\tau_{GL}|\psi|^2}{m\,\xi^2(T)\,\sigma}(\mu_p - \mu) = 0 \qquad (3.14)$$

The coefficient of $\mu_p - \mu$ is itself a function of position and defines a temperature dependent "healing length" for the potential difference which on numerical calculation turns out to be $\simeq 2\xi(T)$ (Appendix B).

The situation is shown in Figure 3-1. μ_p stays constant inside the superconductor S and actually extends slightly into the normal region N as a result of proximity effect until thermal fluctuation destroys the coherence. μ splits from μ_p well inside the superconductor with the localized excess charge generated by the depairing and finally joins up with the usual Ohmic behavior inside the normal metal.

The picture offered here is based on the assumption of a two fluid model and the proposed concept of a different potential for each fluid in a nonequilibrium depairing region. In the experiment to be reported we sought to probe if there is really a difference between those two potentials by placing potential measuring probes inside that region.

3.4 Origin of the Potential Difference

Equation (3.12) which relates the two potentials to the divergence of the supercurrent implies that energy is released in both pairing and depairing processes. Consider a current flowing through a S/N interface from the superconductor side to the normal

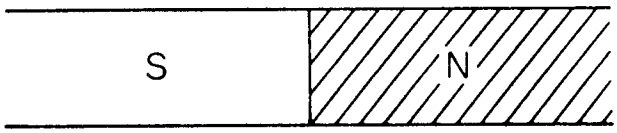

$$\mu_p - \mu = \frac{m\xi^2(T)}{4|e|\tau} \frac{\vec{\nabla}\cdot\vec{j}_s}{|\psi|^2}$$

$$\nabla^2(\mu_p - \mu) - \frac{4e^2\tau|\psi|^2}{m\xi^2(T)\sigma}(\mu_p - \mu) = 0$$

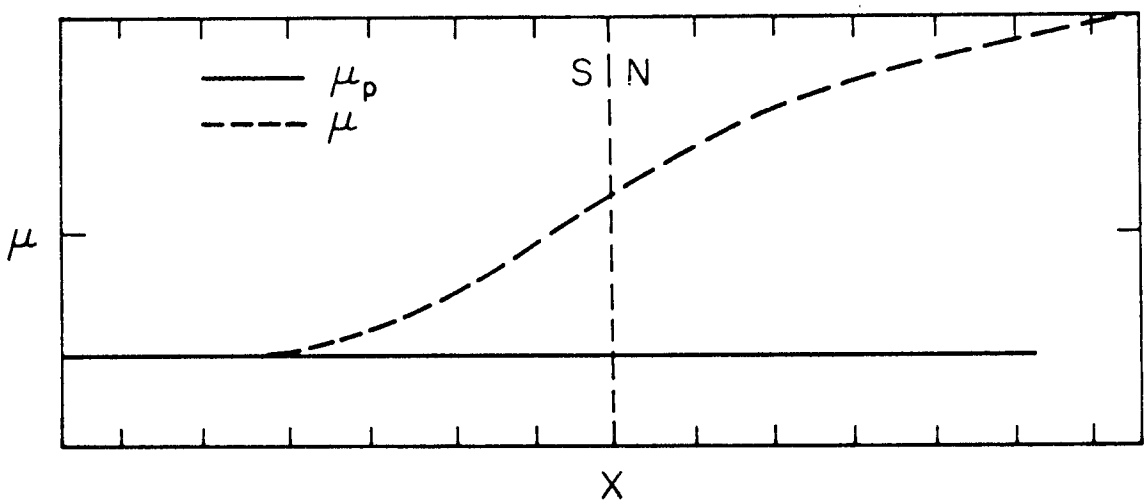

Fig. 3.1 Quasiparticle chemical potential μ and pair potential μ_p as a function of position in the vicinity of the current-carrying S/N interface. Spatial grid marks are 1 coherence length apart.

side. $\nabla\cdot\vec{j}_s$ is negative and hence $\mu > \mu_p$. Electrons flowing in the opposite direction are pairing up in the nonequilibrium region, releasing energy $\mu - \mu_p$ per electron. Similarly a current flowing from the normal side to the superconducting side reverses the pairing process to a depairing process with $\mu_p > \mu$ and a positive $\nabla\cdot\vec{j}_s$. Again energy $\mu_p - \mu$ per electron is released during depairing. This energy release is conceivable as the system naturally goes from a higher energy to a lower energy state.

To trace back the origin of this energy difference, it must be noted that equation (3.12) is a direct consequence of the time dependent Ginzburg-Landau differential equation (2.27) which describes the time evolution of a perturbed condensate. At equilibrium the free energy F of the condensate is at a minimum. A perturbed condensate hence is at a higher free energy state. So as the condensate relaxes back to its equilibrium state, the excess free energy is released, independent of whether it is through pairing, depairing or otherwise. And equation (3.12) describes how this amount of energy is given out as the chemical potential of the perturbed system tries to relax back to its equilibrium value μ_p.

3.5 Probing of Potentials

A direct verification of the two potential concept requires the appropriate potential probes measuring μ_p and μ individually to give different measurements in the nonequilibrium region. The actual magnitude and temperature dependence will give a direct comparison with the Rieger et al theory.

Our experiment was done by making potential measurements within a few microns of a current-carrying S/N boundary. Usual voltmeters measure chemical potential differences (Hunt 1966). In thermodynamic equilibrium, for a high impedance voltmeter that essentially draws no current, the chemical potential difference across the two terminals of the voltmeter produces a nonzero reading. Each terminal shares the same chemical potential as the end of the potential probe with which it is connected and for usual cases that should be the same as the chemical potential at the sample test point with which the other end of the probe is in contact. However, in this nonequilibrium case of more than one potential at a single location, this is no longer valid. A nonequilibrium process is being induced into the potential probe. It is important to recognize the effect of the state of the probe in determining which potential it is going to measure.

Let us first examine the action of a superconducting potential probe. The nonexistence of an accelerating supercurrent implies the constancy of μ_p spatially throughout the nonequilibrium region and also the probe. At the testing point where contact with the nonequilibrium region is made, the quasiparticles in the superconducting probe tends to share the same μ as those in the depairing region. This induces a chemical potential gradient $\nabla\mu$ and also a potential difference $\mu_p - \mu$ at this end of the potential probe. The $\nabla\mu$ so created sets up a normal current flow in the probe*. However, the

*The power dissipated by this normal current is indirectly supplied by the current source which is responsible for the current flowing through the S/N interface.

influx of quasiparticles will upset the equilibrium distribution in the superconducting probe and the quasiparticles start to recombine while supercurrent begins to flow in the opposite direction to maintain charge neutrality, counterbalancing the normal flow such that

$$j_s + j_n = 0 \tag{3.15}$$

The divergence of j_s accounts for the decay of μ from the non-equilibrium value back to μ_p in a few coherence lengths. So at the far end (with respect to the testing point) of a superconducting potential probe few coherence lengths long, same chemical potential is shared by both quasiparticles and pairs and this common potential is the same as μ_p inside the depairing region. Thus a superconducting potential probe more than a few coherence lengths long can be used to measure the pair potential μ_p at its point of contact with the sample.

A potential probe made of normal metal (or a superconductor above its transition temperature) will have its electrons in thermodynamic equilibrium with the electrons in the nonequilibrium region and hence will tend to measure the chemical potential μ. There is some complication at the contact point as the normal probe also creates a S/N boundary. Superconductivity is induced at the tip of the normal probe. The spatial extent of this proximity effect induced superconductivity is the coherence length of the pairs. In a dirty normal metal with mean free path ℓ_N, this induced coherence length is given by $(\ell_N \xi_N)^{1/2}$ where ξ_N may be estimated by equation

(3.1).

$$\xi_N \simeq \frac{hV_F}{6\pi k_B T} \simeq \frac{hV_F}{6\pi k_B T_c} \qquad \text{of the superconductor,}$$

$$\simeq \frac{1}{3}\,\xi_o \qquad \text{(equations (2.6),(2.8))}$$

$$\sim 300\text{Å} \qquad \text{(Hauser and Theuerer 1964)}$$

while $\ell_N \sim 13\text{Å}$ for our film

$$\sqrt{\ell_N \xi_N} \simeq 62\text{Å} \tag{3.16}$$

The same argument as in the case of the superconducting probe indicates that there will be slight decay of the potential μ towards μ_p taking place over the coherence length $\sqrt{\ell_N \xi_N}$ before thermal fluctuations destroy the induced superconductivity. In this experiment $\sqrt{\ell_N \xi_N} = 62\text{Å}$ is very small compared to $\xi(T) \sim 0.2\ \mu\text{m}$ (equation (3.17)) and hence we assume negligible decay of μ can occur inside a normal probe. In this experiment the probe carried negligible current as the impedance of the voltmeter was high. So the chemical potential in the normal probe remained the same value throughout the probe and this value was detected by the voltmeter. Thus a normal potential probe measures μ .

3.6 General Experimental Considerations

As the whole phenomenon extends only a few coherence lengths away from the S/N interface, to optimize the chance of seeing the non-equilibrium effect, potential probes for potential measurement were

placed within one micron to the interface. As the pair potential only extends a very short distance ($\sim \xi_N$) into the normal metal and the effect is masked by the usual Ohmic voltage drop, potential measurements on the superconductor side give a more transparent examination of Rieger et al's two potential concept. Two important consequences of their theory were stressed:

a) There should be a difference between μ and μ_p which can be detected individually with normal and superconducting potential probes.

b) There should exist an electric field on the superconductor side of the interface that can only be measured with normal potential probe.

The way these ideas were tested was to place two potential probes on the superconductor side of the interface with one inside the nonequilibrium region and the other in the equilibrium region. If the first probe (inside the nonequilibrium region) is a normal probe, μ would be sensed. If it is a superconducting probe, μ_p would be sensed and $\mu \neq \mu_p$. However the second probe (in the equilibrium region) will measure the same potential independent of the state of the probe since $\mu = \mu_p$ in the equilibrium region. The assertion that μ_p should remain constant spatially implies that if the first probe is a superconducting probe, no potential difference should be detected across this set of probes. However, if the first probe is a normal probe, a potential difference should be measured. This potential should to a first approximation be linear with the total current

through the interface. $\Delta\mu = \mu_p - \mu$ is also the potential difference required to drive the normal current in the depairing region. If the normal probe is very close to the S/N boundary, the proportionality constant between the potential difference and current should be of the order of the resistance of the metal strip, a healing length long in the current direction. The healing length is approximately $2\xi(T)$.

The region in which nonequilibrium is to be expected is only a few coherence lengths away from the S/N interface. As it was technically difficult to fabricate microvoltage probes of sizes less than 0.5 μm, a longer coherence length would enhance the possibility of seeing the potential difference. The coherence length ξ varies with temperature in the way expressed by equation (2.3). Its value diverges as T approaches T_c. So the experiment stood the best chance when T was just below the superconducting transition temperature T_c. As an estimate:

$$\xi \sim 900\text{Å}, \quad \ell \sim 13\text{Å} \quad \text{in the film}$$

$$T_c \sim 4^\circ\text{K}, \quad T_c - T \sim 10\ \text{m}^\circ\text{K} \tag{3.17}$$

$\xi \sim 0.2$ μm. As the temperature goes down the coherence length becomes shorter than the distance between the interface and the microvoltage probe and the potential difference between μ_p and μ at the probe will disappear.

3.7 Circuit Fabrication

As the measurement had to be done at distances at most a few coherence lengths (~ 1 μm) away from the S/N interface, high precision

voltage probes of size less than one micron had to be fabricated and positioned to within a micron of a well defined super-normal interface. The superconducting thin film substrates originated by Notarys and Mercereau proved to be extremely useful to meet such requirements. Using photoetch masking technique and anodization (Palmer and Decker 1973), such superconducting thin film substrates not only allowed high precision (to 1/2 micron) superconducting microcircuits to be sculptured in a well controlled manner, it also allowed a control over the transition temperature of the film and thus made the fabrication of S/N interface on the same thin film possible.

The superconducting substrates used in this particular experiment were tantalum thin films. (This technique is easily extendable to various superconducting refractory metals, e.g., Nb, W, Zr, Hf.) These hard superconducting films were produced by evaporation onto a sapphire substrate $\sim$250Å of tantalum. The evaporation was done in an ultrahigh vacuum system with pre-evaporation pressure $\sim 10^{-8} - 10^{-9}$ torr (mm Hg). The tantalum melt was 99.99% pure and electron beam heating was used. The cleaned sapphire substrate was heated to 400°C during evaporation. Deposition was usually completed within a minute, with thickness monitored with a quartz crystal thickness monitor.

Tantalum possesses very good anodization properties. The oxide formed during the electrolytic oxidation is structurally compact and strongly adheres to the metal surface protecting it from further oxidation unless a critical electric field in the oxide is reached. Hence with an applied voltage, the oxide will grow to a

thickness such that the electric field is reduced to just below the critical value; the oxidation then stops. Hence the thickness of oxide is proportional to the voltage applied. The rate is about 15Å/volt which corresponds to the removal of $\sim$ 6Å/volt of tantalum metal. Using this technique, thickness of various regions of the tantalum substrate can then be adjusted in a controlled way by anodization with various voltages.

The tantalum substrate itself possesses a very peculiar superconducting property. Its transition temperature is thickness dependent, going to a lower temperature as its thickness decreases. Our 250Å film usually has a T_c of about $4^{\circ}K$ and may drop to $3.5^{\circ}K$ when it is thinned down to $\sim$ 100Å with anodization. The exact mechanism of the thickness dependence is unknown. It is suspected to be related to possible gradual change in crystalline structure with thickness as a result of the influence by the substrate during evaporation. It is also possible that electron-phonon interaction is strongly affected by the change in phonon spectrum as the film thickness changes. However, the fairly broad variation of properties among the films makes this as the major cause not plausible. Thickness less than 50Å was rarely used because of uniformity considerations unless the whole film was to be oxidized away. This superconducting property gives a powerful capability to investigate S/N interface, as in this case where various portions of the superconducting circuit have to stay normal. This is simply attained by working at an appropriate temperature range such that it is above the T_c of certain parts of the circuit.

To sculpture the circuit, photoresist masking technique was used. A thin layer ($\lesssim$ 1 μm) of positive photoresist (Shipley AZ1350, exposed areas are removed by developer) was spun on the 1 inch x 1 inch tantalum thin film on the sapphire substrate at 4000 RPM or higher. For large patterns, ultraviolet exposure with contact masks could be used. For fine detail, masks were inserted in the optical path of a Carl-Zeiss RA microscope so that a diminished image was focused onto the film through the objective. With 1600 magnification and standard oil immersion technique, it was possible to reproducibly work with well defined dimensions down to at least 0.3 μm, the resolution limit of the microscope. Following standard developing procedures a plastic mask was then formed on the film. A drop of weak electrolyte was put on the area to be anodized. Gold wire was used as the cathode and a predetermined voltage was then applied to anodize the film.

Undercutting sets a limitation to the resolution. Anodization sometimes extends under the edges of the plastic covered areas as the electrolyte slips underneath. The sticking power of the photoresist may be weakened by the presence of the electrolyte, or by the stress of the expanding oxide formed which is about 2.5 times the volume of the metal removed. It was observed that undercutting strongly depended on the length of time required for the anodization. For most cases where accuracy was required, a trade-off among the area to be anodized, the anodization time, anodization waveform, and maximum anodization voltage had to be decided. For every film to be used, a calibration procedure had to be performed to determine the

voltage equivalent thickness of the film, surface resistivity (resistance per unit square) and transition temperature as a function of thickness. And based on these data, a particular circuit with proper operating temperature range could then be designed. Electrical connections were made onto the circuit by pressed-on indium contacts.

Such superconducting microcircuits proved to be very reliable and very stable. Thermal cycling from room temperature to $4^{o}K$ and storage over a year did not change the characteristics to any appreciable extent.

The inset in Figure 3. shows one of the typical circuits. The width of the current carrying strip ranged from 3 to 10 μm. The "normal" section on the strip was an anodized region at least 10 μm long, typically 100Å thick, with a depressed transition temperature below the normal working temperature range of the experiment. Potential leads were all located on the superconductor side of the interface. They were in general 1 μm or less wide. One was situated close to the interface and one about 30μm away. The transition temperature of the probes were depressed by anodization. So the whole circuit was fabricated on a single tantalum film and hence boundary scattering due to mismatch of crystalline structure was minimized.

The whole film was immersed in a liquid helium bath within a silvered dewar. This was in turn surrounded by a liquid nitrogen jacket. As the boiling point of liquid helium is a function of its vapor pressure, the temperature of the liquid helium bath was controlled by pumping and regulating the vapor pressure. At about $4^{o}K$

pressure regulation within 1 mm of mercury allows a temperature resolution of 1 $m^{o}K$. Cooling rates as slow as 5 $m^{o}K$ per minute were often used for measurements as a function of temperature. The pumping system allowed a working temperature range of from $4.2^{o}K$ at atmospheric pressure to $\sim 1.4^{o}K$ at 2 mm of mercury.

3.8 Magnetic Shielding

Superconductivity is sensitive to the application of magnetic field (Meissner effect). To avoid complication, measurements were made in an ambient magnetic field of the milligauss level. This was achieved by using two concentric, cylindrical μ-metal shields around the dewars and they were demagnetized before every run. To further minimize any time varying interfering fields, a Meissner effect superconducting lead shield was used inside the helium bath as a final shield for the circuit. A small compensating field, variable up to a few Gauss, produced by a superconducting niobium coil, was also used in some circumstances to minimize the remaining ambient static field.

3.9 Electrical Measurements

This experiment required the measurement of low level voltage signals inside a superconductor. As an estimate, the voltage should be approximately the potential difference developed across a strip of the film ($\sim$ 10 μm wide) and one coherence length ξ long. Taking

$$\xi \sim 0.2\ \mu m$$

$$I = 1\ \mu A$$

Resistance per square of film ~ 2 ohms

$V \sim 40$ nV

a voltage resolution better than 2 nV was required for a 5% accuracy.

To avoid various spurious d.c. voltage as a result of thermoelectric effects, a.c. pickups and typical drift problems with d.c. equipment, a low frequency alternating current technique was used. An alternating current of about 350c/s was driven by a high output impedance (~ 1 MΩ) current source through the S/N interface. Current level was normally limited to 1 μA or lower so that the power dissipation in the circuit was of the order of 10^{-12}watt and heating effects were negligible. The alternating current was well filtered with a low pass filter to prevent spurious radiofrequency interference. Potential differences were measured with a "lock-in" (PAR HR-8) amplifier tuned to the same frequency and in phase with the current. A relatively low impedance (~ 200 ohms) transformer coupled preamplifier (Type B, PAR) provided a low noise figure matching to the very low internal impedance of the circuit (< 1 ohm). The bandwidth used in the experiment is about 1 c/s. The Johnson noise from the circuit was negligible ($\sim 10^{-12}$volt at 4°K).

3.10 The Experimental Results

Based on the two-fluid model and the two potential concept, the results were analyzed in Section 3.5 that a superconducting probe measures the pair potential μ_p and a normal potential probe measures the quasiparticle chemical potential μ, and they should give

different potential measurements when applied to the nonequilibrium region close to a S/N interface. It was this important prediction that this experiment was intended to verify. The experimental results came out to be affirmative. Normal potential probes and superconducting potential probes gave different measurements when they were used to probe the potentials close to a S/N interface. This strongly indicated the validity of the two-potential concept.

With our experimental arrangement, differences between μ_p and μ could be detected only when we used normal potential probes to detect μ close to a S/N interface. The replacement of the normal probe by superconducting probe or the absence of a S/N depairing region should give results identical to that of a usual superconducting strip.

Figure 3.2 shows the superconducting transition of our tantalum thin film strip as measured by potential probes. The temperature width of the transition was less than 5 $m^{o}K$ and was the same for both superconducting and normal probes.

Imposing a S/N boundary near a superconducting potential probe did not materially alter the superconducting transition. In all cases the voltage measured by superconducting probes was zero below the transition region. This supported the prediction that the potential of the pairs stays constant even in the depairing region. For sufficiently small probes ($\sim$ 0.5 μm) fluctuation effects (Hunt and Mercereau 1967) lowered the transition temperature of the probe and broadened the apparent transition by a typical value of $\sim 5 m^{o}K$.

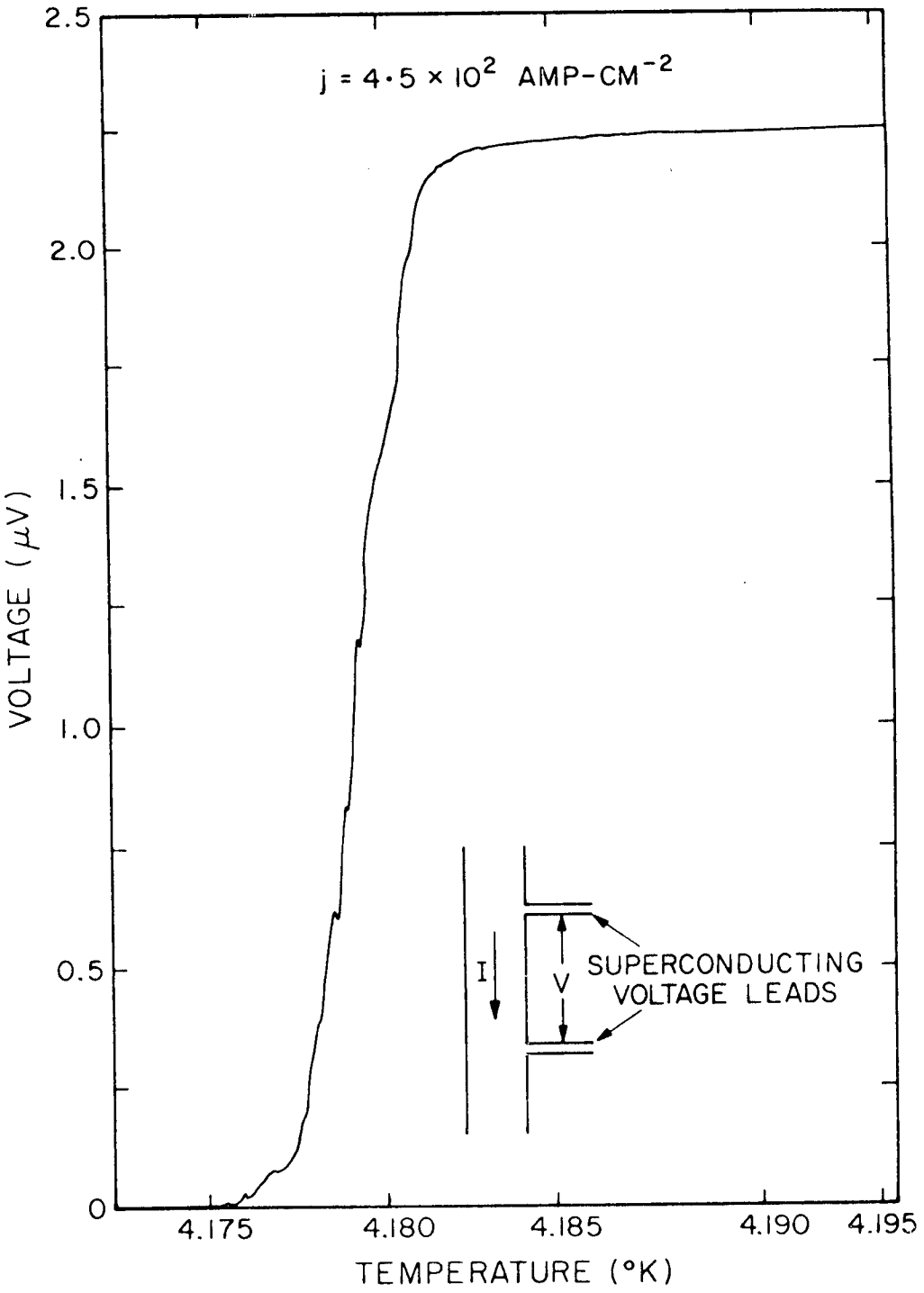

Fig. 3.2 Superconducting transition of the tantalum thin film strip as measured by the potential probes

In each of the many circuits we have tested, small potentials were measured with normal probes on the superconducting side of a S/N interface immediately below the superconducting transition as defined by the similar measurement with a superconducting potential probe. Hence it indicated that there was an electric field on the superconducting side of the interface that could only be detected with a normal potential probe, consistent with the theoretical prediction. Figure 3.3 shows a typical result when measurement was made with normal voltage probes. The potential remained nonzero as far as one-tenth of a degree below the superconducting transition. This potential difference below the superconducting transition, we believe, is the potential difference described by equation (3.12).

Many checks had been made to confirm that this was not a thermal heating effect and that a S/N interface and normality of the potential probe near the interface were essential for the observed results. These tests consisted of different combinations of depressed transition temperatures of the potential probe and of the "normal" side of the interface. The voltage always went to zero either when the "normal" side of the interface went superconducting or when the "normal" potential probe close to the interface turned superconducting. Figure 3.3 is an example. The voltage went to zero at above $3.99^{\circ}K$, the same temperature as the "normal" section went superconducting. Superconductivity or normality of the other probe 30 μm away from the interface did not affect the result.

Experiments also showed that a 5 μm length of superconductor or 3 μm of normal metal in a potential probe were sufficient to make

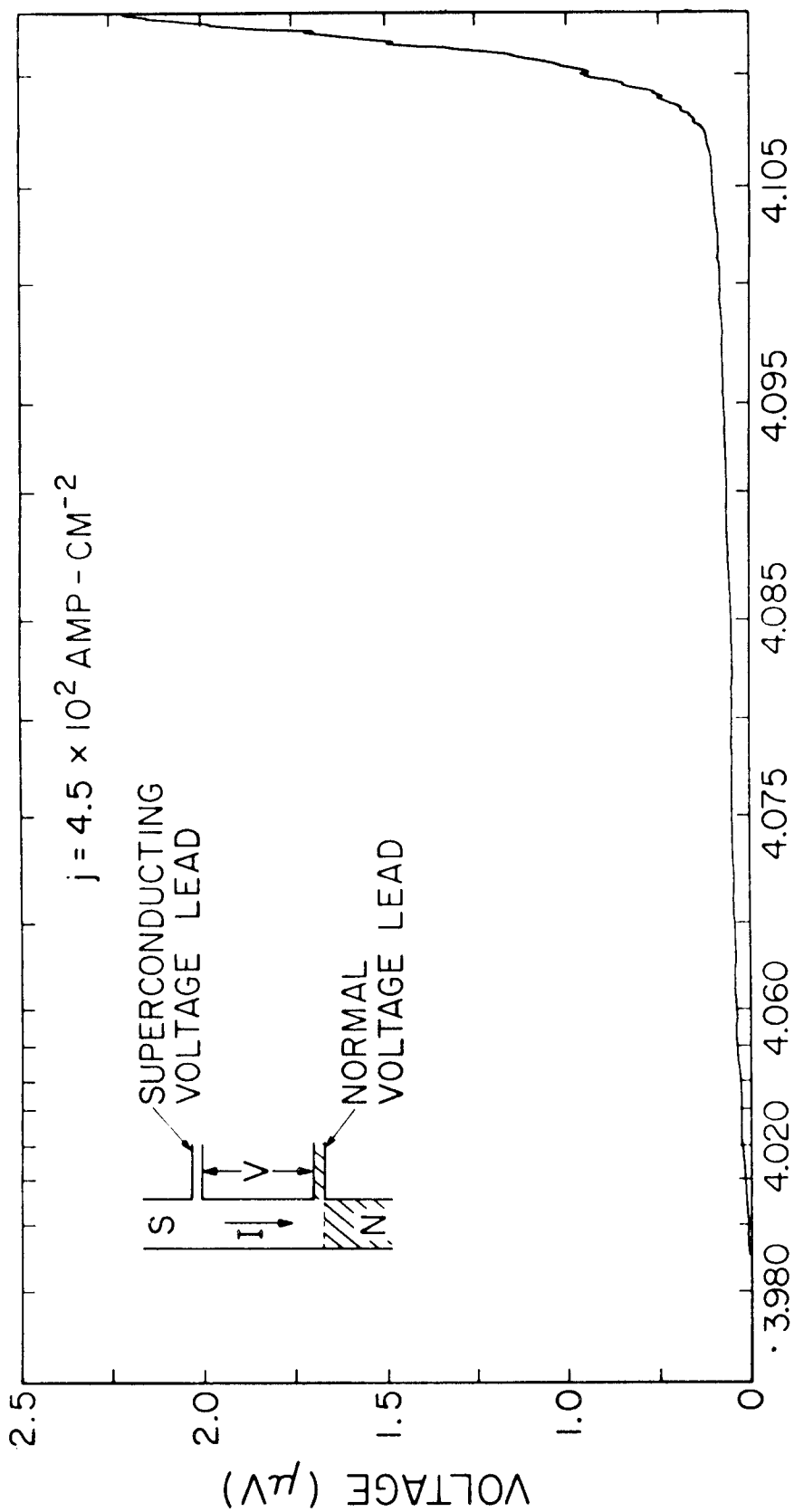

Fig. 3.3 Potential measured below the superconducting transition of a current-carrying interface. This potential is zero if the normal probe is superconducting.

the probe behave as superconducting or normal, respectively. The potential was too small to measure once the S/N interface was over 5 μm away from the nearest potential probe. Most of the experiments were done at power levels below 10^{-12}watt, and thus heat input was very small. As the film was immersed in liquid helium, major portion of the heat was carried away by the helium liquid. Assuming conduction only, the temperature gradient required may be estimated as follows. The heat conductivity for liquid helium is 2.5×10^{-4}watt/cm/deg. (Wilks 1967) and assuming that heat came out from an area of 10 μm × 10 μm, the temperature gradient required was only 4 $m^{o}K$/cm, while temperature of the helium bath was measured up to an accuracy of about 2 $m^{o}K$. Hence heating effects are too small to account for a phenomenon which extends at least $0.1^{o}K$ and may be neglected.

All these results not only confirmed that there exists an electric field on the superconductor side of the interface, it also indicated that different potentials were measured by superconducting or normal potential probe. The latter is a crucial test of the two potential concepts. A confirming test involved putting a superconducting potential probe between the S/N interface and the normal probe. The leads, each slightly less than 1 μm from each other, were situated as close as possible to the interface such that the outermost edge of the normal probe was about 3 μm away from the interface. The geometry is shown in the inset in Figure 3.4. When the whole film was normal a resistive drop was developed across the two probes as indicated to the right of Figure 3.4. However, just below the superconducting transition, this voltage reversed in polarity. This is

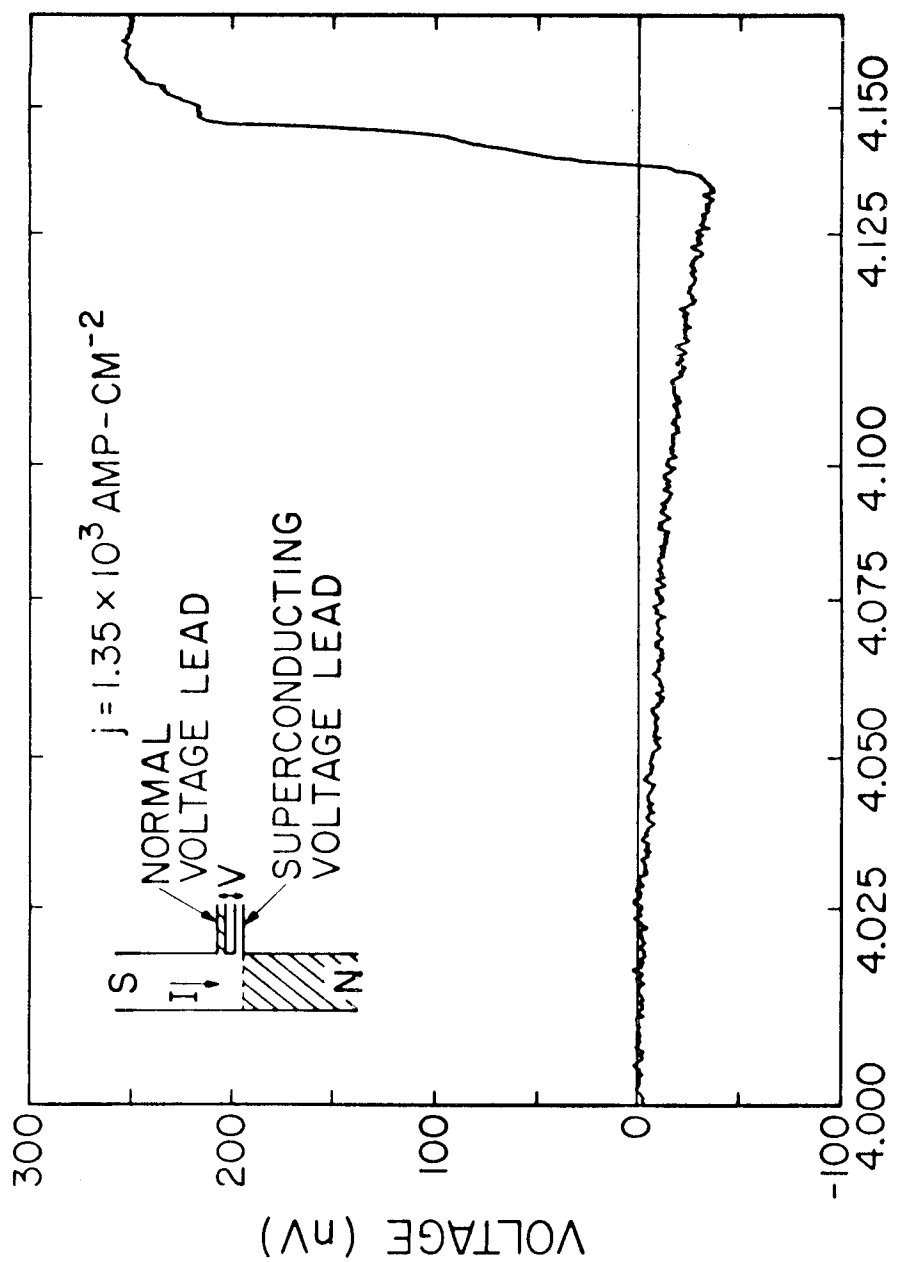

Fig. 3.4 Potential measured by a set of superconducting and normal probes situated within 3 m of a current-carrying S/N interface. Note that the potential of the superconducting probe is higher than that of the normal probe.

additional evidence that the quasiparticles are being subjected to an electric field even though they are relatively further from the boundary, and have an even lower potential than the pairs near the boundary.

The theory also predicted to first approximation a linear relationship between the chemical potential difference and the current through the interface. Experimentally it implies a constant dV/dI or "dynamic resistance". Indeed it was found that the dynamic resistance corresponding to the difference in chemical potential was constant when current was below the temperature dependent critical current of the film itself. Figure 3.5 shows the dynamic resistance measured as a function of the direct current through the supernormal interface. As the dynamic resistance gradually decreased during the superconducting transition of the film, regions of constant dV/dI slowly developed when it went below 0.5 ohms. dV/dI stayed constant until the d.c. current exceeded the critical current and the superconducting film switched back to its normal resistance.

Although the polarity reversal experiment shown in Figure 3.4 gave good grounds that the phenomenon was not a structure effect, this critical current behavior actually ruled out the possibility that the whole experiment was merely demonstrating a gradual superconducting transition in areas adjacent to the boundary, weakened by the regions of depressed transition temperature created by the anodization process. In that case we would expect a gradual increase in dynamic resistance with increasing current similar to that observed during the transition of the film and no well defined critical current.

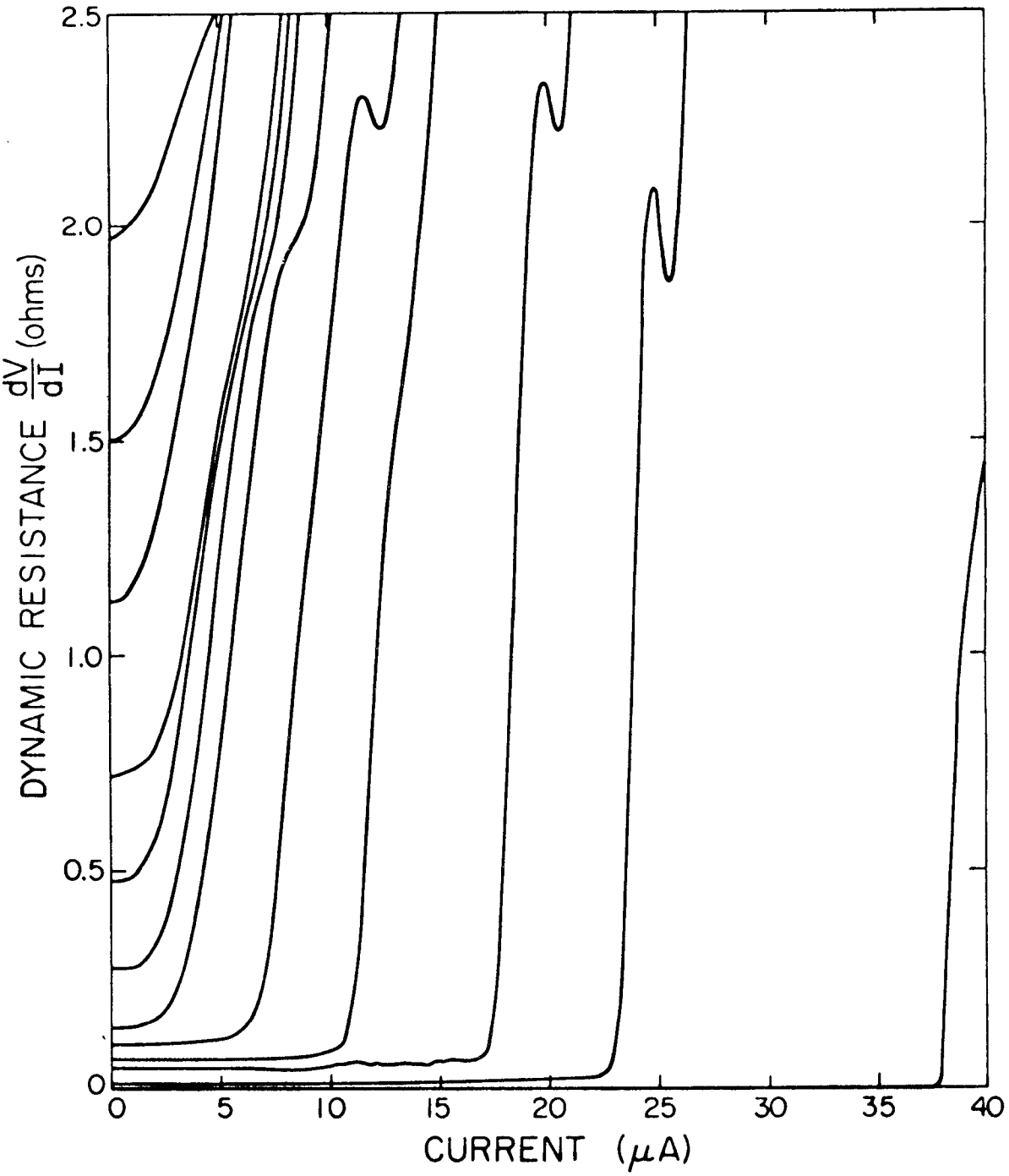

Fig. 3.5 Dynamic resistance dV/dI as a function of the d.c. bias current through the S/N interface as temperature went through the superconducting transition. Below the transition dV/dI stayed constant until the d.c. current exceeded the critical current.

3.11 Quantitative Comparison with Theory

The experimental results indicated that the theoretical prediction and thus the physical model was at least qualitatively correct. To yield a more complete picture, both the actual magnitude of the potential difference $\mu_p - \mu$ and the temperature dependence have to be examined. We use the experimentally determined temperature dependence to compare with theory using the distance of the probe (in coherence lengths) from the S/N interface as a parameter. The coherence length so deduced is then compared with values determined by other investigators using different methods.

The potential difference measured between two given positions is expected to be temperature dependent via the temperature dependence of the "healing length" (equation (3.14)). Since the potential probes were about 1 μm wide, they measured a spatial average of the effect over their width. Equation (3.14) was solved numerically for this average $\mu_p - \mu$ as a function of temperature, leaving the relative probe distance $X/\xi(0)$ from the S/N interface as a parameter. Figure 3.6 shows the result of this analysis along with data points taken with a probe 1 μm from the boundary. The best fit was obtained for $X/\xi(0) = 12$, thus implying that the effective coherence length at zero degree $\xi(0)$ is 830Å in our thin tantalum films. In this sample the transition temperature of the "normal" section is $3.99^{\circ}K$ so the prediction of the simple analysis would be expected to fail near this temperature and $\mu_p - \mu$ should vanish below $3.99^{\circ}K$, as it does.

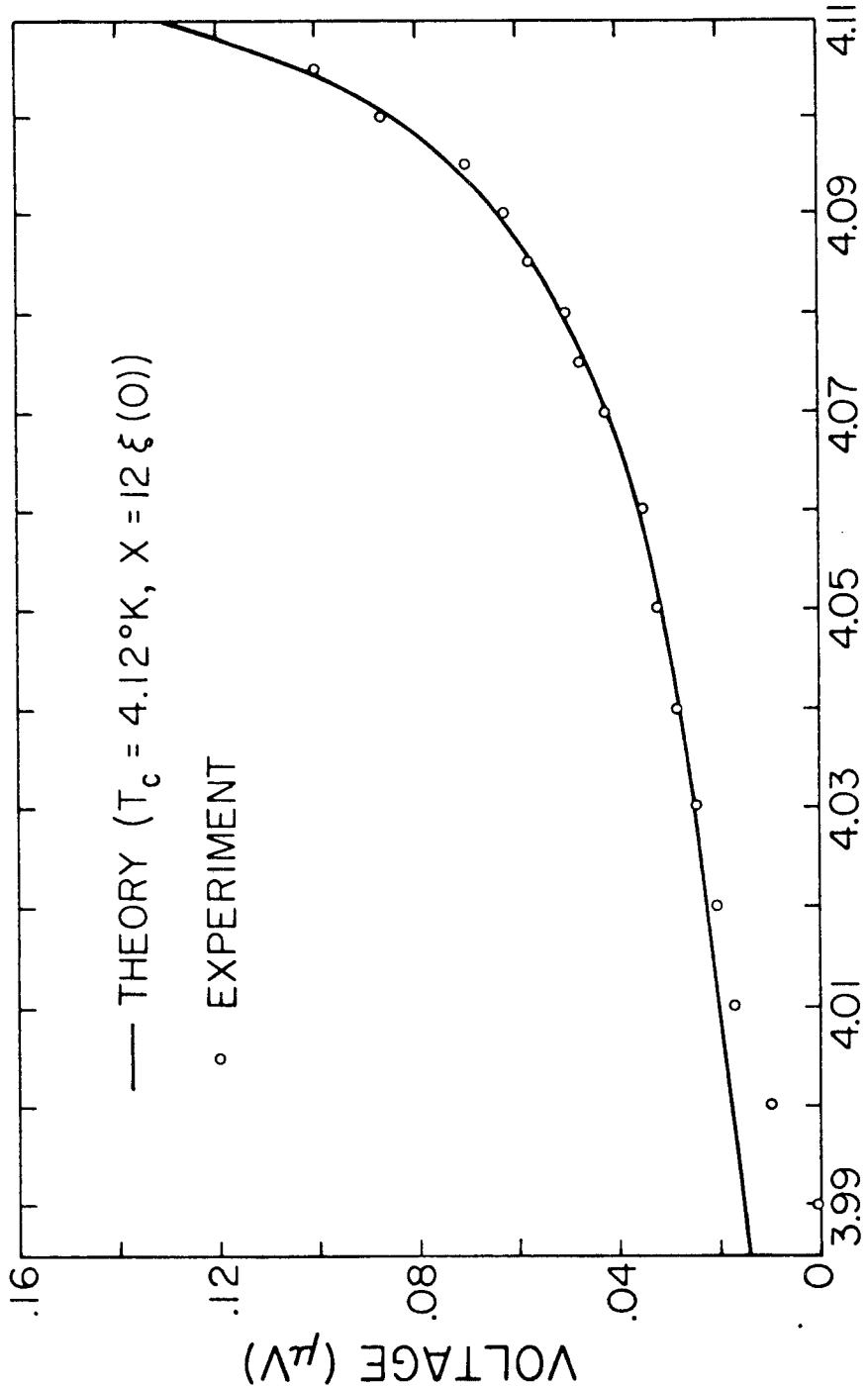

Fig. 3.6 Comparison of Rieger et al's theoretical temperature dependence with experimental results. The theoretical curve was calculated for a voltage probe at a distance X = 12 ξ(0) away from the S/N interface. The normal region went superconducting at 3.99°K.

However in this experiment we were in the mean free path limited situation. The resistivity of the film at $4.2^{o}K$ is about 1.6×10^{-5} ohm-cm. A simple estimation using the free electron model and taking

electron density	$n_o \tilde{=} 0.9$ holes/atom	(Ziman 1958)
effective mass	$m^* \tilde{=} 1.2\ m_e$	(Halloran et al 1970)
Fermi level	$e_F \tilde{=} 0.7$ Rydberg	(Mattheiss 1970)
Fermi velocity	$v_F \tilde{=} 0.24 \times 10^8$ cm/sec	(Shen 1970)

then mean free path $\ell \tilde{=} 13\text{Å}$ for our 250Å thick film which had a resistance ratio $R_{300^oK}/R_{4.2^oK} \sim 5$ to 10. Hauser and Theuerer (1964) estimated the Ginzburg Landau coherence length ξ_o to be ~ 900Å in the clean limit. The effective coherence length for our film should then be $0.85\sqrt{\ell\xi_o}$ or about 92Å at 0^oK, about a factor of 9 less than 830Å inferred from this experiment.

There is also a discrepancy with the magnitude of the potential difference as predicted by the theory. In equation (3.10) we can approximate $\nabla \cdot j_s$ by j/ξ at the interface. Within the superconductor, $|\psi|^2$ is given by $n_o \ell^2/\xi^2$ (Appendix B). Hence

$$eV = \mu_p - \mu$$

$$\simeq \frac{m\xi_{\infty}^3}{4|e|\tau_{GL} n_o} \frac{1}{\ell^2} j \qquad (3.19)$$

Referring to the experimental condition in Figure 3.3

$$j = 4.5 \times 10^2 \text{amp/cm}^2 \qquad (3.20)$$

At $4.10^{o}K$, which is 20 $m^{o}K$ below T_c of the film, ξ $(4.1^{o}K)$ calculated by equation (2.5) with ξ_o = 900Å is 1320Å. The calculated V is then about 8.8×10^{-9}volt at the boundary. And since the probe is about 7.6ξ away from the boundary, the measured value is expected to be about 2×10^{-10}volt instead of which it is over two orders of magnitude lower than the experimental value of 9×10^{-8}volt.

The choice of 830Å for $\xi(0)$ also implies a Ginzburg Landau coherence length ξ_o of 6.3 μm which is far too high for a hard superconductor like tantalum. This experimental result possibly implies that further nonequilibrium effects may coexist whose characteristic length is not the coherence length but a much longer one.

3.12 Andreev Scattering and Branch Mixing

This experiment gave qualitative agreement with the predictions of the two potential concept, but it also indicated that the nonequilibrium process at the S/N interface which leads to two potentials is more complicated than that described by the time dependent Ginzburg Landau formalism. The nonequilibrium depairing and pairing processes extend over distances at least a few times further than expected.

At about the same time that Rieger et al. proposed their theory (RSM1) the important role of the individual branches (hole and electron branches, c.f. Section 2.5) of the quasiparticle excitations at a S/N boundary was realized by Pippard et al (1971). They took up the mechanism suggested by Andreev (1964) by which excitations are reflected at an S/N interface. They assumed a simple picture in

which the interface is regarded as a region where the energy gap Δ varies within a few coherence lengths ξ from zero in the normal side to its equilibrium value Δ_∞ far within the superconducting region. The gap acts as a potential step above the Fermi level by which excitations are scattered.

Consider an electric current flowing across the S/N interface. An electron-like excitation incident onto the interface will be subjected to a force field imposed by the condensate in the superconducting region. According to Andreev, as the excitation effectively interacts with a massive object (the whole Fermi sea of superconducting electrons) its total energy remains constant while its momentum changes. The electron-like excitation with momentum $k_F + \Delta k_e$ is scattered back as a hole excitation with momentum $k_F - \Delta k_h$ and $\Delta k_e \simeq \Delta k_h$ for low-lying excitations. Particle conservation is achieved by the injection of two electrons into the superconducting ground state as a Cooper pair, completing the pairing process. The same argument applies for hole-electron conversion when current direction is reversed.

Hence according to their picture, branch mixing of the quasiparticle excitations (hole electron, c.f., Section 2.5) must accompany pairing or depairing at a S/N interface. However, as was stressed by Pippard et al (1970), the elastic scattering by the spatial inhomogeneity of the gap described above affects only a small fraction ($\sim \Delta/k_B T$) of the excitations at temperatures near T_c and the majority of the excitations has $E > \Delta$ and branch crossing is through the inelastic processes. Tinkham's analysis (1972) is hence applicable. It was argued

both theoretically and experimentally that branch mixing time τ_Q is longer than the usual Ginzburg Landau relaxation time for the condensate (for Sn $\tau_Q(0) = 2 \times 10^{-10}$sec (Tinkham 1972)) and it was estimated that the characteristic length for branch mixing $\tau_Q = \sqrt{\ell v_F \tau_Q}$ is of the order of a micron, much longer than the usual coherence length of the pairs.

Although data on branch mixing properties inside superconducting tantalum are not available, the qualitative argument is general enough tnat tantalum probably follows the same trend. Hence the pairing and depairing processes extend a branch mixing characteristic length rather than a coherence length. We suspect that this might explain why the "healing length" in our experiment is much longer than expected from Rieger et al's theory. Rieger et al's suggestion of two potentials is certainly verified by our experiment. The analysis they gave for $\mu_p - \mu$ probably gives a close description for the condensate. However, quasiparticle nonequilibrium processes may go along at the same time, which may delay equilibrium and explain why the measured $\mu_p - \mu$ is higher than expected.

However, the quasiparticle density spectrum is also perturbed by the induced pairing and depairing processes. The injection of excitations or the extraction of excitation disturb the equilibrium quasiparticle Fermi distribution. It is shown in Appendix C that perturbation of the excitation number density shifts the chemical potential of the gas of electrons. In actual fact,

$$\delta\mu = \frac{A(\Delta')}{N(0)}\,\delta n \tag{3.21}$$

where δn is the deviation from the number of electron-like or hole-like excitations at equilibrium. $A(\Delta')$ is a function depending on the dimensionless parameter $\Delta' = \Delta/k_B T$ and is given in Appendix C. It converges to 2 when $T \to T_c$ and is approximately $(k_B T/2\Delta)^{1/2} \exp(\Delta/k_B T)$ at low temperatures. $N(0)$ is the density of states at the Fermi level.

The amount of excess in excitation number is controlled by the rate of injection and hence the current densities j_n and j_s, and the rate of branch mixing and hence the branch mixing time τ_Q. Normal current is shared equally between the two quasiparticle branches. As the electron-like excitations are injected by the normal current so as to produce an excess δn in population, the hole current going in the opposite direction extracts the holes that are converted from the electrons by Andreev scattering. Electron-like excitations convert with probability $1/\tau_Q$ per unit time into hole-like excitations to maintain a steady state perturbation δn per branch. The derivation given in Appendix C shows that the shift in chemical potential is given by

$$\mu_p - \mu = \frac{A(\Delta')\,\tau_Q}{2N(0)|e|}\,\nabla\cdot\vec{j}_s \tag{3.22}$$

Here both Δ and $\nabla\cdot\vec{j}_s$ vary spatially through the S/N interface region.

In order to compare with the result of Rieger et al, we can write equation (3.12) as

$$\mu_p - \mu = \frac{\tau_{GL}}{12N(0)|e|} \nabla\cdot\vec{j}_s \qquad \text{(Appendix B)} \tag{3.23}$$

Hence in both cases a positive $\nabla\cdot\vec{j}_s$ increases the difference between μ_p and μ ; they add to each other. To compare their magnitude if they coexist

$$\frac{(\mu_p-\mu)_{qp}}{(\mu_p-\mu)_{GL}} = \frac{6A(\Delta')\tau_Q}{\tau_{GL}} \tag{3.24}$$

As $\tau_Q > \tau_{GL}$ and $A(\Delta') \geq 2$, we would expect the quasiparticle mechanism to dominate.

We assume that $\nabla\cdot\vec{j}_s$ has an exponential dependence

$$\nabla\cdot\vec{j}_s(x) = \frac{j}{\lambda_Q} \exp(-\frac{x}{\lambda_Q}) \tag{3.25}$$

Hence the measured potential difference between the two probes should be

$$V(x) = \frac{A(\Delta')\tau_Q\, j}{2N(0)|e|^2\lambda_Q} \exp(-\frac{x}{\lambda_Q}) \tag{3.26}$$

As the temperature range covered in the experiment was very close to T_c , $A(\Delta') \sim 2$. As discussed in Chapter 2,

$$\tau_Q(T) = \tau_Q(0)(\frac{\Delta(0)}{\Delta(T)}) \tag{3.27}$$

$$\lambda_Q(T) = \lambda_Q(0)(\frac{\Delta(0)}{\Delta(T)})^{1/2} \tag{3.28}$$

where $$\lambda_Q(0) = (\ell\tau_Q(0)V_F))^{1/2} \tag{3.29}$$

while $$\frac{\Delta(T)}{\Delta(0)} = 1.76(1 - t)^{1/2} \tag{3.30}$$

$$t = T/T_c \tag{3.31}$$

Substituting

$$V(x) = \frac{j\,\tau_Q(0)}{(1.76)^{1/2}N(0)e^2\lambda_Q(0)(1-t)^{1/4}}$$

$$\cdot \exp\left\{-(1.76)^{1/2}(1-t)^{1/4}\frac{x}{\lambda_Q(0)}\right\} \tag{3.32}$$

This expression predicts both the magnitude and temperature dependence of the potential V measured by a probe at position X. Experimental data shown on Figure 3.6 ranged from $4.020^{\circ}K$ to $4.105^{\circ}K$ * with the mean temperature of the experimental superconducting transition $4.12^{\circ}K$ taken to be the T_c of the S region. A plot of $\log_e\{V(1-t)^{1/4}\}$ vs. $(1-t)^{1/4}$ with these data is shown in Figure 3.7 and gives a good straight line fit, reflecting a correct prediction of the temperature dependence.

The value of $\lambda_Q(0)$ can be deduced from the slope $(= -1.76^{1/2}X/\lambda_Q(0))$ and is $\sim 1900\text{Å}$ since $X \sim 1\ \mu m$. This is longer than the coherence length $\xi(0)$ $(= 92\text{Å})$ as expected. The branch mixing

---

*Below $4.020^{\circ}K$, the normal region started to go superconducting. The few data points below this temperature were hence discarded.

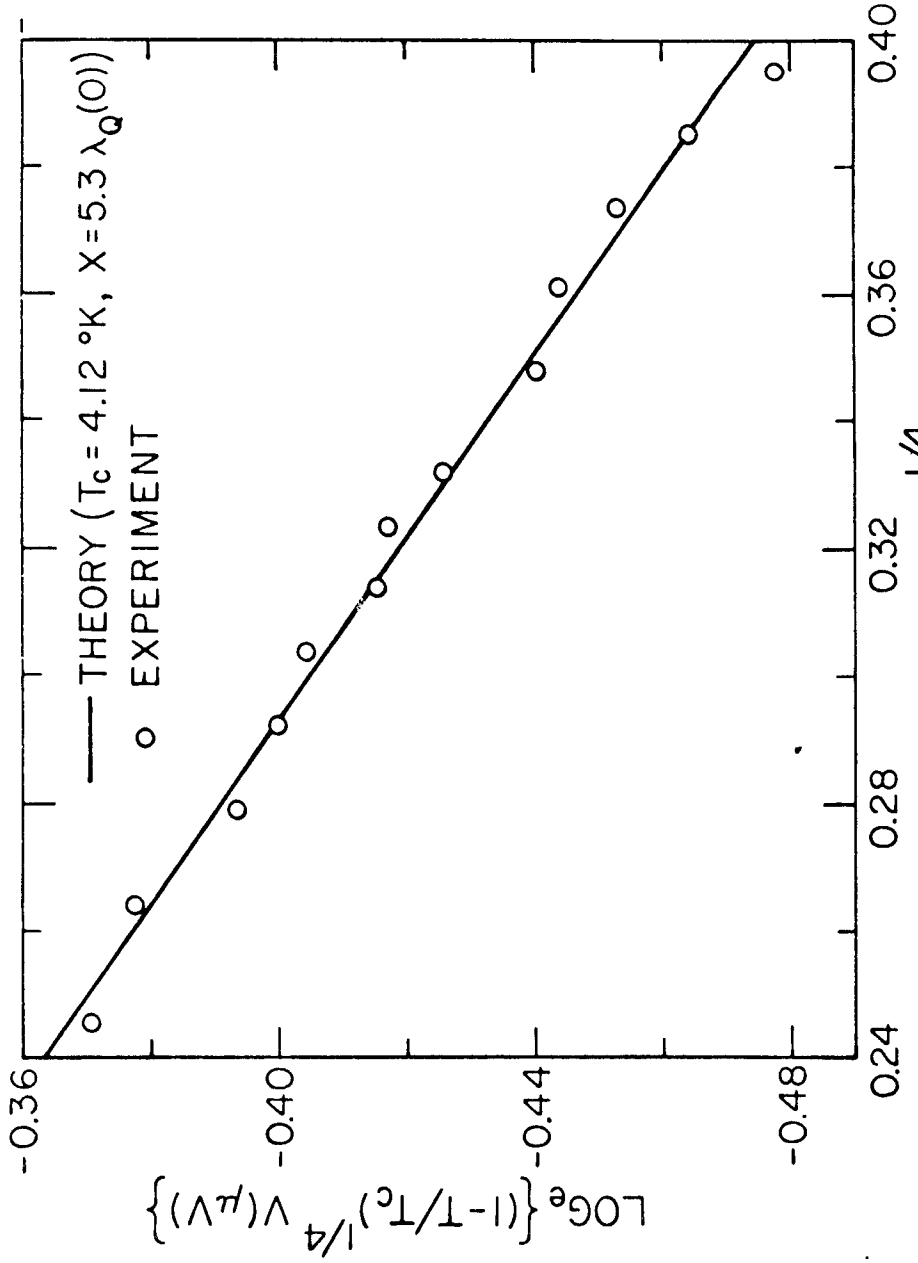

Fig. 3.7 Comparison of the experimental results with the temperature dependence in the quasiparticle nonequilibrium theory. The theoretical curve was calculated for a voltage probe at a distance $X = 5.3\ \lambda_Q(0)$ away from the S/N interface

relaxation time $\tau_Q(0)$ hence estimated by equation (3.29) is equal to 1.2×10^{-10}sec.

To compare with the prediction from the quasiparticle branch mixing theory (Tinkham 1972, also Section 2.5), we take 1.05×10^{-5}ohm-cm for the resistivity of Ta at Debye temperature θ (= 258°K) (CRC Handbook 1971), the electron-phonon scattering time τ_θ is 8.2×10^{-15}sec. Equation (2.25) gives 1.4×10^{-10}sec for $\tau_Q(0)$ which is close to our experimentally estimated value.

With our experimental values of $\tau_Q(0)$ and $\lambda_Q(0)$ and using the fact that

$$N(0) = 0.68 \times 10^{23}/\text{eV-cm}^3 \qquad \text{(Benneman and Garland 1971)}^* \qquad (3.33)$$

for Ta, equation (3.32) gives 12×10^{-8}volts for the potential difference at the probe position at 4.10°K and when $j = 4.5 \times 10^2 \text{amp/cm}^2$, as compared to 8.7×10^{-8}volts measured with the probe. Our quasiparticle interpretation gives a satisfactory agreement with the experiment.

This voltage discrepancy is outside our voltage measurement error. However, there is a possible error in our estimation of the probe position X. The probe of size $\sim$ 1 μm is placed at an average distance 1 μm away from the interface. How the probe averaged the spatial dependence is uncertain. The estimated voltage would agree

---

*Possible slight deviation from this bulk value due to short mean free paths in transition metal thin films had been suggested by Strongin (1972), but the exact amount is still unknown.

with the experimental value if X is chosen to be 0.75 μm, well within the spatial span of the voltage probe. With such correction to the value of X,

$$\lambda_Q(0) = 1400\text{Å} \tag{3.34}$$

and

$$\tau_Q(0) = 0.65 \times 10^{-10}\text{sec} \tag{3.35}$$

for our Ta thin films.

Chapter 4

NONEQUILIBRIUM SUPERCONDUCTIVITY AT S/W INTERFACES

4.1 The S/W Interface

The nonequilibrium process induced by a supernormal (S/N) interface in the current carrying dynamic state was studied and reported in the last chapter. Experiments which have been done tend to verify the concept of separate potentials for electrons and pairs as suggested by Rieger et al (RSM1). In all these measurements the normal metal N was a superconductor above its transition temperature. However, there are two mechanisms by which we may create a normal region. The first is by thermodynamic fluctuation, i.e., the metal is thermodynamically normal, as for example, a superconductor above its transition temperature. The normal regions discussed so far belong to this category. The second is by the kinetic energy of a current. This highly dynamic situation is realized when the "normal" region is a superconductor below its transition temperature but is driven normal by a current larger than its critical current. A second kind of supernormal interface can hence be created at the boundary of a strong superconductor S of higher transition temperature and a weak superconductor W of lower transition temperature by a d.c. bias current above the critical current of the weak region W so that the latter is being driven into a dynamically normal state. In this chapter evidence will be presented for a possible extension of the two-potential concept in the nonequilibrium region to such a S/W

boundary. Besides, experimental results also indicated that the boundary condition for the wavefunction at the supernormal interface is different for the case of a thermodynamically normal ($T > T_c$)(N) region from that of a dynamically normal ($T < T_c$, $I > I_c$) (W) region, leading to a different boundary potential in the two cases.

4.2 Description of the Dynamically Normal State

As a result of the coherence of the superconducting condensate, all the pairs move with the same center of mass velocity and constitute a supercurrent. However, there is a critical velocity at which the kinetic energy associated with the motion is equal to the condensation energy. Above that velocity superconductivity is no longer favorable and the conductor goes into a dissipative voltage sustaining state. The current associated with the critical velocity is defined as the critical current. This picture is described in an elegant way by the time independent Ginzburg Landau equation (de Gennes 1966). The order parameter decreases to $(2/3)^{1/2}$ of its maximum value as the critical current is approached and then goes into an unstable state at which the order parameter falls abruptly to zero.

This process pictures a sudden loss of coherence of the superconducting electrons as the superconductor goes into a voltage sustaining state. However, more careful study of the onset of resistance in narrow superconducting channels (Langer and Ambegaokar 1967) revealed that this is probably not exactly the case. It is suspected that in a voltage sustaining state, there exist states of non-zero

superflow which are metastable and there is always a finite probability for transitions to states of lower supercurrent and lower free energy. Fluctuations in the interior of the superconductor induce such transitions only to be balanced by transitions to higher current states through the acceleration of supercurrent as a consequence of the application of the voltage.

The transition to a lower supercurrent state is through the "phase slippage" process. The supercurrent at a local weak spot with a smaller $|\psi|$ (by fluctuation or otherwise) is accelerated to its critical value. Superconductivity collapses locally and the total phase difference of the wavefunction across the wire

$$\Delta\phi = \int_1^2 (\nabla\phi)d\ell \tag{4.1}$$

decreases by 2π, minimizing the phase gradient and hence the supercurrent. The special case of a short one-dimensional (i.e., no spatial variation in the other two dimensions) inhomogeneous superconducting channel with a single weak point with minimum wavefunction amplitude at which phase slippage is localized was treated extensively by Rieger, Scalapino and Mercereau (RSM2 1972)*. With a voltage V across the channel the increase in phase difference (equation (2.18)) is balanced by the rate of phase slippage,

$$\frac{2eV}{\hbar} = 2\pi\nu \tag{4.2}$$

*This is a model for the proximity effect bridge (Chapter 5).

or frequency of phase slippage

$$\nu = \frac{\hbar}{2eV} \tag{4.3}$$

The results of the analysis were to predict an asymmetric oscillating supercurrent at a finite voltage, in fact

$$I_s(t) \overset{\sim}{=} \frac{I_c}{2}\left(1+\cos\frac{2e}{\hbar}\int V dt\right) \tag{4.4}$$

In the current biased case an oscillating normal flow maintains the current conservation.

When $\langle V\rangle_{dc}$ is small $\langle I_s\rangle_{dc} \simeq I_c$. At higher d.c. voltages, $\langle I_s\rangle_{dc} \simeq \frac{I_c}{2}$.

Our understanding of S/W interface is no better than the W region itself. But phenomenologically nonequilibrium pairing or depairing is expected to behave qualitatively very similarly to an S/N interface at least in its time averaged behavior. In the few experiments to be reported below, evidences were observed that there are differences between these two kinds of supernormal interfaces with respect to the nonequilibrium behavior at the boundary.

4.3 Evidence for Two Potentials at S/W Interface

The existence of two different potentials close to a S/N interface was best illustrated by the voltage reversal experiment (§3.10). A similar experiment was performed with a S/W interface. The tantalum thin film microcircuit similar to the previous experiment is shown schematically in the inset of Figure 4.1. Two voltage leads (Set A)

were placed one at each side of the interface but more than 20 μm away. This set of probes was used to monitor the onset of resistance in the W and S regions. Experimentally it was verified that superconductivity or normality of these probes did not affect the result. This was to be expected as they were far away from the nonequilibrium region. The set B was a pair of superconducting and normal voltage probes each a micron or less wide and less than 1 μm apart which were placed on the superconducting side with the normal probe further away from the interface as in the S/N voltage reversal experiment. The thickness of the W region was controlled such that its transition temperature was slightly lower than S ($\sim .2^{o}K$) but higher than that of the normal probe. The working temperature was chosen such that both S and W were superconducting, with the critical currents of both regions relatively small but well separated in magnitude. Although a moderately large d.c. bias current had to be used, d.c. measurement for the potential difference $\mu_p - \mu$ (~ 0.1 μV) was still very difficult since the background d.c. thermoemfs of the various leads were very large (~ 1 mV). So the "dynamic resistance" dV/dI rather than the actual voltage was measured. This was done by adding a small (~ 1 μA) a.c. modulation current at 350c/s to the d.c. bias current through the interface. The signal voltage at this frequency and phase was detected with a PAR HR-8 lock in amplifier with about 1c/s bandwidth.

Curve A, Figure 4.1, taken with probes A, shows the resistive transition of the W region at critical current I_{CW}, and that of the S region at critical current I_{CS}. Curve B taken with probes B

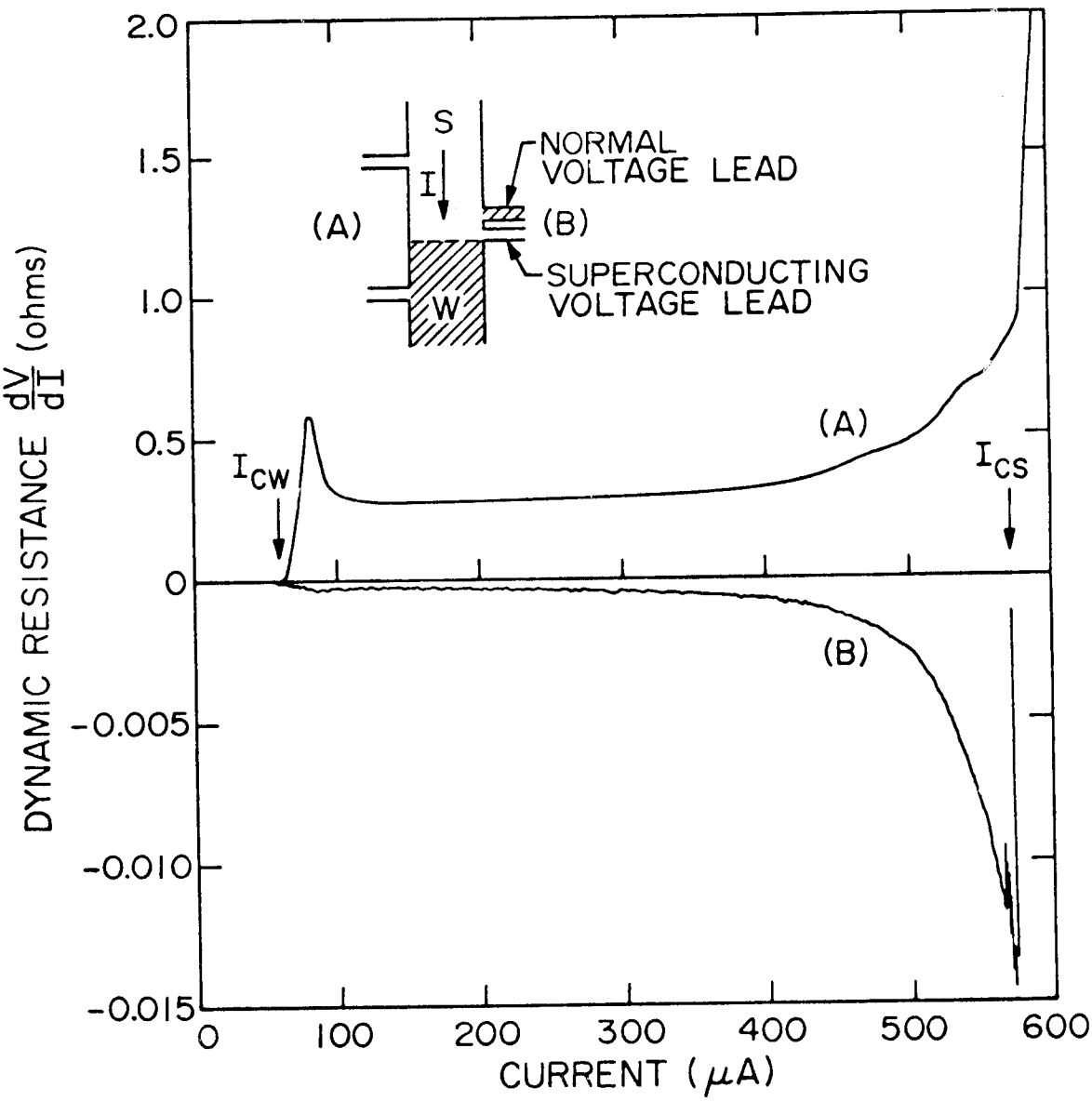

Fig. 4.1 Dynamic resistance dV/dI measured as a function of d.c. bias current. Curve A measured with probes A shows the transition of the region W at critical current I_{CW} and that of the region S at I_{CS}. Curve B is the derivative of the potential difference $(\mu_p - \mu)e^{-1}$ with respect to current.

indicates that a voltage in the reversed direction with respect to the ohmic behavior appeared across the normal superconducting leads as in the case of the S/N interface. The area under the curve gives the actual potential difference. The voltage was linear with current as in the case of the S/N interface, as indicated by the fairly constant dV/dI at the start, but seems to be proportional to $(I - I_{CW})$ rather than I. This phenomenon persisted until the critical current I_{CS} of the strong side was gradually approached, at which time the reverse voltage rose rapidly to about 0.7 μV and then switched polarity back to the normal resistive potential drop.

Thus in this situation the quasiparticle potential probed by the normal voltage probe was also found to be less than the pair potential; probably the result of a nonequilibrium depairing process in the weak superconductor which extends to a short distance into the strong superconductor. Even though the quasiparticles probed were farther away from the S/W interface, they nevertheless had a lower potential than the pairs near the boundary, as in the case of the S/N interface discussed in Chapter 3. The two potential concept thus seems to apply in the S/W situation in a similar manner as to a S/N interface.

4.4 Comparison Between the S/N and the S/W Interfaces

A significant difference of the S/W result from the S/N case is that the potential difference $\mu_p - \mu$ was proportional to $(I - I_{CW})$ when $I < I_{CS}$. This initial proportionality with $(I - I_{CW})$ instead of I allows a smooth transition with no discontinuous jump in potential

difference from the dynamic state with no depairing ($j < j_{CW}$) to the dynamic state with depairing ($j > j_{CW}$) . This means when the critical current on the W side is exceeded, the potential difference $\mu_p - \mu$ resulting from the depairing process is smaller by an amount proportional to $\nabla \cdot \vec{j}_{CW}$ than it would be if W were thermodynamically normal.

Another significant difference of the S/W result from the S/N case was the rapid increase in the potential difference $\mu_p - \mu$ as I_{CS} was approached. This rise was not observed in the case of the S/N boundary (Figure 3.5). This, together with the initial proportionality with $I - I_{CW}$ instead of I , indicated that the boundary condition for the wavefunction at the S/N interface is different for the case of a thermodynamically normal ($T > T_c$) N region from that of a dynamically normal ($T < T_c$, $I > I_c$) W region, leading to different potentials for these two cases.

4.5 Evidence for Boundary Potential at a S/W Interface

The possibility of a boundary potential as a result of non-equilibrium pairing or depairing at the S/N interface was suggested and experimentally observed by Pippard et al (1971). They considered the contribution to resistivity as a result of Andreev scattering at the boundary. This boundary potential is ohmic in character and acts as an additional resistance to the conducting strip.

A non-ohmic boundary potential which is practically independent of current density was observed near a S/W interface in this highly dynamic situation. This showed up when we examined the current voltage

characteristics of S/W/S structures where the W region ranged from 2 to a few tens of microns in length. Such circuits, as shown in the inset of Figure 4.2, were again fabricated on a tantalum thin film substrate using the standard photoetch and selective anodization technique.

There were two sets of probes. Probes A measured the potential between superconductors and hence included the boundary potentials at the two S/W interfaces besides the voltage across the W region. Probes B measured only the potential drop across a section of W . When $T > T_{CW}$ so that W is thermodynamically normal, this structure (now a S/N/S circuit) gives a linear I-V curve ("a" in Figure 4.2) indicating a normal ohmic behavior. When the temperature is lowered, W becomes superconducting and the I-V curves change as shown in the figure where $T_a > T_b > T_c > T_d > T_e$. Data from probes B (Figure 4.2B) show that at high current the resistance of the section of W returned to the same value as in the normal state. However, data from probes A (which include the effects of the boundaries) indicated that although the dynamic resistance dV/dI approached the normal value, the voltage was discretely less than that at the normal state. This difference is a potential developed across the two S/W interfaces and decreased only very slowly with increasing total current and still existed up to potentials of a few tens of millivolts across the S/W/S circuit, off the scale on Figure 4.2. By positioning the voltage probes along the S/W strip, it was observed that this d.c. boundary potential was developed on the W side of the interface and was localized within a micron from the interface. Superconductivity

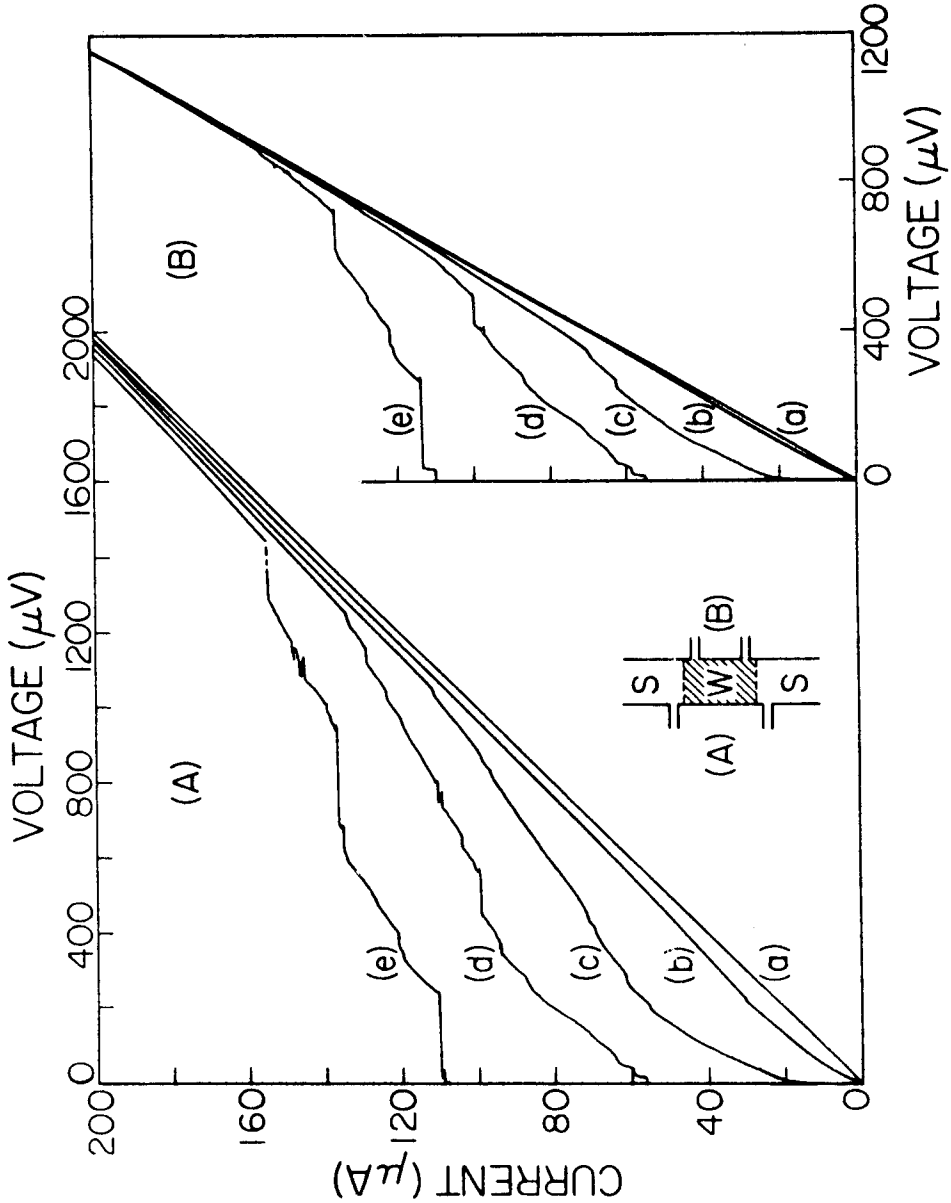

Fig. 4.2 I-V characteristics of a S/W/S structure. The sets of curves (A) and (B) were measured with probes A and B respectively. Curves (a) were the characteristics when W was normal and (b),(c),(d),(e) were those when W was superconducting and they are in order of decreasing temperature.

or normality of the voltage probe did not give any noticeably different results.

To determine the temperature dependence of the boundary potential the linear high voltage part of the I-V curves were extrapolated back to $I = 0$ and the voltage intercept was taken to be the difference in boundary potential ΔV_b, which develop in S/W relative to S/N. This boundary potential began to develop near T_{CW} even at temperatures where fluctuations prevented the zero voltage critical current as shown in curve "b", Figure 4.2. These experimental results lead us to ascribe the voltage drop ΔV_b to a difference in boundary potential between the S/W and S/N situation as

$$\Delta V_b = V_b(S/N) - V_b(S/W) \tag{4.15}$$

The temperature dependence of ΔV_b for a single S/W interface near T_{CW} is exponential in $\beta(T_{CW} - T)$, where β is somewhat structure dependent. Figure 4.3 shows a typical result, where β is approximately $(0.06^{o}K)^{-1}$.

4.6 Possible Physical Processes at the S/W Interface

Both the two-potential $(\mu_p - \mu)$ measurement and the existence of the boundary potential ΔV_b imply different boundary conditions for S/N and S/W interfaces. The $\mu_p - \mu$ experiment indicated that the two-potential concept applies in the S/W situation but with modifications, in particular, $\mu_p - \mu$ is proportional to $(I - I_{CW})$ instead of I.

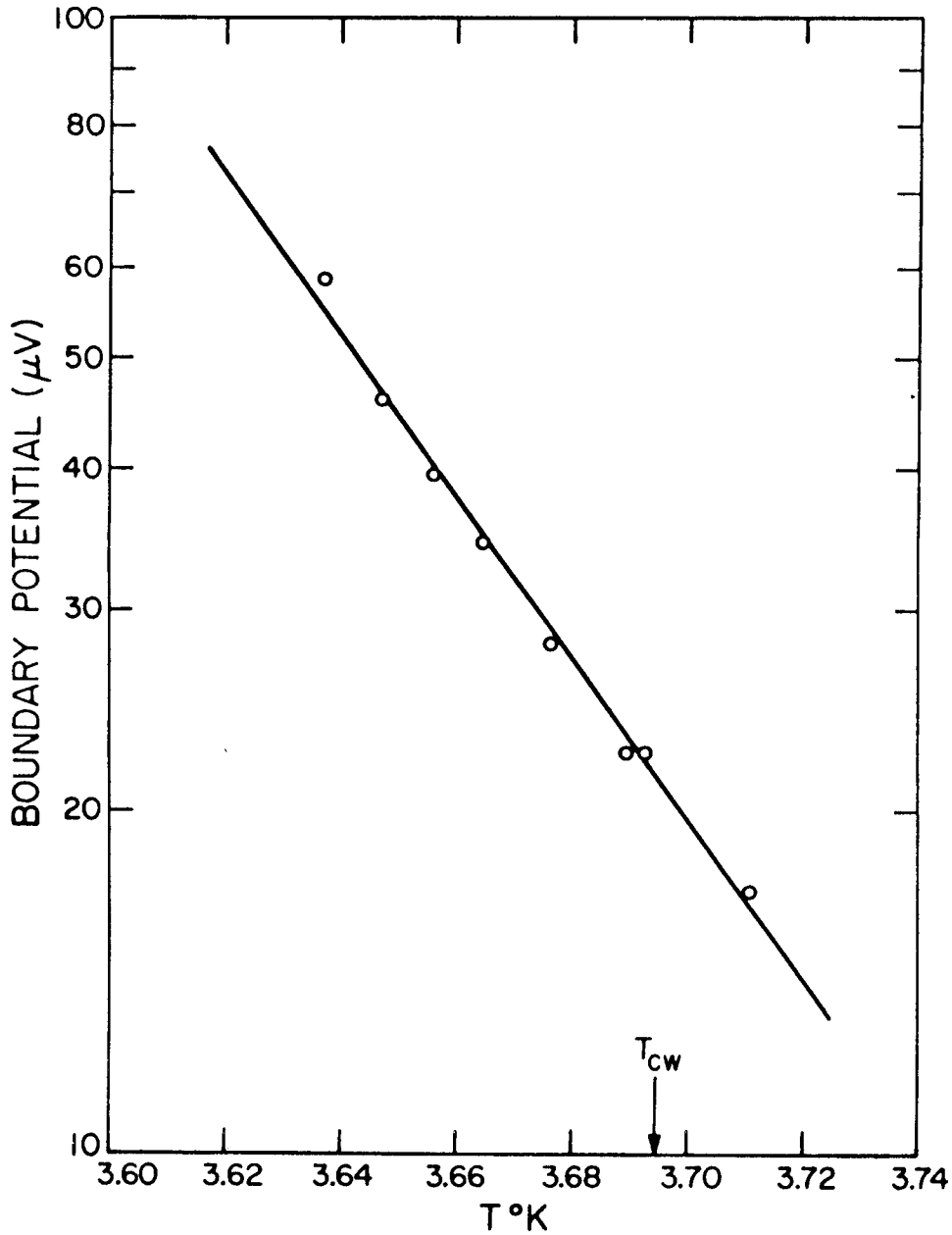

Fig. 4.3 Temperature dependence of the boundary potential ΔV_b across a S/W interface. T_{CW} is the transition temperature of the W region.

As current passes through a supernormal interface, the non-equilibrium depairing and pairing processes induce a splitting between the potentials μ and μ_p and

$$\mu_p - \mu \propto \nabla \cdot \vec{j}_s \tag{4.16}$$

Deep inside the superconducting region there is no depairing and hence $\nabla \cdot \vec{j}_s = 0$, $\mu_p = \mu$. Deep inside the normal region depairing is essentially complete, $\vec{j}_s$ and hence $\nabla \cdot \vec{j}_s$ are both zero; so again, $\mu_p = \mu$. However, μ has to satisfy the boundary condition that

$$\vec{j} = - \frac{\sigma}{e} \nabla \mu \tag{4.17}$$

which implies $\nabla \mu_p \neq 0$ in the normal region.

At an S/N interface, superconductivity extends only a very short distance into the N region before thermal fluctuation upsets the pairing interaction and μ_p is not defined further into the normal region. Hence the pair potential μ_p can stay constant ($\nabla \mu_p = 0$) in the region where it is defined so that there is no acceleration of the supercurrent and hence no time dependent phase slip. However, this is no longer true for a S/W interface since there is pairing interaction inside the W region. μ_p cannot stay spatially constant throughout the entire depairing region as discussed above and the acceleration of any remaining supercurrent must become proportional to the gradient of μ_p deep in the W region.

When j_{CW} is exceeded, there will thus be phase slip in the W region instead of a steady state solution inside the N region of a S/N

interface. We will use this phase slippage picture and the quasiparticle nonequilibrium process (Section 3.12) to explain why $\mu_p - \mu$ is proportional to $j - j_{CS}$ at S/W interfaces.

At the S/W interface, the proximity effect enhances pairing interaction in the W material above the intrinsic value so that the amplitude of the wavefunction $|\psi|$ is larger at the interface and tapers off to the intrinsic value $|\psi_o|$ in W in about the quasiparticle diffusion length λ_Q as suggested by the S/N experiment. The wavefunction near the boundary thus resembles closely that of the short phase slippage region considered by Rieger et al (RSM2 1972). As discussed above, the pairs at the W side of the interface are being accelerated. When j_{CW} is exceeded phase slippage is most likely to happen where $|\psi|$ is small, i.e., after $|\psi|$ has been tapered down to $|\psi_o|$. However phase slippage is no longer always at the same spot and hence smears out the frequency spectrum of the oscillating supercurrent. Attempts to detect coherent oscillation at the S/W interface gave negative results*. But otherwise the RSM2 analysis for the time averaged behavior is largely appropriate.

For a typical S/W/S circuit with a 20 μm long W region and less than 2 mV across it, the voltage governing the phase slippage rate

---

*To investigate this point, an external rf radiation ranging from 30 MHz to 2 GHz was applied to the structure while the voltage across the structure was scanned. It was expected that this external radiation would modulate any oscillation within the structure if coherent phase slippage existed. This modulation should show up on the V-I characteristics as constant voltage steps such as induced in proximity effect bridges or Josephson junctions. RF response at both S/N and S/W interfaces in long S/W/S ($W > 10\,\mu m$) structures was examined by measurement of voltage V_b across the boundary but aside from suppression of critical current by the rf radiation, no rf response was seen.

is less than approximately

$$\frac{\lambda_Q}{20\ \mu m} \times 2\ mV$$

and by taking $\lambda_Q \sim 0.1\ \mu m$, this voltage is $\sim 10\ \mu V$ which gives ~ 5 GHz or a time scale of $\sim 2 \times 10^{-10}$ sec. This time scale is generally longer than $\tau_Q(0)$ estimated from the S/N experiment and hence the nonequilibrium quasiparticle process applied in the S/N case should still contribute to the potential difference $\mu_p - \mu$ (equation (3.22)) especially at lower voltages. In the current biased case $\vec{j}$ is independent of position, i.e.,

$$\nabla \cdot \vec{j} = 0 \tag{4.18}$$

and since

$$\vec{j} = \vec{j}_s + \vec{j}_n \tag{4.19}$$

$$\nabla \cdot \vec{j}_s = - \nabla \cdot \vec{j}_n \tag{4.20}$$

Combining equations (3.22) and (4.20) within each phase slip cycle,

$$\mu_p - \mu = - \frac{A(\Delta')\tau_Q}{2|e|N(0)} \nabla \cdot \vec{j}_n \tag{4.21}$$

$$\simeq - \frac{\tau_Q}{|e|N(0)} \nabla \cdot \vec{j}_n \quad \text{as} \quad A(\Delta') \simeq 2 \tag{4.22}$$

As discussed in Section 4.2, the time average over one phase slip cycle

$$\langle j_n \rangle \simeq j - j_{CW} \quad \text{when} \quad j \gtrsim j_{CW} \tag{4.23}$$

Therefore

$$\langle \mu_p - \mu \rangle \simeq - \frac{\tau_Q}{|e|N(0)} \frac{j - j_{CW}}{\lambda_Q} \tag{4.24}$$

This explains the initial proportionality of the potential difference $\mu_p-\mu$ with $I - I_{CW}$. However, as current goes higher, the potential difference gradually increases more rapidly than linearly (i.e., instead of staying constant, $d(\mu_p-\mu)/dI$ increases as shown in Fig. 4.1) and rises rapidly as I_{CS} is approached. To explain this we notice that as voltage goes higher the oscillation is more sinusoidal (Section 4.2) and

$$\langle j_s \rangle \sim j_{CW}/2 \tag{4.25}$$

So

$$\langle \mu_p-\mu \rangle \simeq -\frac{\tau_Q}{|e|N(0)\lambda_Q}\left(j - \frac{j_{CW}}{2}\right) \tag{4.26}$$

instead of $\propto (j - j_{CW})$. This can account for part of the gradual increase in $d(\mu_p-\mu)/dI$ as current increases. Also, since measurement was made in the S side and $\tau_Q \sim (\frac{\Delta(0)}{\Delta})$, $\frac{\tau_Q}{\lambda_Q} \sim (\frac{\Delta(0)}{\Delta})^{1/2}$, at high current densities, the effective gap Δ becomes smaller, and a larger τ_Q/λ_Q contributes to a larger $d(\mu_p-\mu)/dI$. When I_{CS} is approached τ_Q may increase to such an extent that the phase slippage rate overtakes $1/\tau_Q$ and renders the above description invalid. This phenomenon was not observed in S/N interfaces where there is no phase slippage.

In addition, the two-potential description has to be modified for the S/W interface, to account for the difference in boundary potential ΔV_b between the S/N and S/W situations. Experimentally this difference starts to develop well above T_{CW} (ΔV_b is exponential in $(T_{CW} - T)$) and probably reflects the gradual spread of superconducting coherence into the weak region W only to be inhibited by thermal

fluctuations. This boundary potential difference ΔV_b implies that when a current I flows through the interface, the induced pairing interaction minimizes dissipation by the amount $I \cdot \Delta V_b$.

That there is a supercurrent contribution even at temperatures above T_{CW} is further supported by an experimental fact that for short S/W/S circuits (proximity effect bridges with $W < 1$ μm , c.f. Chapter 5)--so short that the two-proximity effect induced wavefunctions at the two S/W interfaces overlap--there is an induced critical current which is exponential in T with a comparable coefficient β (Section 4.5). Both of these are phenomena associated with a dynamic fluctuating superconducting state at a current-carrying S/W interface.

From the temperature dependence of ΔV_b the following analysis gives some idea of the temperature variation of the boundary condition at the interface. When $T >> T_{CW}$ proximity extends only a small distance into the W region and we may approximate the situation by writing

$$\vec{j} = - \frac{\sigma}{e} \nabla \tilde{\mu} \tag{4.27}$$

When T is close to T_{CW} , the superflow accounts for part of the current and the above equation should be replaced by

$$\vec{j}_n = - \frac{\sigma}{e} \nabla \mu \tag{4.28}$$

$$\nabla(\tilde{\mu}-\mu) = - \frac{e}{\sigma}(\vec{j} - \vec{j}_n)$$

$$= - \frac{e}{\sigma} \vec{j}_s \tag{4.29}$$

Hence the variation of boundary potential with temperature near T_{CW} can be written in terms of the supercurrent induced near T_{CW} as:

$$\Delta V_b = -\frac{1}{e}\int_0^\infty \nabla(\tilde{\mu}-\mu)\, dx = \frac{1}{\sigma}\int_0^\infty j_s(x)\, dx \qquad (4.30)$$

At large current densities we assume that the voltage is so high that the phase slippage cycle is faster than the recovery time of the superconducting state (τ_{GL} of the W region) and coherence is destroyed except close to the interface where proximity effect maintains the pairing interaction. We may then assume an exponential decay of j_s :

$$j_s(x) = j_{so}(T)\, e^{-x/\lambda(T)}$$

on the W side of the interface similar to the exponential decay of $|\psi|^2$. Hence

$$\Delta V_b = \frac{j_{so}(T)}{\sigma}\int_0^\infty e^{-x/\lambda(T)}\, dx$$

$$= \frac{j_{so}(T)\lambda(T)}{\sigma}$$

At the high current density limit we expect $j_{so}(T)$ is the critical current density ($j_{co}(T)$) at the interface (x=0) which is proportional to the magnitude of the wavefunction $|\psi|^2$. The S/N experiment suggested that $\lambda(T)$ is probably the branch mixing characteristic length which has a slow variation with temperature in this temperature range (equations (3.28) and (3.30)). Thus the exponential behavior of our experimental measurements of ΔV_b can be interpreted as an

exponential temperature dependence for j_{co} and hence for $|\psi|^2$ induced on the W side by the proximity effect at the interface.

4.7 Possible Relationship with Other Experiments

Many experiments investigating fluctuation induced resistive transition of narrow superconducting channels had electrical arrangements very similar to the present experiment. Superconducting voltage and current leads used create S/W interfaces. The boundary potentials reported above may be important in the interpretation of these data. Quite a few investigators have also reported "voltage steps" (i.e., constant current voltage jumps) in transition curves and voltage-current characteristics of current-carrying superconducting thin wires and whiskers (Meyer et al 1972). We have also observed "voltage steps" in the V-I characteristics of the S/W/S structure (Fig. 4.2). We suspected that this behavior might be associated with inhomogeneities in T_c and the resulting S/N and S/W interfaces. This situation has been simulated with a series of weakened regions with different transition temperatures and hence different critical currents on a tantalum thin film strip as shown in the inset of Fig. 4.4. The voltage jumps agreed well with the resistance of these different regions. Transition curves of these structures when d.c. current biased also gave voltage steps similar to those reported as temperature went through the transition temperature of different regions. Attempts to see any Josephson type radiofrequency response by modulating with external rf also gave negative results. Although inhomogeneities in T_c can produce voltage step effects such as those

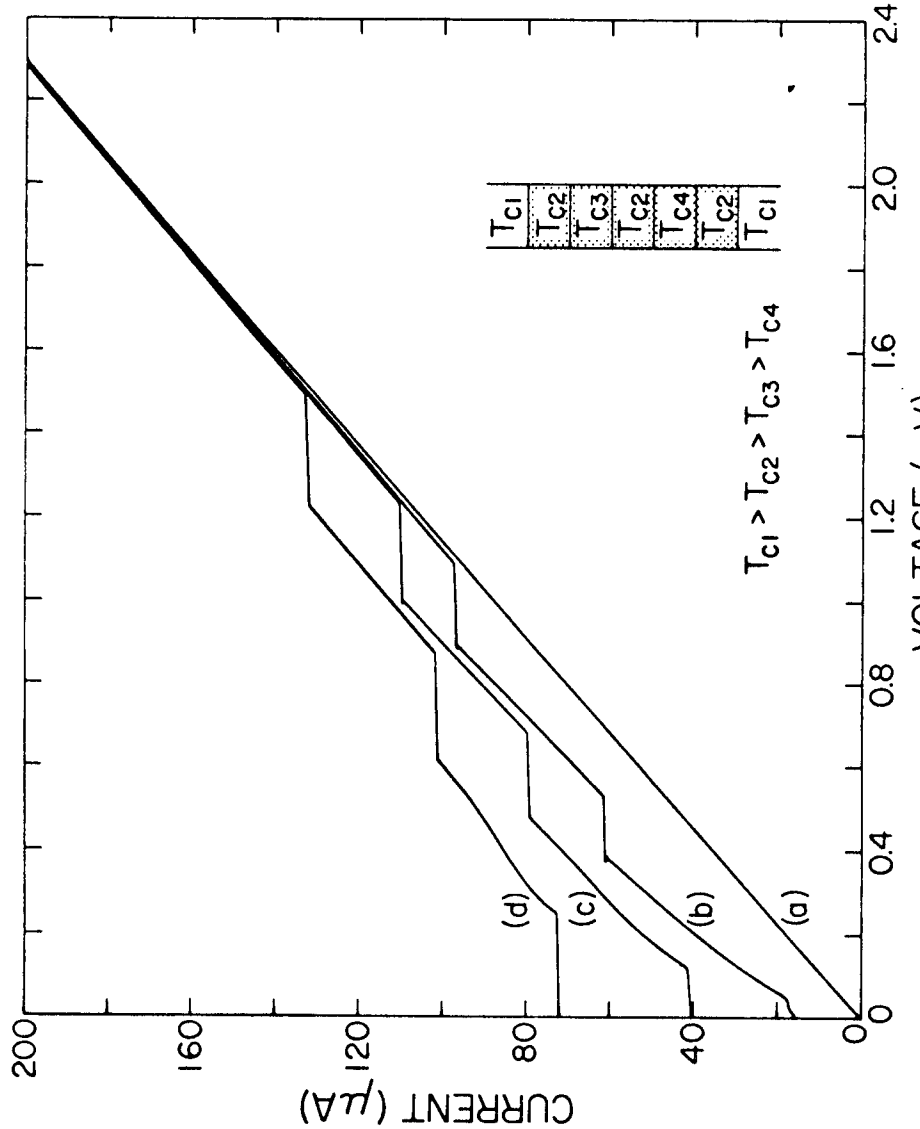

Fig. 4.4 I-V characteristics of an inhomogeneous superconducting strip as shown in the inset. Curve (a) was taken when regions 2,3,4 were all normal. The others were taken when all were superconducting. Curves a,b,c,d are in order of decreasing temperature.

reported by Meyer et al, our experiments with inhomogeneous thin film certainly do not rule out more fundamental processes such as suggested, e.g., by Fink (1973) and Tinkham (1973) which might be occurring in the more perfect superconducting whiskers.

Chapter 5

TIME DEPENDENT SUPERCONDUCTIVITY IN PROXIMITY EFFECT BRIDGES

5.1 The Proximity Effect Bridge and Time Dependent Superconductivity

The previous experiments have revealed many interesting features of the time independent (d.c.) behavior of nonequilibrium pairing and depairing processes that occur at a single supernormal or superweak interfacial region. However, it has been found (Kirschman 1972) that when two interfaces are brought very close together, in the order of one micron apart, the intervening region acts as a link between the two superconductors, establishing phase coupling between the order parameters or macroscopic wavefunctions of the two strong superconductors. Such quantum phase coherence and interference result in Josephson-like phenomena (Josephson 1962,1965) in both the zero voltage and finite voltage sustaining state. The zero voltage critical current of this "proximity effect bridge" can be modulated periodically with an external magnetic field applied perpendicularly to the direction of current flow, similar to the d.c. Josephson effect. When current is above the critical current of the bridge so that there is a finite voltage V between the two strong superconductors, the supercurrent oscillates with a frequency given by the Josephson voltage frequency relationship,

$$\nu = 2eV/h \tag{5.1}$$

similar to the a.c. Josephson phenomenon.

The best understood example of two strong superconductors weakly coupled with each other is the Josephson tunneling junction.

The two superconductors are connected by a very thin layer (< 20Å) of oxide such that Cooper pairs can tunnel through this barrier. The supercurrent density j_J is proportional to the sine of the phase difference $\phi_1 - \phi_2$ between the two macroscopic wave functions:

$$j_J = j_o \sin(\phi_1 - \phi_2) \tag{5.2}$$

It is this equation together with the Josephson relation (equation (5.1)) that results in the d.c. and a.c. Josephson effects. However, neither the tunneling barrier nor equation (5.2) are vital for Josephson-like phenomena. In actual fact the proximity effect bridge belongs to a general category of structures consisting of a pair of superconductors weakly coupled to each other through a superconducting weak link and in general show Josephson-like phenomena. As for example, the Dayem bridge has a very narrow constriction (Anderson and Dayem 1964) $\sim$ 1/2 μm coupling between two superconducting films or a point contact (Zimmerman and Silver 1964,1966) which is a superconducting sharp point pressed against another piece of superconductor. A common feature of all these metallic superconducting weak link structures is a small inhomogeneous region where the magnitude of the superconducting order parameter is relatively small when compared to the two adjoining superconductors. In the voltage sustaining state, contrary to equilibrium superconductivity, there is an electric field inside this weak link region with a time varying superflow. The weak link region is in a time dependent nonequilibrium superconducting state.

In this chapter a brief review of previous results on fabrication, electrical characteristics, a.c. and d.c. Josephson effects will

be given. The major emphasis will be on a new interpretation of the quantum interference in these bridges and experiments to test these ideas.

5.2 Bridge Fabrication

The proximity effect bridge in the thin film form consists of a short (in the current direction) inhomogeneous region which defines the bridge. This inhomogeneous region should have an intrinsic transition temperature T_{CW} lower than that of the adjoining film. T_{CW} is usually well separated ($\sim 1^{\circ}K$) from the transition temperature T_{CS} of the main film. Such inhomogeneity may be achieved through material inhomogeneity in both soft superconductor films and hard superconductor films. Techniques used through the experiments are to be described below. Detailed and more general discussion is contained in the paper by Notarys and Mercereau (1973).

The soft superconductor system used in the course of the experiment was the Sn/Au system with the Sn film as the strong superconductor. The inhomogeneous region is a narrow (~ 1 μm) line of SnAu alloy perpendicular to the current direction. The procedure is to evaporate a fine Au line onto a glass or sapphire substrate then follow by evaporation of a Sn film on top. Sn alloys with a Au line forming the bridge region. The intrinsic transition temperature T_{CW} is controlled by the ratio of the thicknesses of Sn and Au. The Sn film, usually 1000Å thick, has a transition temperature T_{C1} of about $3.8^{\circ}K$. The most commonly used ratio for Sn/Au is 1000Å/250Å with $T_{CN} \sim 2.5^{\circ}K$ and a resistance of about 0.5 ohm/square. With other ratios, T_{CN} can vary

from $3.6^{\circ}K$ to $1.3^{\circ}K$. The length of the line ranged from $\sim$ 0.3 μm to 100 μm.

Before evaporation the glass or sapphire substrate is thoroughly degreased and cleaned with chromerge*. To form the mask for the gold line, a thin (few μm) layer of collodian was spun on the substrate. The mask for the Au line is formed by drawing the edge of a sharp razor blade across the collodian. Then the desired thickness of Au is evaporated. The collodian film is subsequently dissolved away leaving a narrow strip of gold film along the scratched line. It was found that sapphire gives better adherence to the Au line.

After another chromerge cleaning cycle, Sn is evaporated. All evaporations were done at a pressure of about 2×10^{-5} torr at room temperature with a heated molybdenum boat. A Sloan quartz crystal thickness monitor was used to control electronically the source shutter for accurate deposition. The final step is to cut the weakened section to the desired width which ranged from a few μm to 100 μm , allowing the resistance of the bridge to vary from ohms to milliohms. This was done either by scratching with a tungsten point mounted on a micromanipulator under a microscope, or using standard photoresist masking technique (Section 3.7) followed by chemical etching.

These Sn/Au structures are in general easy to fabricate and usually give pronounced quantum coherence effects. However, their properties (e.g., T_{CW} and resistance) gradually degrade with time,

---

*Chromerge is a solution of potassium dichromate in concentrated sulfuric acid.

presumably due to atomic diffusion of gold. Probably, for the same reason, when examined under a scanning electron microscope, it was observed that the weak link region is not well defined and homogeneous.

A hard superconductor system has been developed to achieve a better reproducibility and control. It is based on the multilayer superconducting substrate originated by Notarys and Mercereau (1973). Layers of Nb, Ta, W, Zr, etc. of hard superconducting materials of various thicknesses are evaporated on a sapphire wafer. The local intrinsic transition temperature depends on the proximity effect in the direction normal to the plane of film which in turn is a function of that particular local combination of material. Figure 5.1 shows the principle used in the fabrication of these bridges. t_s and t_n are the thicknesses of superconducting films of higher T_c and lower T_c respectively. This combination has a transition temperature T_{CS}. At the narrow region at which the bridge is desired, part of the film with higher T_C is removed so that it has a lower t_s'/t_n' ratio and results in a lower transition temperature T_{CW}.

To prepare the bridges 200Å Ta was first evaporated onto a heated (400°C) clean sapphire substrate, then followed by deposition of 100Å of Nb. Evaporation was done in an ultrahigh vacuum with pre-evaporation pressure $\sim 10^{-8}$-10^{-9}torr. A discrete change in anodization properties of the subsequent multilayered film indicated that alloying did not take place to an appreciable extent. Then the standard photoresist masking technique and controlled anodization described in Section 3.7 were used to sculpture the circuit and to fabricate the

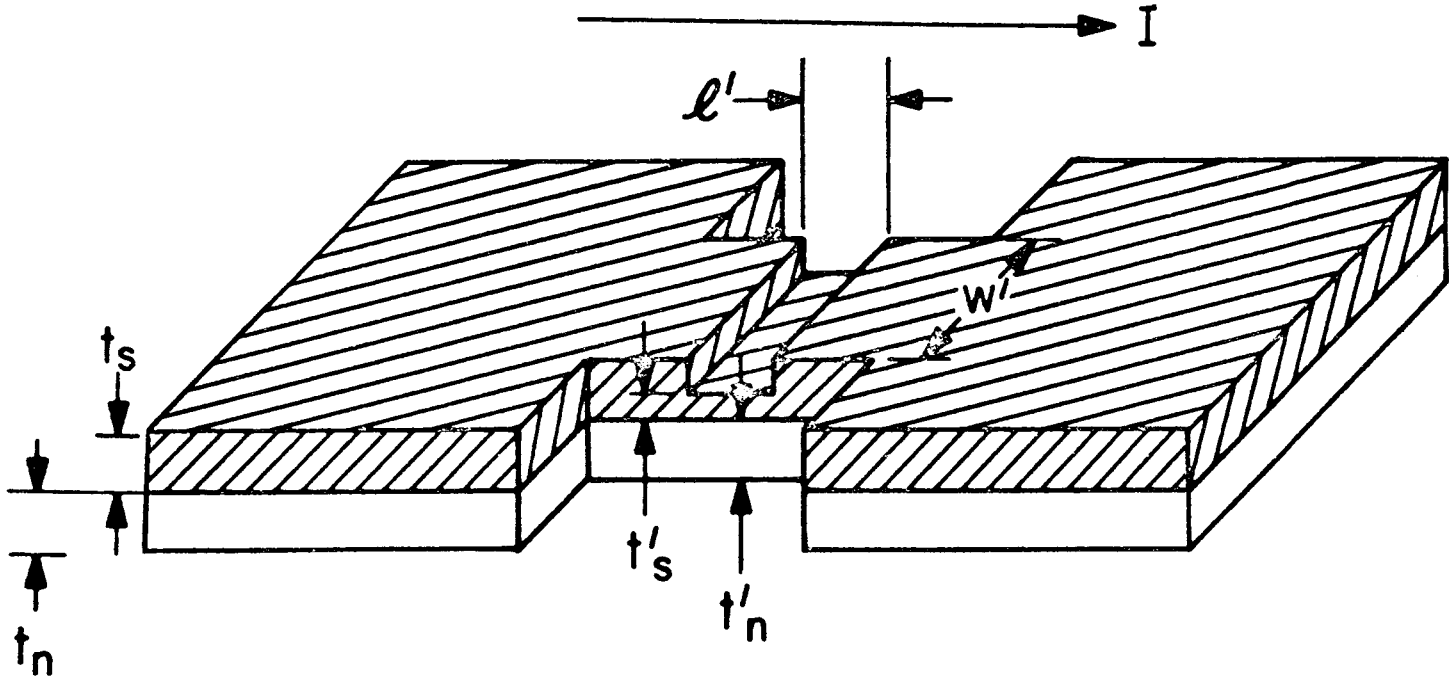

Fig. 5.1 Artist's representation of proximity effect bridge constructed in layered films. t_s and t_n are the thicknesses of superconducting films of higher T_c and lower T_c respectively. The bridge region has length ℓ' along the current I direction, width W' and local thickness ratio t'_s/t'_n.

bridge. The present limitation of the length of the bridge is about 0.3 μm which is also the resolution limit of our optical system. Press-on indium contacts were used for electrical connections.

T_{CS} of the main film was about $7^{o}K$ while the T_{CW} of the bridge was usually about $4^{o}K$ or lower for experimental convenience. Josephson-like effects were observed for lengths varying from 0.5 μm to about 5 μm . Widths ranged from a few μm to 100 μm and weak link resistance ohms to tens of milliohms. This technique gives a well defined and homogeneous weak link region which makes many control experiments possible. Its reproducibility and long lifetime (years) are additional good features.

5.3 General Electrical Characteristics

At temperature T lower than T_{CS} of the film, but above T_{CW} of the bridge, the bridge can already sustain a zero voltage critical current I_c . It is believed that this critical current I_c is a result of the overlap of the two-proximity effect induced wave functions associated with the two supernormal interfaces bounding the bridge region. This interpretation is supported by the following experiment. Bridges of various lengths (0.5 μm to 5 μm) were fabricated on the same Nb/Ta substrate. Anodization was done with the same voltage pulse to ensure the same thickness and thus the same intrinsic transition temperature T_{CW} . The critical current I_c of the bridges for a fixed temperature T ($< T_{CS}$) was observed to increase steadily with decreasing length suggesting that the proximity effect from the adjoining stronger superconducting material decreases with distance as

it penetrates into the bridge region. The maximum overlap at the center of the bridge of the two-proximity effect induced wave function which determines the critical current hence decreases with increase in length . For long bridges (> 2 μm) the overlap is small and I_c is small when $T > T_{CW}$. When $T < T_{CW}$ the intrinsic superconductivity of the bridge region comes into play and the critical current I_c is proportional to $(T_{CW} - T)^{3/2}$ as expected from the Ginzburg-Landau theory for a one-dimensional system (Section 4.2). For short bridges this dependence holds at very low temperature but is exponential in $T_{CW} - T$ when $T > T_{CW}$ which was anticipated from an analysis of S/N/S structures (Bardeen and Johnson 1972). When $T < T_{CW}$ the intrinsic superconductivity of the bridge also comes into play. However, Josephson-like properties still persist.

When the critical current is exceeded, the bridge goes into a voltage sustaining state. With a rapid rise in voltage, the bridge approaches a constant dynamic resistance dV/dI approximately the same as that when the bridge is thermodynamically normal ($T >> T_{CW}$). However, the d.c. current-voltage characteristic fails to return to the ohmic characteristic for the thermodynamically normal state. For the same voltage the nonlinear characteristic shows an "excess current" over the ohmic one. This "excess current" is believed to be partly attributable to the boundary potential described in Chapter 4, and partly to a superflow which is responsible for the Josephson-like phenomena. It was shown by Kirschman, Notarys and Mercereau (1971) that for their Sn/Au proximity effect bridges the following empirical relation for the supercurrent held:

$$I_s = \frac{I_c}{2} [1 + \cos (\phi_1 - \phi_2)] \quad , \tag{5.3}$$

$$\phi_1 - \phi_2 = \frac{2e}{\hbar} \int V \, dt \tag{5.4}$$

and the contribution of the superflow to the excess current was hence $\simeq I_c/2$.

As the critical current goes up, the bridge starts to show hysteresis. When the critical current is exceeded, the bridge rapidly switches to the constant dynamic resistance region. On the return path, the bridge stays on the resistive state and switches back to zero voltage state at a much lower current. The exact mechanism of the hysteresis is still unknown.*

Self-heating has been suggested as a possible explanation for these effects in some situations (Shocpol, Beasley and Tinkham 1973). However, for our circuits no abrupt change in characteristics has been observed as the helium bath temperature went through the λ-point at which there is an abrupt increase in heat conductivity. Also, it has been observed that hysteresis could be induced by the application of

---

*When the I-V characteristics were traced with a d.c. voltage source instead of a high impedance current source, the hysteresis was replaced by an unstable negative dynamic resistance region bound by the two current limits of the hysteresis loop. The experiment was done by shunting the bridge with a resistance wire whose resistance was at least an order of magnitude below that of the bridge. By d.c. biasing the bridge in the negative resistance region, the circuit had been made to oscillate in the megahertz range. Frequency was tunable through at least a factor of two by changing the bias point.

high frequency microwave radiation. The radiation sharpened the resistive transition, that is, increased the initial dynamic resistance, and induced hysteresis at high microwave power. For frequencies less than 1 GHz, such effects were not observed (Palmer 1973). Consequently we believe that classical heating effects do not play a significant role in these bridges and that the hysteresis may be related to the intrinsic noise of the bridge similar to the Dayem-Wyatt effect to be discussed later.

5.4 The d.c. Josephson Effect

When a magnetic field is applied normal to the film, the critical current shows a periodic dependence with the field strength. This is very similar to the behavior of the Josephson junction. The proximity effect bridges which are flat film structures have large demagnetizing effects and Meissner effect tends to concentrate the magnetic field on the weaker part of the film which is the bridge. Phase coherence of the superconductor requires the fluxoid to be quantized. This can be seen from the following. Writing the wave function of the superconductor in the form

$$\psi = \sqrt{\rho_s}\, e^{i\phi} \tag{5.5}$$

as in equation (2.14), the supercurrent is given by equation (2.17)

$$\vec{J}_s = \frac{2e\hbar\,\rho_s}{m}\vec{\nabla}\phi - \frac{4e^2\rho_s}{mc}\vec{A} \tag{5.6}$$

or

$$\vec{\nabla}\phi = \frac{\pi m}{e\hbar\rho_s}\vec{j}_s + \frac{4e\pi}{\hbar c}\vec{A} \tag{5.7}$$

As ψ should be a single valued function, integrating along a closed path around the edge of the bridge gives

$$\oint \vec{\nabla}\phi \cdot d\vec{\ell} = 2\pi n \qquad n=0,1,2,\cdots \tag{5.8}$$

while

$$\oint \vec{A}\cdot d\vec{\ell} = \Phi \quad , \quad \text{the magnetic flux} \tag{5.9}$$

Hence

$$\frac{mC}{4\rho_s e^2}\oint \vec{j}_s \cdot d\vec{\ell} + \Phi = \frac{n\hbar c}{2e} \tag{5.10}$$

The quantity on the left hand side is defined as the fluxoid and it should be quantized in units of $\hbar c/2e = \Phi_o$, the flux quantum. The circulating current $\vec{j}_s$ that is required to fulfill the quantization conditions would raise the energy of the superconductor and thus decrease the critical current (Kirschman 1971). So the critical current would be a periodic function of the flux and thus periodic in the magnetic field.

The d.c. Josephson effect is in essence a demonstration of the actual two-dimensionality of the system. In subsequent experiments, in order to ensure one-dimensionality of the actual experimental situation, a compensating magnetic field was applied perpendicularly to the bridge to cancel out stray fields until the critical current was maximized. This corresponds to zero net magnetic field on the bridge and uniform phase difference along the width of the circuit.

5.5 The a.c. Josephson Effect

When the bridge is biased at a d.c. voltage V, it was found that the circuit oscillates with a frequency ν obeying the Josephson voltage-frequency relationship

$$\nu = \frac{2eV}{\hbar} \tag{5.11}$$

Such oscillation has been directly observed by Kirschman et al (1971). An indirect way to prove the existence of such oscillations is to irradiate the bridge with an EM wave of frequency ν. The a.c. voltage would phase modulate the Josephson oscillation, producing side bands at frequencies $2eV/h \pm n\nu$, $n=0,1,2,\cdots$ with amplitudes proportional to integral order Bessel functions $J_n(2eV_{rf}/\hbar\nu)$ as in usual FM analysis. So when the bridge is biased at voltage $V = n\hbar\nu/2e$, the zero beat results in a d.c. current which appears on the I-V characteristic as a constant current step. The n^{th} step size is proportional to $J_n(2eV_{rf}/\hbar\nu)$. This was also verified by Kirschman (1973) and is very similar to that of the Josephson junction.

To see how the bridge responds to external radiation, the bridge is mounted directly under an open ended waveguide with the current direction the same as that of the electric field. Bridges have been tested from 9.5 to 12.0 GHz, 35 GHz, and 90 GHz in this way. For lower frequencies (< 2 GHz) rf current was allowed to flow through coaxial cables in parallel with the d.c. bias current. The rf and bias current sources were isolated from each other with appropriate low pass and high pass filters. The cable was terminated with the bridge

(generally < 1 ohm) in series with 50 ohms and with very short leads to cut down inductances. Such care was taken to minimize the frequency dependence of the coupling coefficient. RF power was measured with an rf power meter together with calibrated attenuators. Figure 5.2 shows the V-I characteristics with and without rf radiation, showing the step structures.

5.6 The Dayem-Wyatt Effect

When a proximity effect bridge is subjected to an external rf radiation of high enough frequency (> 1 GHz for Sn/Au bridges and 35 GHz for Nb/Ta bridges), the critical current in many cases is enhanced contrary to decrease expected from a Josephson-like analysis. In many cases superconductivity could even be "switched on" (or created) by the external rf radiation as indicated by an induced zero d.c. voltage critical current at temperatures where none existed without radiation. A similar critical current enhancement has also been observed by Dayem and Wiegand (1967) and Wyatt et al (1966) in other structures. This phenomenon has been an unresolved dilemma in superconductivity for many years. It is usually observed only with high frequency radiation which may indicate that it is connected with the intrinsic noise of the superconducting circuit. It has never been reported to be observed in bulk material or Josephson junctions.

However, the proximity effect bridges show a very prominent Dayem-Wyatt phenomenon and we have used them to carefully examine this phenomenon and have proposed a modification of the Josephson quantum interference effects to account for the process. The final

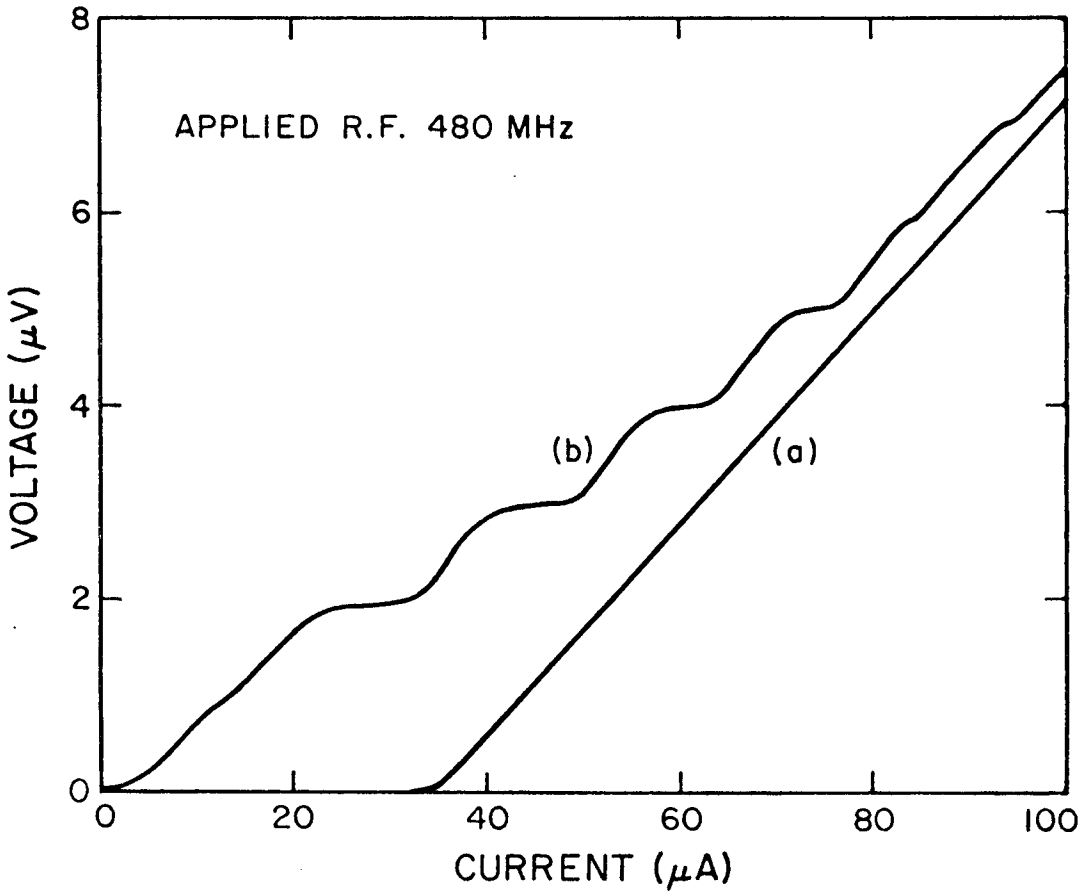

Fig. 5.2 Voltage-current characteristics of a proximity effect bridge (a) without and (b) with 480 MHz applied rf. To show the rf power modulation, in (b) the rf power is adjusted to minimize the first voltage step (at ~ 1 μV).

part of this thesis concerns these experiments and ideas. It was suspected that the Dayem-Wyatt effect in the proximity effect bridges was related to the phase coherence behavior of the weak link circuit. A high current density, two-phase model, to be described below, suggests a possible explanation for the Dayem-Wyatt effect and its connection with the intrinsic noise of the device itself.

5.7 Physical Models for the Proximity Effect Bridges

Unlike the Josephson junction which has a tunneling barrier, the proximity effect bridge has a metallic connection through which the electronic state must transfer from one superconductor to the other. A two-fluid model for the weak link is usually assumed in which both a time varying superflow and a dissipative normal flow coexist with possible nonequilibrium interconversion between the two.

Models have been suggested to describe the process inside the weak link region at finite voltage in which the superflow is subjected to an electric field. The most promising models are the phase slippage model proposed by Rieger, Scalapino and Mercereau (RSM2 1972) and the high current density two-phase model proposed by Notarys, Yu and Mercereau (NYM 1973) and the latter will be presented in detail in the following sections.

5.8 The Two-Phase Model

The proximity effect bridge can be described as two supernormal interfaces brought very close to each other such that the two macroscopic wavefunctions $\psi_1 e^{i\phi_1}$ and $\psi_2 e^{i\phi_2}$ overlap within the weak link "normal" region. There are two main physical consequences of the overlap:

(1) The existence of a zero voltage critical current for the bridge of the S/W/S circuit;

(2) Establishment of phase coupling between the macroscopic wavefunctions of the two superconductors.

In equilibrium the two-component wavefunctions phase lock to each other (i.e., $\phi_1 = \phi_2 = \phi$) so that they couple together to create a single quantum phase coherent state. Current in this state is then determined by the local gradient of the quantum phase,

$$j = \frac{2e\hbar}{m} |\psi|^2 \nabla\phi \tag{5.12}$$

However, at finite voltage, the system is out of equilibrium and the strong coupling condition $\phi = \phi_1 = \phi_2$ cannot be maintained. Instead we adopt a model in which the two-component wavefunctions decouple from each other, though individual components are still phase coherent with their respective strong adjoining superconductors.

Aslamazov and Larkin (AL 1969) proposed a similar model and used it to treat the bridge as a two-phase region in which the amplitude of the separate wavefunctions was strongly position dependent. They assumed that the total wavefunction was a linear combination of

the two components

$$\psi = \psi_1 + \psi_2 = \psi_o[f(x)e^{i\phi_1} + \{1 - f(x)\} e^{i\phi_2}] \tag{5.13}$$

where $f(x)$ is a function which rapidly goes to unity in superconductor 1 and zero in superconductor 2, and ψ_o is the undisturbed amplitude far from the bridge. With the strong phase coupling condition relaxed, this form of the wavefunction implies quantum interference between the two-component superconducting wavefunction within the weak region. AL asserted that both ϕ_1 and ϕ_2 were position independent constants whose time evolution depends only on the respective pair potential of the condensates. With this assumption and using the usual quantum current operator (eq. (2.17)), AL showed that the current resulting from this wavefunction is

$$j_s = \frac{2e\hbar}{m} \psi_o^2 \, f \, \nabla f \, \sin(\phi_1 - \phi_2) \tag{5.14}$$

This has the same functional dependence with the phase difference $\phi_1 - \phi_2$ as a Josephson tunnel junction and hence offers a general explanation for Josephson-like phenomena in any weakly connected circuit except the Dayem-Wyatt effect.

5.9 The Two-Phase Model at High Current Density

However, in the proximity effect bridges, with a typical supercurrent of 100 μA flowing through a cross-section of about 10^{-8} cm^2, the current density ($\sim 10^4$ amp/cm^2) is about 10^3 times that in usual superconductor tunnel junctions (Clarke 1968). The gradient of the phase, as shown by equation (2.17), depends linearly on current and the

deBroglie wavelength ($= 2\pi/|\nabla\phi|$) becomes comparable to the coherence length as current reaches the current densities of the proximity effect bridge. The approximation of a position independent phase that both Josephson and AL took is not an adequate representation of this high current density situation and the effects of a spatial variation of quantum phase within the junction region must be considered.

Notarys, Yu and Mercereau (NYM 1973) recently attempted to include these effects in a two-phase model and their results are included below.

For simplicity, S_1 and S_2 (Fig. 5.3) are assumed to be identical superconductors, with amplitude of the superconducting wavefunction deep inside the metals equal to ψ_o. Let the wavefunction that describes the superconducting state induced in the weak region by superconductor S_1 be $\psi_o f(x)\, e^{i\phi_1(x)}$ and by the second superconductor be $\psi_o g(x) e^{i\phi_2(x)}$ where f, g, ϕ_1 and ϕ_2 are all real functions of position x, and f and g are normalized such that

$$f(-\infty) = g(\infty) = 1 \tag{5.15}$$

and drop off rapidly inside the weak link region W as shown in Figure 5.3. $f(x)$ and $g(x)$ are governed by the spatial variation of the induced pair interaction along the S/W/S circuit and as a first approximation are assumed to be independent of current density. This assumption does not change the qualitative features of the physical process underlying the working of the proximity effect bridge.

The conduction electrons inside the bridge region are subjected to the simultaneous induced pair interactions by the two strong

superconductors S_1 and S_2. We assume that the long-range coherent nature of the interaction results in a wavefunction for the whole system which is the linear superposition of the two components given above:

$$\psi = \psi_1 + \psi_2 = \psi_o\{f(x)\, e^{i\phi_1(x)} + g(x)\, e^{i\phi_2(x)}\} \tag{5.16}$$

The wavefunction does not conserve the number of pairs, since the two terms can interfere with one another to cause $\psi = 0$. This quantum interference is thus a simple functional way to introduce time dependence into the amplitude of the wavefunction by having ϕ_1, ϕ_2 evolve with time and without the discontinuities involved in "phase slip" (Section 4.2).

The supercurrent j_s is calculated from first principles with the current operator (eq. (2.16)) in a manner similar to that of AL. The result is

$$j_s = \frac{2\hbar|e|}{m}\psi_o^2[(f\nabla g - g\nabla f)\sin(\phi_2 - \phi_1)$$

$$+ f^2\nabla\phi_1 + g^2\nabla\phi_2 + fg\nabla(\phi_1 + \phi_2)\cos(\phi_2 - \phi_1)] \tag{5.17}$$

The term which is proportional to sine of the phase difference is the Josephson current term obtained in AL's analysis. The other terms which are not included in AL's theory express the effect of high current density by the inclusion of the gradient of the phases.

This current depends not only on the phase difference $\phi_1 - \phi_2$ but also on $\nabla\phi_1$ and $\nabla\phi_2$. Consequently some relation between these quantities and experimental quantities must be found. The gradient

of the phase $\nabla\phi$ for a single phase system is proportional to the linear momentum of the superconducting pairs. Physically, coherence implies that pairs at a particular position x should all have the same linear momentum no matter from which strong superconductor they are originated. So a simple momentum conserving coupling condition is

$$\nabla\phi_1(x) = \nabla\phi_2(x) \quad * \tag{5.18}$$

or $\phi_1(x) - \phi_2(x)$ is independent of position. With this coupling condition the supercurrent reduces to

$$j_s(x) = \frac{2h|e|}{m} \psi_o^2[(f\nabla g - g\nabla f) \sin(\phi_2 - \phi_1) + \nabla\phi\{f^2 + g^2 + 2fg \cos(\phi_2 - \phi_1)\}] \tag{5.19}$$

where ϕ_1, ϕ_2, f , g , $\nabla\phi$ are all measured at the same spatial point x .

The properties of the bridge will be determined essentially by the weakest spot of the link which for the simple case of a symmetric weak link is the center of the bridge at which $f = g$. The expression reduces to

---

*Pictorially, we may represent the amplitude and phase angle of each component wavefunction locally by a polar vector. The tip of this vector hence traces out a helix of varying radius. These two helices overlap onto each other inside the bridge region. Locking is most natural when they have the same pitch which is equivalent to the phase coupling condition that $\nabla\phi_1(x) = \nabla\phi_2(x)$.

$$j_s = \frac{4\hbar|e|}{m} \psi_o^2[f\nabla f \sin(\phi_1 - \phi_2) + f^2\nabla\phi\{(1 + \cos(\phi_1 - \phi_2)\}] \quad (5.20)$$

As a rough estimation, $f\nabla f \sim f^2/\xi$ while $\nabla\phi \sim 1/\xi$ so both terms can be of comparable importance. Which term contributes more probably depends on the actual structure of individual bridges. In actual fact, to accurately determine the current an appropriate average should be taken over the two-phase region.

Hence the supercurrent in a proximity effect bridge can be expressed by

$$\vec{j}_s = \vec{j}_J \sin(\phi_1 - \phi_2) + C\vec{\nabla}\phi \{1 + \cos(\phi_1 - \phi_2)\} \quad (5.21)$$

where both $\vec{j}_J$ and C are functions of the wavefunction amplitudes and their gradients which for simplicity will be assumed to be temperature dependent but time independent. The time evolution of the phases depends on the pair potentials of the component wavefunctions (eq. (2.18)).

$$\frac{\partial\phi_1(x)}{\partial t} = \frac{2\mu_{p1}}{\hbar} \quad (5.22)$$

$$\frac{\partial\phi_2(x)}{\partial t} = \frac{2\mu_{p2}}{\hbar} \quad (5.23)$$

The gradient of phase $\nabla\phi$ in general depends on the current source. The maximum allowable supercurrent j_s sets a maximum value $\nabla\phi_c$ for the phase gradient in this phenomenological theory. When $\nabla\phi$ is time dependent, there is a gradient of the pair potential associated with the time variation of the phase gradient. From eqs. (5.22) and (5.23) and combining with the phase coupling condition $\nabla\phi = \nabla\phi_1 = \nabla\phi_2$,

$$\nabla\phi = \frac{2}{\hbar}\int \nabla\mu_{p1}\, dt$$

or

$$\nabla\phi = \frac{2}{\hbar}\int \nabla\mu_{p2}\, dt \tag{5.24}$$

as

$$\nabla\mu_{p1} = \nabla\mu_{p2} \tag{5.25}$$

Both terms in eq. (5.21) are results of quantum mechanical interference of the two components. The Josephson term arises from the spatial variation of the amplitude of the wavefunction ∇f . The second term is a coupling between the phase gradient and the phase dependent pair density

$$\rho = \psi_o^2 f^2[1 + \cos(\phi_1 - \phi_2)] \tag{5.26}$$

As was noted previously, this phase dependent pair density is a result of the nonconservation of pairs for this wavefunction and physically must result in interconversion of pairs and normal electrons to conserve the number of electrons. The $1 + \cos(\phi_1 - \phi_2)$ factor arises from the constructive and destructive interference of the two-component wavefunctions. The total current thus depends both on the sine and cosine* of the phase difference as well as the phase gradient. For

---

*The cosine dependence in this case does not have the same physical origin as the similar cosine dependence in Josephson tunnel junctions (Josephson 1965). In tunnel junctions, current with a cosine dependence on the relative phase occurs only at finite voltage because of pair quasiparticle interference effects. Here the cosine term exists even at zero voltage and reflects the dependence of the amplitude of the wavefunction ψ on the relative phase of the two components ψ_1 and ψ_2 .

the Josephson term the direction of the current flow depends on the phase difference $\phi_1 - \phi_2$. For the second term the direction is determined by the direction of the phase gradient and the phase difference only modulates the amplitude of the current.

Throughout this analysis, one-dimensionality is assumed. That is, current is taken to be uniform in the perpendicular direction to the flow so that variation along the current direction only has to be considered. Another simplification is that temperature is assumed to be above the intrinsic transition temperature of the weak link region so that we may neglect the constant contribution to the wavefunction as a result of the intrinsic pairing interaction. However, we expect that as long as we have the two-phase system, quantum interference effect will still bring out the main features of the coherence phenomenon. This is actually verified experimentally. Josephson effects were still observed at $T < T_{cw}$.

5.10 Comparison with the Josephson Tunnel Current

Our supercurrent expression (5.21) has a distinct contrast with the Josephson analysis for tunneling current. For expression (5.21) the supercurrent $j_s(x)$ depends on ϕ_1, ϕ_2, j_2 , C , and $\nabla\phi$ at the same spatial position x , while the Josephson tunneling current depends on the phase difference $\phi_1 - \phi_2$ across a tunneling barrier,

$$j_s = j_o \sin(\phi_1 - \phi_2) \tag{5.27}$$

This difference comes about here since we assume that the mechanism for the quantum effects in our bridges depend on the actual electronic

state inside the bridge region. In order to relate the phase difference within the bridge to experimental parameters we define points 1 and 2 as being sufficiently deep within the adjoining superconductors that superconductivity is in equilibrium and may be defined in terms of a single phase θ_1 and θ_2 and chemical potential μ_{p1} and μ_{p2}. Then the phase within the bridge can be obtained by integration as:

$$\phi_1(x) = \theta_1 + \int_1^x \nabla\phi \cdot dx \tag{5.28}$$

$$\phi_2(x) = \theta_2 - \int_x^2 \nabla\phi \cdot dx \tag{5.29}$$

so

$$\phi_1(x) - \phi_2(x) = \theta_1 - \theta_2 - \int_2^1 \nabla\phi \cdot dx \tag{5.30}$$

Expression (5.21) becomes:

$$j_s(x) = j_J \sin(\theta_1 - \theta_2 - \int_2^1 \nabla\phi \cdot dx) + C\,\nabla\phi\,\{1 + \cos(\theta_1 - \theta_2 - \int_2^1 \nabla\phi \cdot dx)\} \tag{5.31}$$

This degenerates to the simple Josephson form (5.27) if we completely neglect the current density effect and set

$$\nabla\phi \equiv 0 \tag{5.32}$$

The inclusion of $\nabla\phi$ in our model brings in the inductive feature of a supercurrent. By definition of $\mu_p \equiv \frac{\hbar}{2}\frac{\partial\phi}{\partial t}$ it follows that

$$\nabla\mu_p = \frac{\hbar}{2}\frac{\partial}{\partial t}(\nabla\phi) \tag{5.33}$$

Physically this says a pair potential is required to accelerate or decelerate the supercurrent as a result of the kinetic inductance of the latter. Hence if the supercurrent is oscillating sinusoidally in time, $\nabla\phi$ varies in phase with the current while μ_p would be leading by $\pi/2$ over the time variation of $\nabla\phi$.

An important consequence is that $\phi_1(x) - \phi_2(x)$ need not have the same time variation as $\theta_1 - \theta_2$. By definition, since θ_1 and θ_2 are defined at an equilibrium point in the superconductor, then:

$$\frac{\partial}{\partial t}(\theta_1 - \theta_2) = \frac{2}{\hbar}(\mu_{p_1} - \mu_{p_2}) \tag{5.34}$$

$$= \frac{2e}{\hbar} V_{12} \tag{5.35}$$

Thus

$$\phi_1(x) - \phi_2(x) = \frac{2e}{\hbar}\int V_{12}dt - \int_2^1 \nabla\phi \cdot dx \tag{5.36}$$

by eqs. (5.31). As will be shown in Section 5.12, it is this $\nabla\phi$ with its inductive character carried into the 2-phase state that gives the Dayem-Wyatt effect which the Josephson tunnel current expression (5.27) fails to predict.

Experimentally the impedance of our bridges (normally $<$ 1 ohm) is very much lower than those of the d.c. and a.c. current sources; both d.c. and a.c. current biased. So our bridges are essentially current controlled circuits. In our model $\nabla\phi$ of individual component wavefunctions is set by the external current source, as if there is no quantum interference, only to be modified slightly by the requirement

of phase coupling condition $\nabla\phi_1 = \nabla\phi_2$. The subsequent quantum interference of these two-coherent component supercurrents modulates the amplitude rather than the velocity of the superconducting pairs. Also to conserve current in this current biased situation, a normal current is required to compensate the variation of the superflow.

In order to make the physics more transparent, we shall concentrate on the high current density term and assume that it dominates over the Josephson-like term. Since all the pairs have the same center of mass momentum, we shall assume that

$$\nabla\phi = \text{constant spatially} \tag{5.37}$$

From eqs. (5.22) and (5.23), this implies $\nabla\mu_{p1}$ and $\nabla\mu_{p2}$ are also independent of position.

5.11 The a.c. Josephson Effect in the Two-Phase Model

When the bridge is biased with a d.c. current exceeding the critical current, a voltage is developed across the bridge. Our two-phase model is then applicable in the resulting nonequilibrium state. We are going to show that the a.c. Josephson effect follows from the quantum interference of the two-component wavefunctions as the voltage causes their relative phase $\phi_1 - \phi_2$ to evolve with time.

In this d.c. current biased situation there is no acceleration or deceleration of the supercurrent

$$\nabla\phi = \text{constant in time} \tag{5.38}$$

and

$$\nabla\mu_{p1,2} = 0 \quad \text{by equation (5.32)} \tag{5.39}$$

$$\frac{\partial}{\partial t}(\phi_1 - \phi_2) = \frac{2eV_{12}}{\hbar} \tag{5.40}$$

and $V_{12} \neq 0$, the pair density (5.27) and hence the supercurrent changes with time as a consequence of the quantum interference. The voltage V_{12} also drives a normal current whose magnitude is proportional to V_{12} (Ohm's law for quasiparticles, Section 2.3). In actual fact, a time varying normal current is required to conserve current in this current biased situation. This implies V_{12} is also oscillating with the supercurrent and has the same period time τ.

The quantum interference completes one cycle when $\phi_1 - \phi_2$ goes through 2π, so that in one period τ

$$\begin{aligned} 2\pi &= \int_0^\tau \frac{\partial}{\partial t}(\phi_1 - \phi_2)dt \\ &= \int_0^\tau \frac{2eV_{12}}{\hbar}\, dt \\ &= \frac{2e\tau}{\hbar} \langle V_{12} \rangle \end{aligned} \tag{5.41}$$

where $\langle V_{12} \rangle$ is the time averaged voltage across the bridge. So the voltage oscillates with frequency

$$\begin{aligned} \nu &= \frac{1}{\tau} \\ &= \frac{2e\langle V \rangle}{h} \end{aligned} \tag{5.42}$$

which is just the Josephson frequency (eq. (5.11)).

5.12 The Dayem-Wyatt Effect in the High Current Two-Phase Model

An important feature where the proximity effect bridge differs from the Josephson tunnel junction is the prominent Dayem-Wyatt effect (Section 5.6). External radiation of high enough frequency induces (or enhances) a d.c. supercurrent even above the apparent transition temperature of the bridge. We are going to show the high current density term in our supercurrent expression indeed leads to a Dayem-Wyatt effect.

Since the bridge is essentially a.c. and d.c. current biased (c.f. Section 5.10), an applied rf radiation of frequency ω induces an rf current in the bridge circuit. In the strong superconductor S where the current is carried completely by the supercurrent, the phase gradient $\nabla\phi$ is given by

$$\nabla\phi = \nabla\phi_1 \sin \omega t + \nabla\phi_o \tag{5.43}$$

where $\nabla\phi_o$ accounts for the d.c. bias current and $\nabla\phi_1$ is proportional to the rf current. This phase gradient is spatially constant (eq. (5.37)) and is the same inside the bridge region.

As a result of the inductive character of the pairs associated with the acceleration and deceleration of the supercurrent is a gradient of μ_p which is $\pi/2$ out of phase with $\nabla\phi$ (eq. (5.33)):

$$\nabla\mu_{p1,2} = \frac{\hbar\omega}{2} \nabla\phi_1 \cos \omega t \tag{5.44}$$

Since there is no d.c. voltage bias across the bridge as we are measuring the zero d.c. voltage supercurrent, we expect the voltage

V_{12} to have a similar time dependence as in (eq. (5.44)). V_{12} which also accounts for the normal flow is in general not sinusoidal. But in the small voltage limit, we shall take only the first harmonic component and neglect possible phase shift due to the dissipative normal flow. So after the integration of V_{12} with respect to time, expression (5.36) for $\phi_1 - \phi_2$ becomes

$$\phi_1(x) - \phi_2(x) = \frac{2eV_o}{\hbar\omega} \sin \omega t + \beta \tag{5.45}$$

where V_o in this small voltage limit is proportional to the rf current (and hence to $\nabla\phi_1$) and β is an integration constant set by the initial condition of the phases.

Hence the high current density term of eq. (5.21) becomes

$$C(\nabla\phi_1 \sin \omega t + \nabla\phi_o) \left\{1 + \cos\left(\frac{2eV_o}{\hbar\omega} \sin \omega t + \beta\right)\right\} \tag{5.46}$$

The beating of the two oscillating terms: one from the gradient of the phase and one from the cosine of the relative phase, besides giving many high frequency terms, gives a rectified component j_B proportional to $\sin^2\omega t$ and using the fact that V_o is proportional to $\nabla\phi_1$,

$$j_B \propto \left(\frac{2eV_o}{\hbar\omega}\right) J_1\left(\frac{2eV_o}{\hbar\omega}\right) \sin \beta \tag{5.47}$$

J_1 is the first order Bessel function. This rectified current represents a d.c. supercurrent induced by an a.c. source which is exactly the experimental observation in Dayem-Wyatt effect. Such a d.c. rectification term comes only from the phase gradient term in eq. (5.21)

and does not occur in the low current approximation where we have the Josephson current term only. This unique feature provides a test ground for this high current density two-phase model.

The two phase gradients and their locking are subjected to disruption by the noise voltage on a time scale set by the noise bandwidth. Hence the measured critical current which is a time average over many noise periods is much less than the maximum supercurrent the bridge can carry if there is no phase disruption. For the same reason, at low frequencies within the noise band, such rf induced oscillating terms fail to give a time averaged d.c. component. But at frequencies above the noise band, mixing can proceed to result in a rectified supercurrent (eq. (5.48)) within a noise period. This provides an explanation for the requirement for a high frequency rf to produce the Dayem-Wyatt effect and a condition for the lower cut-off frequency. It was shown (Kirschman 1972) that the intrinsic Johnson noise current in these bridges has a bandwidth of approximately $RI_c\Phi_o^{-1}$ where R is the bridge resistance, I_c is the critical current and Φ_o is the flux quantum. Hence in order to observe Dayem-Wyatt effect, the frequency is expected to be at least above this value. This was observed experimentally.

Figure 5.3 shows an example from a 10 milliohm Sn/Au proximity effect bridge. This bridge was 1 μm long, 39 μm wide and 1000Å thick and was mounted directly under an open ended X-band waveguide with the current direction the same as that of the electric field of the 10 GHz microwave. The critical current was determined with a feedback circuit. The bridge was biased with a small unidirectional

current slightly higher than the critical current. The error signal hence created across the bridge was amplified and fed back to the bias current loop to minimize the difference with the critical current. The unidirectional current was chopped at about 300 c/s so that the error signal might be detected with phase lock technique to minimize noise. The minimal error of the feedback loop was limited by the noise of the circuit which was about 5 nV. This gave a current noise of about 0.5μA for the critical current in this 10 mΩ bridge.

RF enhanced supercurrent was observed at and above 2 GHz for this Sn/Au bridge. This is above the Johnson noise bandwidth $RI_c\Phi_o^{-1}$ which is about 10^7Hz (taking $R = 10^{-2}$ohms, $I_c \sim 4$ μA ; Φ_o the flux quantum $= 2 \times 10^{-15}$weber) as predicted. Nb/Ta bridges of comparable characteristics failed to show any Dayem-Wyatt effect at 10 GHz but it was observed at 35 GHz and 90 GHz.

As further experimental evidence for this interpretation of the Dayem-Wyatt effect, the rf power dependence of the induced d.c. supercurrent was examined experimentally. The induced d.c. supercurrent should have a maximum amplitude ($\beta = \pi/2$, corresponding to the critical current) which is periodic in V_{rf} through the first order Bessel function J_1 .

The data shown in Fig. 5.3 were taken at about 3.6^oK nearly 0.4^oK above the temperature at which supercurrent appears without radiation. In this bridge supercurrent to be "created" in this fashion was actually observed up to 3.9^oK, just below T_{CS} of the main Sn film. Equation (5.47) has been fitted to the data (solid line) by adjusting

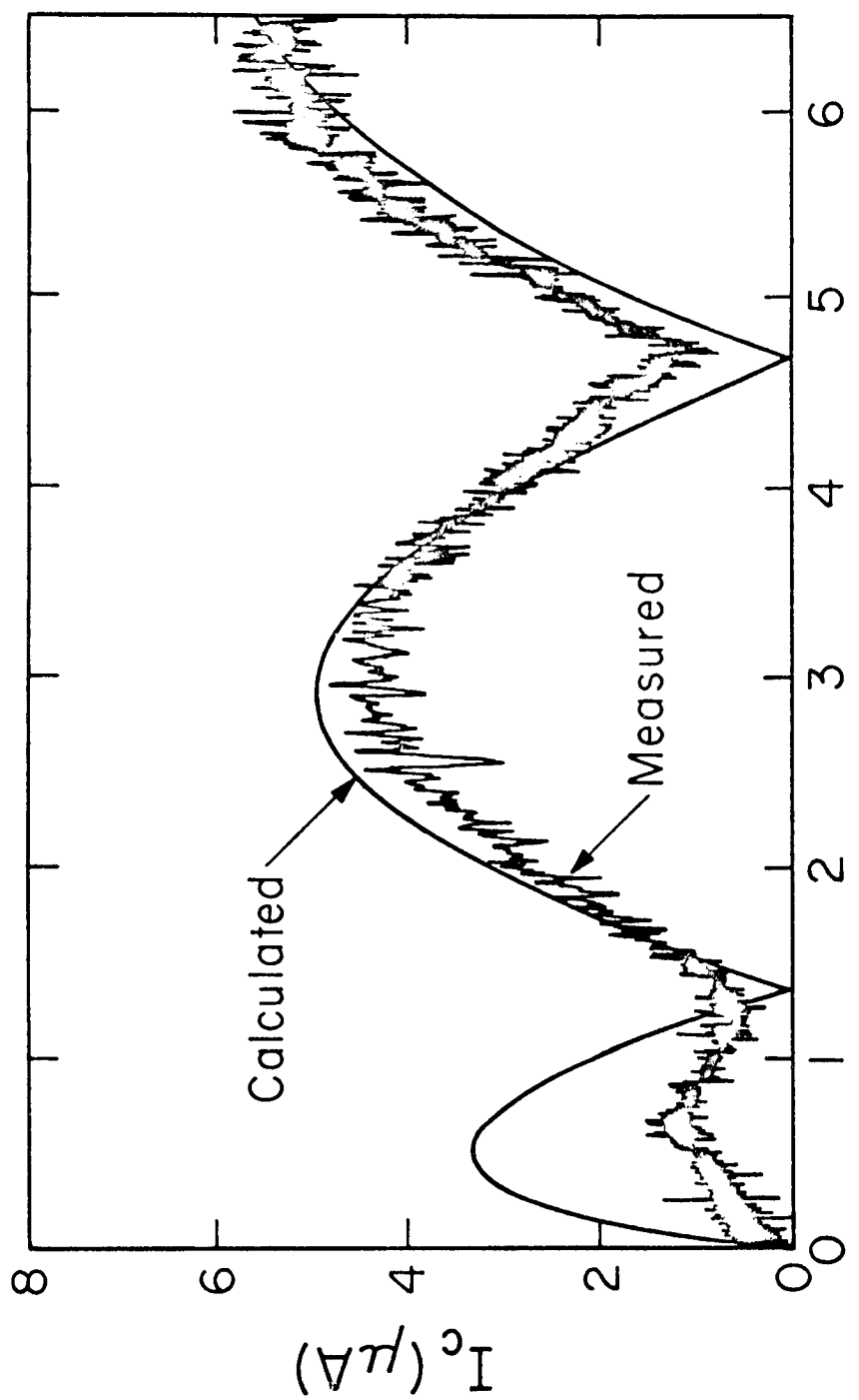

Fig. 5.3 Enhanced supercurrent as a function of 10 GHz microwave power. These data were taken at 3.6^{o}K where no supercurrent was observed without external radiation. Similar effects persist up to 3.9^{o}K. Smooth solid line, power dependence to be expected from eq. (5.47).

the period of the Bessel function to the zeros of the data and the scaling factor for the magnitude. The theoretical prediction agrees well except at low voltage where fluctuations still predominate. At high rf levels beyond the scale on the figure, the effect goes away which probably corresponds to the breakdown of the small voltage approximation. We interpret this agreement with the theoretical prediction as a strong support for the validity of the present two-phase model and the importance of the high current density modification, and also that it establishes the Dayem-Wyatt effect as a manifestation of macroscopic coherence of the condensate.

5.13 Effect of Static Magnetic Field on the Dayem-Wyatt Effect

It was pointed out in Section 5.4 that in order to understand the effect of an applied magnetic field it is necessary to consider the actual two-dimensionality of the experimental situation. Analysis given in the previous section involves only one dimension. Experimentally a magnetic field applied normal to the plane of the bridge was found to change the Besseling behavior of the enhanced supercurrent with rf power. Figure 5.4 shows how the rf power dependence varies with magnetic field. Data were taken when there was a small critical current at zero rf. Magnetic field was set to maximize the zero rf critical current in the upper curve of Fig. 5.4 and set to the first minimum in the lower curve of Fig. 5.4. The maxima and zeros of the Besseling pattern are shifted and the amount of shift depends on the magnetic field. Here we suggest a plausible explanation of this behavior.

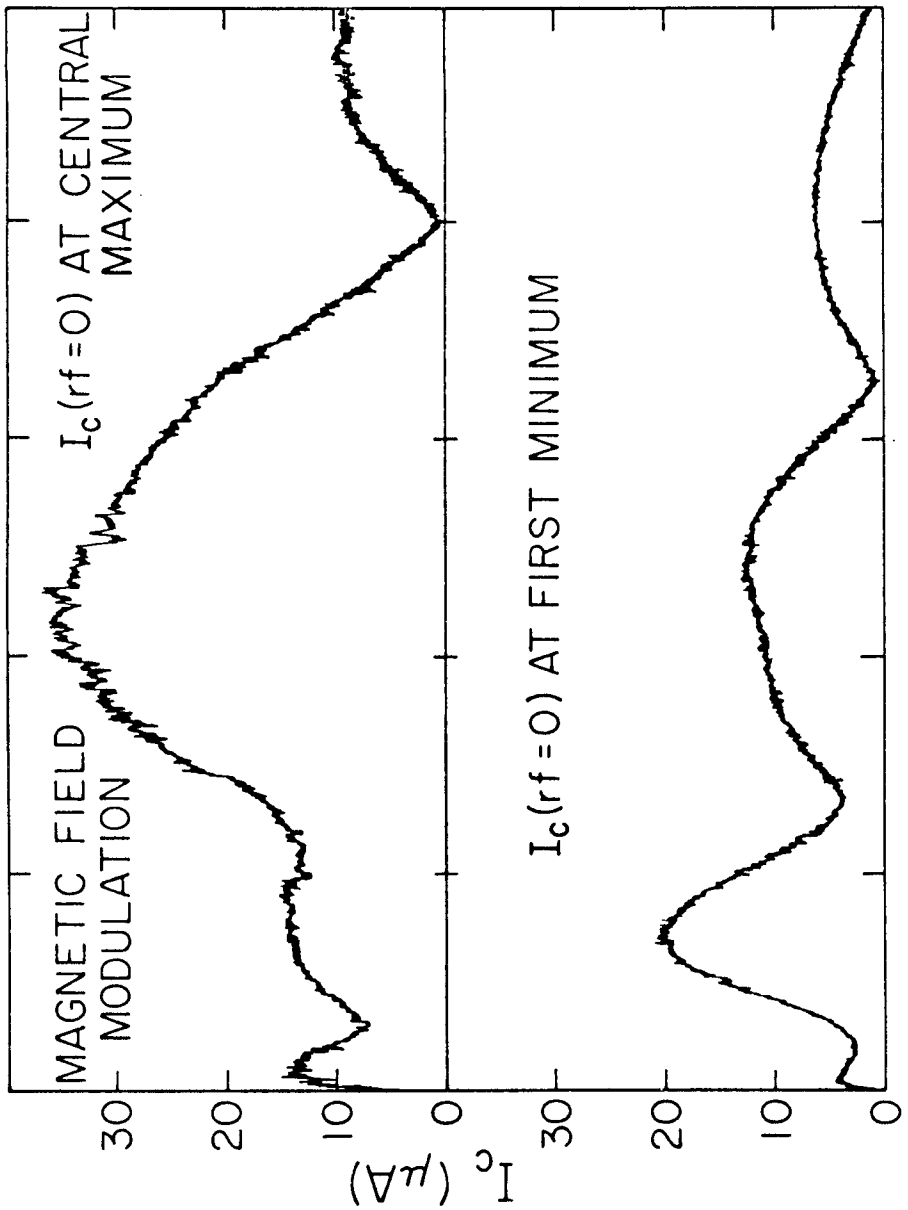

Fig. 5.4 Enhanced critical current as a function of 10 GHz microwave power at various magnetic fields. Magnetic field was set to maximize the zero rf critical current in the upper curve and set to the first minimum in the lower curve. Notice the shifting of positions of maxima and zeros.

The application of a magnetic field creates a phase gradient on the transverse (y) direction (perpendicular to the direction of current I). This implies that the phase angle β in expression (5.47) is position dependent in the y direction. In the voltage sustaining state it was shown (Mercereau 1973) that this shifts the phase of the oscillating supercurrent along the y-axis thus resulting in rf current loops round the bridge region. It is suspected that the inductive effects of these current loops contribute to $\phi_1(x) - \phi_2(x)$ through the $\int_2^1 \nabla\phi \cdot dx$ term in eq. (5.35), hence causing a nonuniform distribution of the rf current and hence a transverse position dependence of V_{rf} in the argument of the Bessel function in (5.47). The Besseling behavior is therefore modified as the detected d.c. supercurrent is the integrated sum along the width of the bridge. It is also suspected that the "self-field" produced by the induced d.c. supercurrent also acts back on the bridge, causing deviation from the Bessel behavior although the external magnetic field was compensated to maximize the zero rf critical current for the data shown on Fig. 5-4 taken with a wide bridge (width $\simeq 40 \times$ length).

5.14 The Characteristic Length and Time Constant of the Phase Slippage Process in a Proximity Effect Bridge

The working of the bridges depends on the overlap of the two proximity effect induced wavefunctions. Each component wavefunction is a function of temperature T and decays with a decay length $\tilde{\lambda}$ as it penetrates into the bridge region. We can approximate the situation by writing each component in the form

$$\psi(x,T) = \psi_o(T)\ e^{-x/\tilde{\lambda}(T)} \tag{5.48}$$

where x is measured from the S/W boundary and $\psi_o(T)$ is the wavefunction induced on the W side at the interface ($x = 0$).

Our experiments with supernormal interfaces indicated that the restoration of equilibrium at the interfaces in the current-carrying dynamic state is slowed down by the quasiparticle processes from the Ginzburg-Landau relaxation time τ_{GL} of the condensate to the branch mixing time τ_Q of the quasiparticles (Section 3.12). This allows the information of the nonequilibrium process to propagate to a longer distance, e.g., the branch mixing characteristic distance λ_Q instead of the coherent length ξ. In the S/N experiment, $\lambda_Q(0) = 1400\text{Å}$ as compared to $\xi(0) \sim 92\text{Å}$ in our Ta thin films. Thus we would expect enough overlap between the component wavefunctions to produce quantum interference effects if L, the length of the bridge, is within a few times of the decay length $\tilde{\lambda}$. If $\tilde{\lambda}$ is λ_Q the length L would be typically a micron. But if λ is ξ, L would be of the order of 1000Å.

For both the Sn/Au and the Nb/Ta system, the typical working length L is indeed about a micron and phase coherence phenomena were observed for bridges as long as 5 microns over a fairly wide temperature range ($\sim 0.5^{\circ}\text{K}$). Hence we conclude that the coherence length ξ is not the characteristic length. The branch mixing length λ_Q is probably the controlling length for our bridges.

The temperature dependence of the d.c. critical current is also consistent with our understanding of the S/W interface (Section

4.6). The critical current is proportional to the maximum overlap of the two components at the center of the bridge. That is,

$$j_c(T) \propto |\psi|^2$$

$$\propto |\psi_o(T)|^2 \, e^{-L/\tilde{\lambda}(T)} \tag{5.49}$$

Our measurement of the boundary potential ΔV_b at S/W interfaces indicated that

$$|\psi_o(T)|^2 = |\psi_o|^2 \, e^{-\beta T} \tag{5.50}$$

where β ranged from 10 to $20^{\circ}K^{-1}$ depending on the particular Ta circuit. As for the temperature dependence originated from that of λ_Q,

$$\frac{x}{\lambda_Q} \sim \frac{x}{\lambda_Q(0)} (1.76)^{1/2} \left|\frac{T_c - T}{T_c}\right|^{1/4} \tag{5.51}$$

For a 1 μm bridge with $T_c \sim 4^{\circ}K$ and $\lambda_Q \sim 0.2$ μm,

$$e^{-x/\lambda(T)} \sim e^{-2|T_c - T|^{1/4}} \tag{5.52}$$

The exponential dependence on T is far slower than that of $|\psi_o(T)|^2$ so the latter completely dominates. Hence j_c is expected to vary with T as

$$j_c = j_{co} \, e^{-\tilde{\beta} T} \tag{5.53}$$

where $\tilde{\beta}$ is expected to run from 10 to $20^{\circ}K^{-1}$, depending on individual Nb/Ta bridges. Experimentally, $\tilde{\beta}$ is found to be about $12^{\circ}K^{-1}$ (Decker 1973) for Nb/Ta bridges and about $8^{\circ}K^{-1}$ for Sn/Au bridges. This result further confirms that the amplitude of the wavefunction

induced at the W side of the interface varies exponentially with temperature.

The quantum interference process inside the bridges results in time variation of the pair density of the condensate and these give all the Josephson-like phenomena.(Section 5.9). Experimentally, frequency response up to about 200 GHz had been observed in short (< 0.5 μm) Nb/Ta and Sn/Au bridges which corresponds to a time of about 5×10^{-12}sec, much shorter than the quasiparticle relaxation time τ_Q ($\tau_Q(0) = 6.5 \times 10^{-11}$sec for Ta, 2×10^{-10}sec for Sn). Quasiparticles, however, are directly involved, especially in the periodic conversion of superflow to normal flow and vice versa. Our experiment indicated that the background of nonequilibrium quasiparticle excitations does not qualitatively affect the quantum interference process of the condensate.

Incidentally, it was also observed experimentally that the upper frequency response decreases as the length of the bridge increases, implying that it also depends on the strength of the coupling. A bridge more than two microns long rarely responds above a few GHz. This dependence may be related to the actual electron-electron coupling energy at the weak link region. As the energy of the quantum $\hbar\omega$ approaches or exceeds the pairing energy in the condensate, the phase coherence is disrupted.

Chapter 6

VOLTAGE MEASUREMENT INSIDE A PROXIMITY EFFECT BRIDGE

6.1 The Experimental Situation

Experiments reported in Chapters 3 and 4 measured voltages at and across the supernormal interfacial region. In a proximity effect bridge two S/W interfaces are in close proximity with each other with a time dependent superconducting state in between. This is expected to modify the characteristic of the voltage across the supernormal interface drastically. A direct experimental approach with voltage probes inside and outside the bridge region was used. With these probes, the time averaged potential across the boundaries was monitored. The time dependent state was examined by coupling the bridge oscillation with an external rf radiation, so that the result of the mixing would appear on the d.c. I-V characteristics. This is the same idea behind the examination of the rf response of the proximity effect bridge which provided the experimental background support for the high current density two-phase model.

A voltage probe less than 0.5 μm wide at the tip was cut out from the Nb/Ta substrate using the photo-etch and anodization technique right at the edge of a usual bridge of about 1 micron or less long (c.f. inset in Fig. 6.1). Bridges about 100 μm wide were used to keep the resistance low ($\lesssim$ 50 milliohm*) so that the noise bandwidth

---

*This impedance is very low when compared to those of the d.c. and rf current sources. So the bridges were essentially both d.c. and a.c. current biased.

is narrow enough to allow the bridge to operate at 50 MHz up (Section 5.11). Radiation was coupled to the bridge using an inductive loop placed close to the film. Frequency ranged from 50 to 500 MHz. A d.c. magnetic field coil was used to apply a compensating (for stray fields) or bias magnetic field on the bridge.

Owing to the technical limitation of resolution, the size of the probe was comparable to the length of the bridge. So a spatial average of the voltage was measured. Both superconducting and normal probes were used. They showed no essential qualitative difference in their measurements. However, the present geometry does not allow simultaneous comparison between the voltage probed by a superconducting and a normal probe.

6.2 Voltage Measurements in the Absence of RF

The d.c. characteristic as measured across the boundary of the weak link showed no qualitative difference from the I-V characteristic of the bridge as a whole. The probe inside the link only acted as a potential divider, sampling part of the voltage. It indicates that the internal Josephson oscillation once averaged does not modify appreciably the d.c. behavior inside the bridge.

6.3 Potential Across the Interface in the Presence of RF

In the presence of external rf radiation, the bridge as a whole showed the usual a.c. Josephson phenomenon as described in Section 5.5. In particular, phase modulation by the applied rf modulates the zero d.c. voltage critical current. The functional

dependence is proportional to $J_o(2eV_{rf}/h\omega)$. But despite the zero net voltage across the bridge including both boundaries, measurements indicated that there can be a d.c. potential across the individual S/N interfaces and it can be a negative potential against the direction of current flow.

Figure 6.1 shows two such cases. Potentials were measured along the weak link structure as indicated by the inset. On the left hand curves $V_{S_1S_2}$ is the voltage across the whole rf coupled bridge region and shows the existence of a zero d.c. voltage critical current. However, the voltage across one of the interfaces V_{S_1W} monitored simultaneously showed a negative potential across the boundary. That is, an external rf can induce a time averaged potential distribution inside the phase slippage region. The right hand curves show the case when the critical current was suppressed by the applied rf. Again there was a negative potential V_{WS_2} across one boundary, even when the bridge was in the voltage sustaining state. The potential V_{S_1W} across the other boundary actually went up to compensate the first, giving a "normal" V-I curve ($V_{S_1S_2}$) for the entire bridge including both boundaries.

It was found that for a fixed d.c. bias current ($< I_c$), the potential at a single boundary oscillates in sign with rf power. Figure 6.2 shows the variation of the potential across a single boundary with rf amplitude. At high rf excitation, the oscillating behavior ceases and the potential finally settles down to a constant value corresponding to the resistance of the boundary region under investigation. A d.c. magnetic field also modulates this rf induced

Fig. 6.1 DC potentials across the individual S/W interfaces and the whole bridge when there is external 480 MHz rf. On the left hand curve V_{S_1W} across one of the interfaces is negative while the net voltage $V_{S_1S_2}$ across the whole bridge is zero. The right hand curves show a similar negative potential V_{WS_2} while $V_{S_1S_2}$ across the bridge is finite. The potential V_{S_1W} across the other boundary goes up to compensate V_{WS_2} giving a "normal"V-I curve $V_{S_1S_2}$ for the entire bridge.

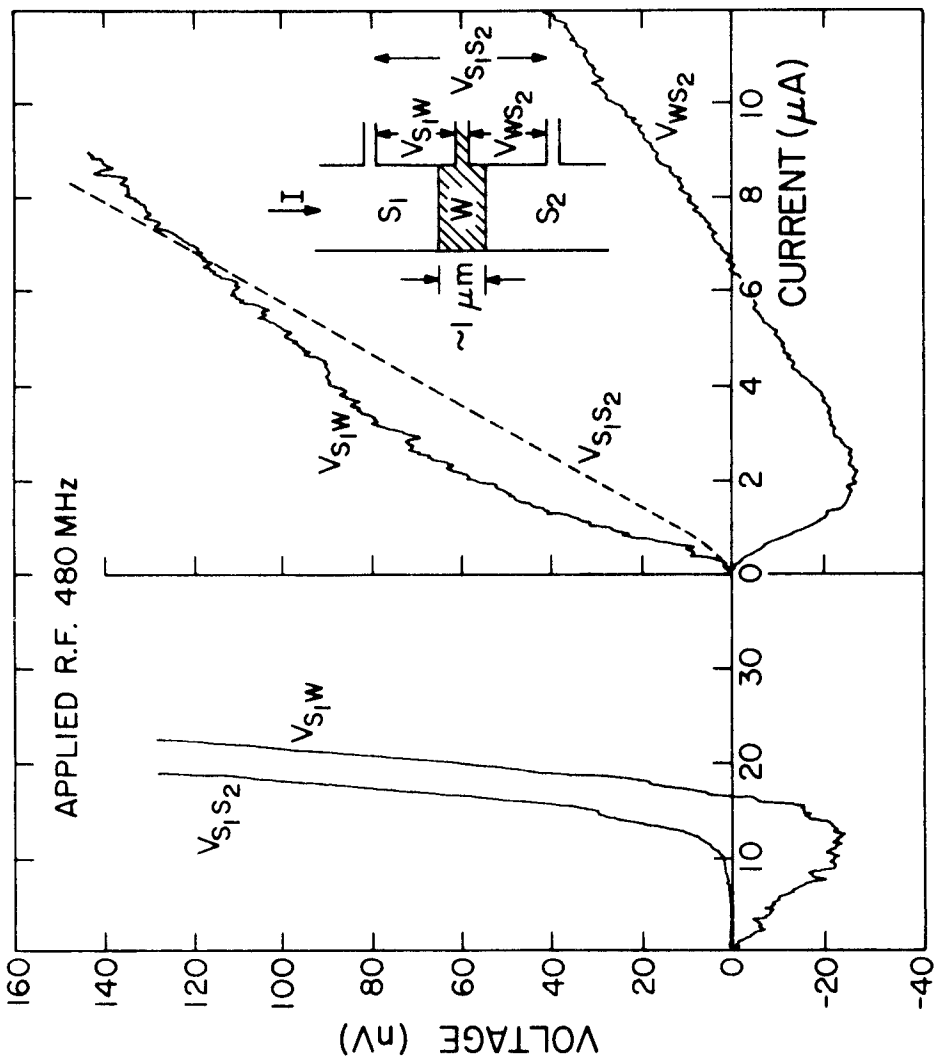
APPLIED R.F. 480 MHz
VOLTAGE (nV)
CURRENT (μA)
V_{S_1W}
$V_{S_1S_2}$
V_{WS_2}
I
S_1
W
S_2
~1 μm
160
140
120
100
80
60
40
20
0
-20
-40
0
2
4
6
8
10
10
20
30

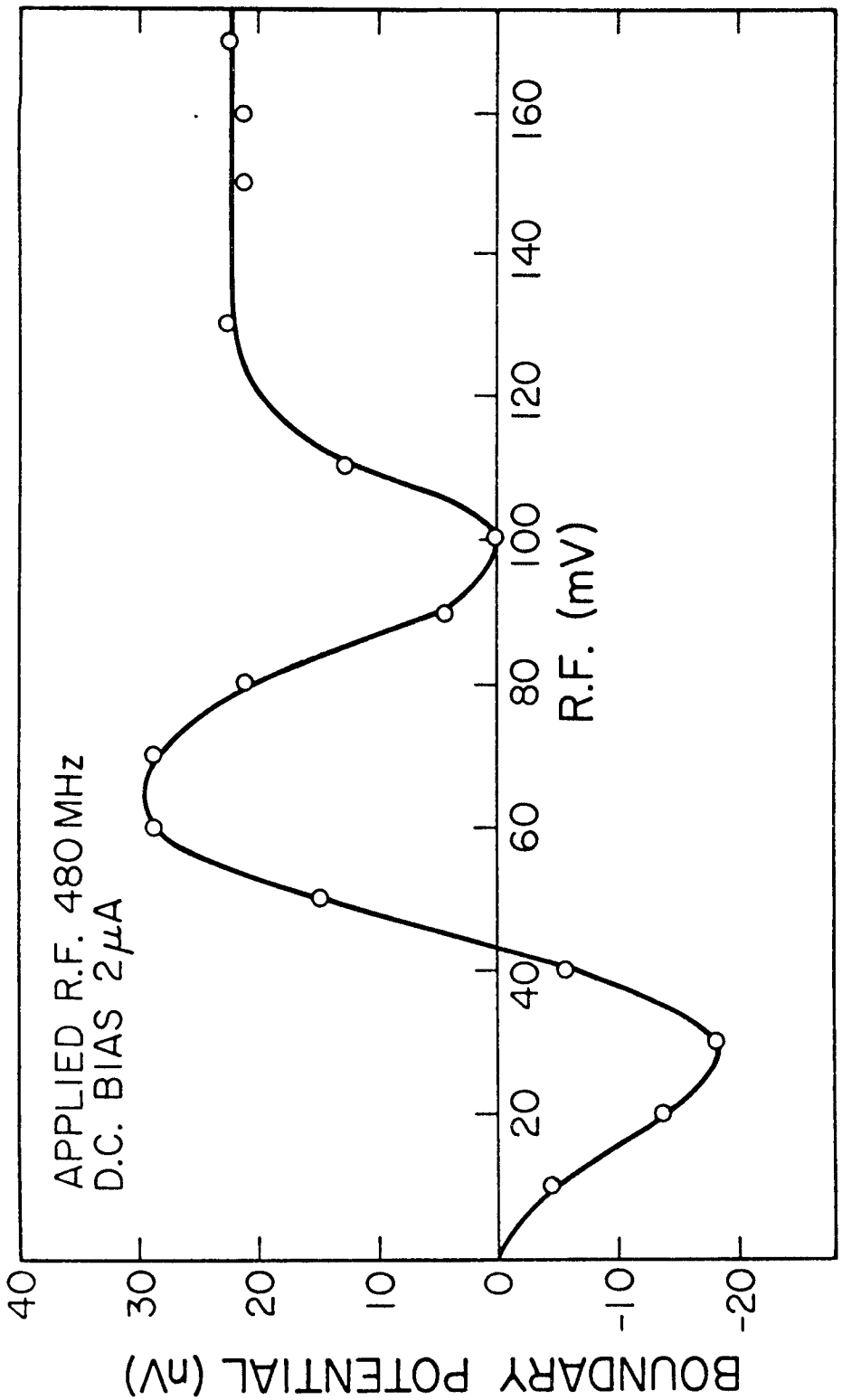

Fig. 6.2 Variation of the potential across a single S/W interface with rf amplitude

boundary potential making it oscillate in sign for a fixed rf level.

With the bridge at a finite voltage, the mixing of the internal Josephson oscillation with the external rf radiation results in constant voltage steps across the bridge at voltages $V = nh\nu/2e$, $n=1,2,\ldots$ and step sizes proportional to $J_n(2eV_{rf}/h\nu)$ as shown by curve $V_{S_1S_2}$ in Figure 6.3 at ~ 1 and $2\ \mu V$. (The nonzero slope of the "steps" is a result of noise intrinsic to the bridge (Section 5.11)). The boundary potential V_{S_1W} monitored simultaneously across only one boundary has essentially the same "step" features, with steps at the same current values but at voltages that violate the Josephson voltage frequency relationship, indicating that the voltage probe was really sampling only part of the time dependent process.

Simultaneous monitoring of both boundaries separately can show both positive and negative "steps" as shown in Fig. 6.4. The constant voltage step was replaced by an equivalent region of negative dynamic resistance as shown on curve V_{WS_2} in Fig. 6.4 or bumps in its complementary characteristic V_{WS_2} across the other supernormal boundary. Their sum however gives back the normal constant voltage steps for the whole bridge and at the correct voltages. This phenomenon is very similar to the observed negative resistance at the "zeroth" step where the net d.c. voltage across the bridge was zero. The negative resistance is now replaced by a negative dynamic resistance. These two phenomena probably have a similar origin; both require an external rf radiation together with a d.c. bias current. A plausible mechanism is suggested in Appendix D.

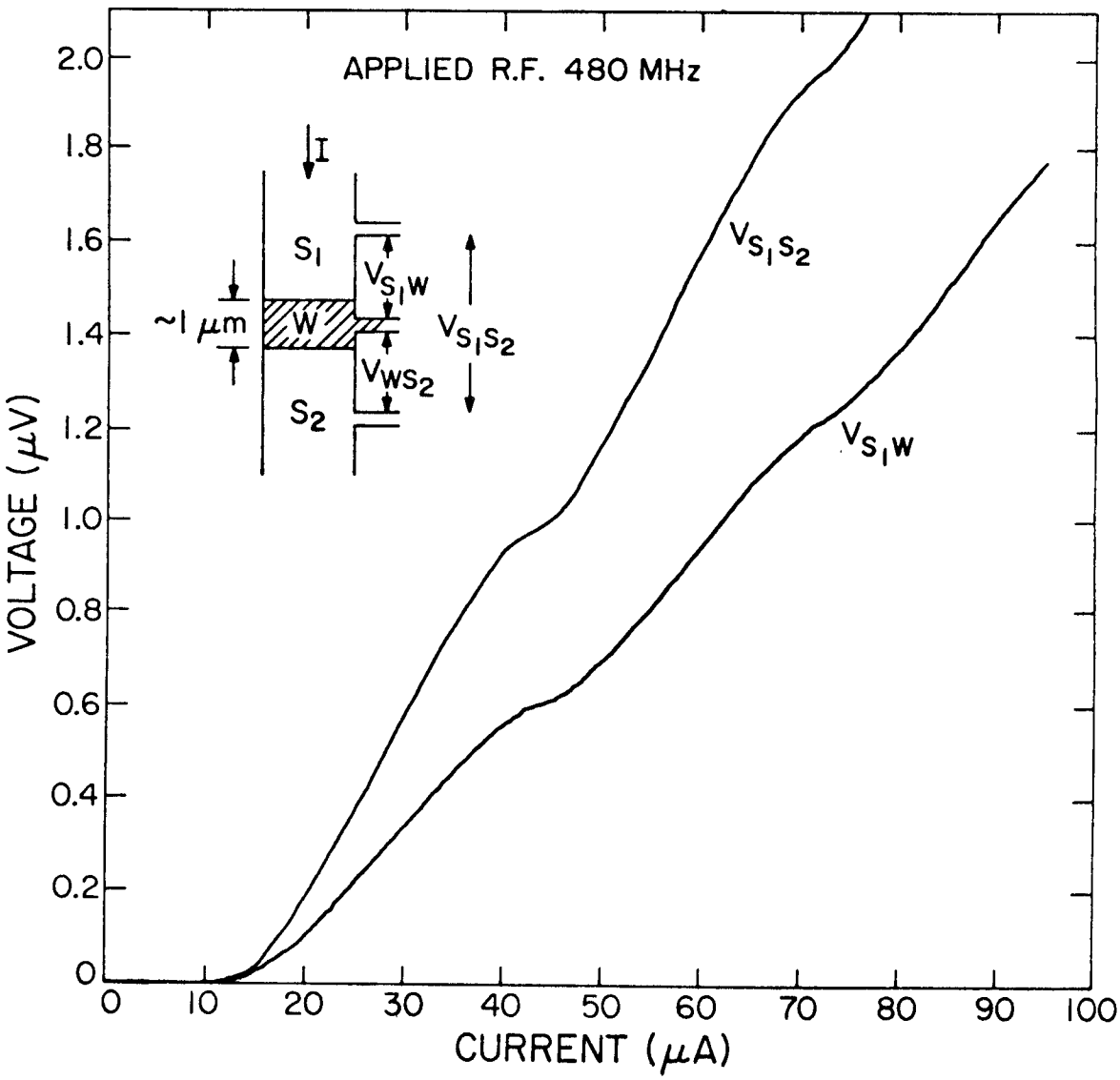

Fig. 6.3 RF induced step structures on V-I characteristics of a S/W boundary (V_{S_1W}) and the entire proximity effect bridge ($V_{S_1S_2}$).

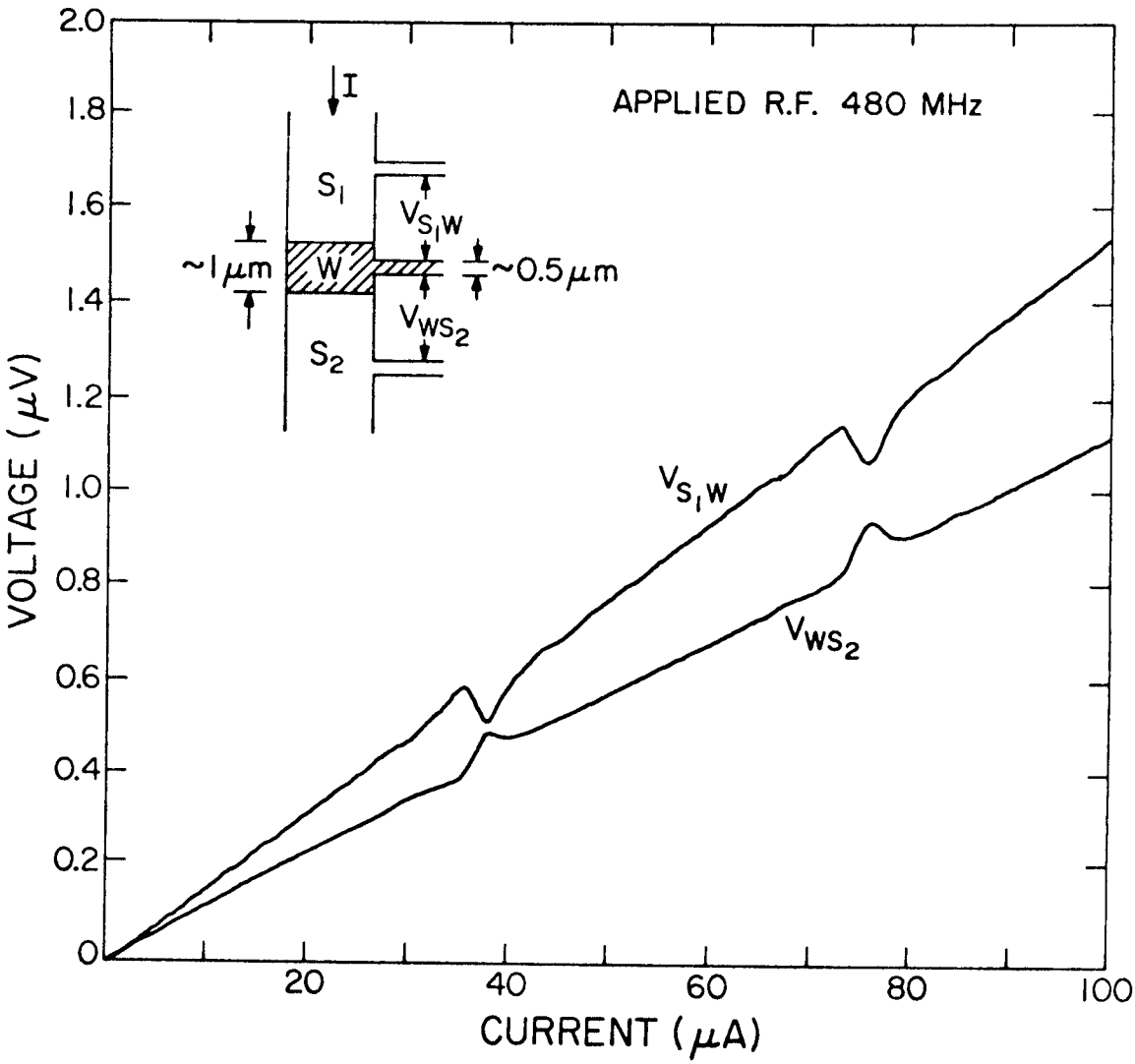

Fig. 6.4 RF induced positive (V_{WS_2}) and negative (V_{S_1W}) "step" structures on the V-I characteristics of the two S/W boundaries of a proximity effect bridge.

Appendix A

ELECTRICAL CONDUCTIVITY FOR QUASIPARTICLE CURRENT

In the two-fluid model we assumed that both the superfluid and the normal fluid contribute to the current. In the limit of negligible coupling between the two, the total current density j may be taken as a sum of the individual components,

$$j = j_s + j_n \tag{A.1}$$

Here j_n, the normal current, is caused by the quasiparticle excitations which obey Fermi statistics. The quasiparticles are believed to be scattered by inhomogeneities of the periodic lattice similar to usual unpaired electrons. Here we may assume the collision time τ_c when the metal is normal to be the same for all the quasiparticles. The effective conductivity is given by

$$\sigma_{eff} = \sum_{\substack{\text{all} \\ \text{quasiparticles}}} \frac{e^2 \tau_c}{m_i^*} \tag{A.2}$$

where m_i^* is the effective mass of the i^{th} quasiparticle. The collective interaction of the condensate strongly modifies the effective mass of the quasiparticles. The effective mass m^* is given by

$$\frac{1}{m^*} = \frac{1}{\hbar^2} \frac{\partial^2 E}{\partial k^2} \tag{A.3}$$

When applied to the dispersion (k-E) relationship for the quasiparticle excitations,

$$E(k) = \sqrt{(\frac{\hbar^2 k^2}{2m} - \mu)^2 + \Delta^2} \qquad (A.4)$$

above μ , the chemical potential or the Fermi level of the electrons.

$$\frac{1}{m^*} = \frac{1}{mE}[\sqrt{E^2 - \Delta^2}\ \{1 + 2(\frac{\Delta}{E})^2\} + 2\mu(\frac{\Delta}{E})^2\ ] \qquad (A.5)$$

Unless T is very close to T_c , $k_B T$ is of the order of Δ . Few quasiparticles would be excited by more than a few Δ's from the bottom of the excitation spectrum, which is itself Δ above the Fermi level. Taking a typical value of $E \sim 2\Delta$, the first term gives

$$\sqrt{3}\ \Delta(\frac{3}{2}) \sim \Delta$$

the second term gives

$$2\mu(\frac{\Delta}{E})^2 \sim \frac{\mu}{2}$$

Typical value of $\mu \sim 5$ eV , while that for $\Delta \sim 0.5$ mV . The first term may be neglected in that case and

$$\frac{m^*}{m} \simeq \frac{1}{2}(\frac{E}{\mu})(\frac{E}{\Delta})^2 \qquad (A.6)$$

So we see for most cases m^* is less than m by 3 or 4 orders of magnitude. In particular, at the bottom of the energy spectrum $E = \Delta$

$$\frac{m^*}{m} = \frac{1}{2}(\frac{\Delta}{\mu}) \qquad (A.7)$$

The amazingly small quasiparticle effective mass is very unique in electronic systems. However the conductivity σ_{eff} is not appreciably affected because there is an equally small number of quasiparticles being excited above the gap. Using the quasiparticle density

of states and the Fermi function as given by equations (2.11) and (2.12),

$$\sigma_{eff} = 2 \int_{\Delta}^{\infty} \frac{N(0)E}{(E^2 - \Delta^2)^{1/2}} \frac{2}{m}\left(\frac{\mu}{E}\right)\left(\frac{\Delta}{E}\right)^2 \tau e^2 \frac{1}{1+\exp\left(\frac{E}{k_B T}\right)} dE \qquad (A.8)$$

The factor of 2 comes about as we have to count both hole and electron branches. Since the density of states goes to infinity as $E \to \Delta$, and the Fermi factor tapers off rapidly through the exponential factor, the main contributions to the conductivity are those close to the gap edge. So we may factor the Fermi factor out of the integral with $E \overset{\sim}{=} 2\Delta$.

$$\sigma_{eff} \overset{\sim}{=} \frac{4\tau e^2 N(0)}{m} \frac{\Delta^2 \varepsilon_F}{1+\exp\left(\frac{2\Delta}{k_B T}\right)} \int_{\Delta}^{\infty} \frac{dE}{E^2 (E^2 - \Delta^2)^{1/2}}$$

$$= \frac{6}{1+\exp\left(\frac{2\Delta}{k_B T}\right)} \cdot \frac{n\tau e^2}{m} = \frac{6}{1+\exp\left(\frac{2\Delta}{k_B T}\right)} \sigma_{normal} \qquad (A.9)$$

For $k_B T \sim \Delta$,

$$\frac{6}{1+\exp\left(\frac{2\Delta}{k_B T}\right)} \sim 1 \qquad (A.10)$$

At temperatures not too far from the transition temperature, the electric conductivity is roughly the same as its normal value. Experimentally, the resistance of proximity effect bridges supports this point (Chapter 5).

Appendix B

COEFFICIENTS IN THE TIME DEPENDENT GINZBURG LANDAU EQUATION (TDGL) AND EQUATIONS (3.12) AND (3.14)

From the theory given by Gor'kov and Eliashberg (1968), the coefficients in the TDGL equation are related to microscopic properties of the electrons inside the superconductor. The equation is

$$\left(\frac{\partial}{\partial t} + \frac{2i\mu}{\hbar}\right)\psi = \frac{1}{\tau_{GL}}\left\{1 - \eta|\psi|^2 + \xi^2(T)\left(\nabla - \frac{2ie}{\hbar c}\vec{A}\right)^2\right\}\psi \qquad (B.1)$$

Here $\eta = \xi^2(T)/3Dn_1$

n is the electron number density

V_F is the Fermi velocity

τ_1 is the scattering time of the electrons

D is the diffusion constant, and

$$D = v_F^2\tau_1/3 \qquad (B.2)$$

The relaxation time is

$$\tau_{GL} = \xi^2/D = \frac{3\xi^2}{v_F^2\,\tau_1} \qquad (B.3)$$

At equilibrium both the left hand side of TDGL and the kinetic energy contribution are zero. So

$$|\psi_o|^2 = \frac{1}{\eta} = \frac{n\ell^2}{\xi^2} \qquad (B.4)$$

since mean free path $\ell = v_F\tau_1$.

Hence equation (3.12) may be written in the following forms:

$$\mu_p - \mu = \frac{m\xi^2}{4|e|\tau} \frac{\nabla \cdot \vec{j}_s}{|\psi|^2}$$

$$= \frac{1}{18|e|} \frac{\mu_o \tau_{GL}}{n} \nabla \cdot \vec{j}_s \qquad (B.5)$$

where free electron Fermi energy $\mu_o = mv_F^2/2$. Since the density of states of free electrons at the Fermi level

$$N(0) = \frac{1}{2\pi^2} \left(\frac{2m}{\hbar^2}\right)^{3/2} \mu_o^{1/2} \qquad \text{(Kittel 1968)} \qquad (B.6)$$

and

$$\mu_o = \frac{\hbar^2}{2m} (3\pi^2 n)^{2/3} \qquad (B.7)$$

then

$$\mu_p - \mu = \frac{\tau_{GL}}{12N(0)|e|} \nabla \cdot \vec{j}_s \qquad (B.8)$$

The differential equation (3.14) governing the spatial variation is of the form

$$\nabla^2(\mu_p - \mu) - \frac{1}{\lambda^2}(\mu_p - \mu) = 0 \qquad (B.9)$$

where the characteristic healing length λ is given by

$$\frac{1}{\lambda^2} = \frac{4e^2 \tau_{GL} |\psi|^2}{m\xi^2 \sigma} \qquad (B.10)$$

The numerical calculation of RSM1 showed that $\lambda \sim 2\xi(T)$. This result is more basic than just a coincidence. From the above we may do the

substitution for $|\psi_o|^2$, τ_{GL} and conductivity $\sigma(=\frac{ne^2\tau_1}{m})$. The coefficient

$$\frac{4e^2\tau_{GL}|\psi_o|^2}{m\xi^2\sigma} = \frac{12}{\xi^2} \tag{B.11}$$

As $|\psi|$ in the depairing region is actually smaller than $|\psi_o|$, the healing length is longer than $\frac{\xi}{\sqrt{12}}$ but expected to be of the order of ξ .

Appendix C

EFFECT OF OCCUPATION DENSITY PERTURBATION ON THE CHEMICAL POTENTIAL OF QUASIPARTICLES CLOSE TO A S/N INTERFACE

The population density of quasiparticles with energy $\mathcal{E}(k)$* in either branch (electron or hole) of the quasiparticle spectrum is given by

$$n = \int_{\Delta}^{\infty} \frac{N(0)E}{(E^2 - \Delta^2)^{1/2}} f \, dE \tag{C.1}$$

Here E is the energy measured above the Fermi level μ, i.e.,

$$E(k) = \mathcal{E}(k) - \mu \tag{C.2}$$

and the Fermi function

$$f = \frac{1}{1 + \exp(\frac{\mathcal{E} - \mu}{k_B T})} = \frac{1}{1 + \exp(\frac{E}{k_B T})} \tag{C.3}$$

The energy spectrum

$$E(k) = \sqrt{(\frac{\hbar^2 k^2}{2m} - \mu)^2 + \Delta^2} \tag{C.4}$$

$N(0)$ is the density of state at Fermi level. Perturbation of the occupation density is related to a change in the distribution f :

$$\delta n = \int_{\Delta}^{\infty} \frac{N(0)E}{(E^2 - \Delta^2)^{1/2}} \delta f \, dE \tag{C.5}$$

---

* k is the linear momentum in units of $\hbar$.

Assuming that thermalization to temperature T takes less time than the process concerned here (Section 2.5) so that Fermi distribution is restored, there will be a shift in the Fermi level (chemical potential) μ . There are two mechanisms by which μ can shift. We shall discuss them individually.

The overpopulation of quasiparticles actually perturbs the energy-momentum spectrum $E = E(k)$ with a resulting change in μ . This may be calculated from equations (C.3) and (C.4).

$$\delta f = - \frac{\exp(\frac{E}{k_B T})}{k_B T\{1 + \exp(\frac{E}{k_B T})\}^2} \delta E \qquad (C.6)$$

and

$$\delta E = \mp \frac{(E^2 - \Delta^2)^{1/2}}{E} \delta\mu \qquad (C.7)$$

where the upper sign applies for the electron-like branch and lower sign is for the hole-like branch. Combining them with equation (C.5),

$$\delta n = \pm \frac{N(0)}{k_B T} \delta\mu \int_{\Delta}^{\infty} \frac{\exp(\frac{E}{k_B T})}{\{1+\exp(\frac{E}{k_B T})\}^2} dE$$

$$= \pm \frac{N(0)}{1+\exp(\frac{E}{k_B T})} \delta\mu \qquad (C.8)$$

That electron-like and hole-like excitations have different signs in their expressions comes from the fact that increasing the number of electron excitations increases the number of electrons in the Fermi sea and hence raises the Fermi level, while an increase in the number of hole-like excitations is equivalent to a decrease in the number of

electrons and hence lower the Fermi level.

However, as a result of this sign difference, this mechanism fails to give any chemical potential difference in our particular situation at the S/N interface where electrons are converted into holes through Andreev scattering (Section 3.12). As there is an excess of electron-like excitations being injected to the interface region, there is at the same time an equal excess of holes converted from the electron-like excitations at the boundary at the steady state. This assures the balance of charges and is consistent with the symmetry between the two branches of excitations in this problem.

The other effect of overpopulation is on the Fermi distribution itself. $E(k)$ in equation (C.4) is the energy above the equilibrium Fermi level μ_o. Hence actual energy $\xi(k) = E(k) + \mu_o$. So as the quasiparticles are injected $\xi(k)$ is not changed, although the equilibrium distribution is disturbed with μ_o changing into $\mu = \mu_o + \delta\mu$ and

$$\delta f = \frac{\exp(\frac{E}{k_B T})}{\{1+\exp(\frac{E}{k_B T})\}^2} \frac{\delta\mu}{k_B T} \qquad (C.9)$$

Hence equation (C.5) gives

$$\delta n = N(0)\ \delta\mu \int_{\Delta'}^{\infty} \frac{y}{(y^2 - \Delta'^2)^{1/2}} \frac{\exp(y)}{\{1+\exp(y)\}^2}\, dy \qquad (C.10)$$

where the dimensionless parameter $\Delta' = \Delta/k_B T$. This relation holds for both electron-like and hole-like excitations. Hence

$$\delta\mu = \frac{A(\Delta')}{N(0)}\,\delta n \tag{C.11}$$

where

$$A(\Delta') = \left\{ \int_{\Delta'}^{\infty} \frac{y}{(y^2 - \Delta'^2)^{1/2}} \frac{\exp(y)}{\{1+\exp(y)\}^2}\, dy \right\}^{-1} \tag{C.12}$$

Let us assume Pippard's model of the S/N interface at which the energy gap Δ varies within a few coherence lengths from zero in the normal side to its equilibrium value Δ_∞ far within the superconducting region. And we also assume that we have a local excitation spectrum (C.4) all along this transition region with Δ now a function of position.

Consider a current flowing from the superconductor side to the normal side so that electron-like excitations are flowing towards the interface (from N to S) while hole-like excitations are leaving the interface. According to Andraev's picture (Andreev 1964) one incoming electron-like excitation is associated with one outgoing hole excitation. The normal current is equally split up between the two branches of the quasiparticle spectrum. Let us treat the electron-like branch first.

The particle flux is $\vec{j}_n/2e$. The factor 1/2 comes from the fact that the electron-like branch only takes care of half the normal current. The continuity equation for the number of particles is

$$\frac{1}{2e}\,\nabla\cdot\vec{j}_n + \frac{\partial n_e}{\partial t} = 0 \quad \text{when there is no branch mixing,}$$

or

$$\frac{\partial n_e}{\partial t} = -\frac{1}{2e}\,\nabla\cdot\vec{j}_n \tag{C.13}$$

However, the electron to hole conversion balances this gain in n_e in the steady state. Since it takes the branch mixing time τ_Q on the average to change an electron-like excitation to a hole-like excitation, the rate of conversion is equal to $\delta n_e/\tau_Q$. So in the steady state

$$-\frac{1}{2e}\nabla\cdot\vec{j}_n - \frac{\delta n_e}{\tau_Q} = 0$$

or

$$\delta n_e = -\frac{\tau_Q}{2e}\nabla\cdot\vec{j}_n$$

$$= \frac{\tau_Q}{2|e|}\nabla\cdot\vec{j}_n \qquad (C.14)$$

To write this in a more familiar form, we notice that inside the equilibrium region,

$$\nabla\cdot\vec{j}_n = 0 \qquad (C.15)$$

And as μ_p stays constant spatially, we can write

$$\delta\mu = \mu - \mu_p \qquad (C.16)$$

Using the two-fluid model

$$\vec{j} = \vec{j}_s + \vec{j}_n \qquad (C.17)$$

and at the steady state, continuity equation requires $\nabla\cdot\vec{j} = 0$.

Hence,

$$\mu_p - \mu = \frac{A(\Delta')\ \tau_Q}{2|e|\ N(0)}\ \nabla\cdot\vec{j}_s \qquad (C.18)$$

Hence

The temperature dependence of $A(\Delta')$ is given in the following table:

$\Delta' = \Delta/k_B T$	$A(\Delta')$
0	2.0
1	2.48
2	4.22
3	8.85
4	20.5
5	49.7

In the limit of $T \to T_c$, $A(\Delta')$ converges to 2. At low temperatures quasiparticles are excited up to the narrow band of width $k_B T$ above Δ and $k_B T << \Delta$. The integral then approaches

$$\frac{\exp(\Delta')}{\{1+\exp(\Delta')\}^2} (2\Delta')^{1/2} \simeq \sqrt{\frac{2\Delta}{k_B T}} \exp(-\frac{\Delta}{k_B T}) \qquad (C.19)$$

and hence $A(\Delta')$ goes as $\sqrt{k_B T/2\Delta} \exp(\frac{\Delta}{k_B T})$. This expression is very similar to that obtained by Tinkham and Clarke (1972) except with $A(\Delta')$ replacing the inverse of the normalized conductance g_{NS} of the tunnel junction. And as $g_{NS} \sim \sqrt{2\pi\Delta/k_B T} \exp(-\frac{\Delta}{k_B T})$ (Douglass and Falicov 1964) they share similar exponential dependence on $\Delta/k_B T$. Such a dependence on temperature was actually observed in Clarke's experiment. However, the workable temperature range of our experiment was too narrow to show this effect.

Appendix D

Voltage Distribution Inside a RF Coupled Proximity Effect Bridge

The magnetic field modulation of the rf induced d.c. voltage indicates that we have to consider the actual two-dimensionality of the problem (Section 5.4). Here we shall propose a few possible modes of d.c. voltage distribution that are consistent with our observation.

The lowest mode is to have a symmetric voltage distribution about the center of the bridge in the longitudinal direction (along the length of the bridge) but antisymmetric in the transverse direction (along the width of the bridge). It was shown (Mercereau 1973) that the applied magnetic field causes and modulates a transverse rf current inside the bridge. This may in turn produce the above mode of voltage distribution with the observed magnetic field dependence.

A higher order mode is to have an antisymmetric d.c. voltage distribution along the length of the bridge whose magnitude depends on the local current density which is modulated by the application of the magnetic field. Here we are going to present a possible mechanism of this mode of rf induced d.c. component of μ_p within the two-phase scheme. In this experiment, both μ and μ_p were probed <u>inside</u> the bridge region with superconducting and normal probes respectively.

The wavefunction $|\psi_o| he^{i\phi}$ inside the bridge is the sum of the two components (eq. (5.16)):

$$he^{i\phi} = fe^{i\phi_1} + ge^{i\phi_2} \tag{D.1}$$

The pair potential μ_p that a superconducting voltage probe will measure governs the time evolution of ϕ :

$$\mu_p = \frac{\hbar}{2} \frac{\partial \phi}{\partial t} \tag{D.2}$$

Using eqs. (D.1) and (D.2) we can express μ_p in terms of the component pair potentials μ_{p1} and μ_{p2} defined by

$$\mu_{p1} = \frac{\hbar}{2} \frac{\partial \phi_1}{\partial t} \tag{D.3}$$

$$\mu_{p2} = \frac{\hbar}{2} \frac{\partial \phi_2}{\partial t} \tag{D.4}$$

It comes out to be

$$\mu_p(x) = \frac{f^2 \mu_{p1} + g^2 \mu_{p2} + fg(\mu_{p1} + \mu_{p2}) \cos(\phi_1 - \phi_2)}{f^2 + g^2 + 2fg \cos(\phi_1 - \phi_2)} \tag{D.5}$$

and

$$\phi_1 - \phi_2 = \frac{2}{\hbar} \int (\mu_{p1} - \mu_{p2}) \, dt + \alpha \tag{D.6}$$

where α is the constant of integration. All quantities are to be evaluated at the same position x .

We shall consider the case with external rf of frequency ω applied to a bridge <u>without</u> a net d.c. voltage bias across the bridge. So we can write μ_{p1} and μ_{p2} as:

$$\mu_{p1}(x) = eV_1(x) \cos \omega t \tag{D.7}$$

$$\mu_{p2}(x) = eV_2(x) \cos \omega t \tag{D.8}$$

The voltage measured with a superconducting probe would be:

$$V(x) = \frac{\mu_p(x)}{e} = \frac{\{f^2V_1 + g^2V_2 + fg(V_1 + V_2)\cos(v \sin \omega t + \alpha)\} \cos \omega t}{f^2 + g^2 + 2fg \cos(v \sin \omega t + \alpha)} \quad (D.9)$$

where

$$v = \frac{2e(V_1 - V_2)}{h} \quad (D.10)$$

This fails to give any time averaged component as the term $\cos(v \sin \omega t + \alpha)$ is exactly a quarter of a period out of phase with $\cos \omega t$.

However in a circuit with both reactive and resistive elements, the voltage along the circuit in general is out of phase with the source voltage. In our proximity effect bridge with a rf voltage, the superflow is reactive* while the normal flow is resistive. The difference in phase depends on the local ratio of the normal and superflow. Condition (5.25) ($\nabla\mu_{p1} = \nabla\mu_{p2}$) implies that $\mu_{p1}(x) - \mu_{p2}(x)$ is independent of position. Hence inside the bridge we expect the pair potential μ_p and its components $\mu_{p1,2}$ to have a position dependent phase shift β relative to $\mu_{p1} - \mu_{p2}$. Thus

$$V(x) = \frac{\{f^2V_1 + g^2V_2 + fg(V_1+V_2)\cos(v \sin \omega t + \alpha)\} \cos(\omega t + \beta)}{f^2 + g^2 + 2fg \cos(v \sin \omega t + \alpha)} \quad (D.11)$$

In the small voltage limit, we may expand the expression in Bessel functions and

---

*This can be seen by noting that $\langle I.V \rangle_{av} = 0$.

$$V_{d.c.}(x) \simeq \frac{2\{f^2V_1 + g^2V_2 + fg(V_1+V_2)\ J_o(v)\cos\alpha\}\ fgJ_1(v)\sin\alpha\sin\beta}{\{f^2 + g^2 + 2fg\ J_o(v)\ \cos\alpha\}^2} \qquad (D.12)$$

This d.c. voltage distribution is antisymmetric about the center of the bridge and is zero at the center. Numerical calculations of expression (D.9) for $V(x)$ indicated that even for a small $\beta(=\pi/10)$ $V_{d.c.}$ can go up to values comparable to V_o close to the center of the bridge as can be seen from the large contribution to the time average when $\phi_1 - \phi_2 = \pm\pi$ at positions where $f \simeq g$, and then it changes polarity rapidly at the center. The Bessel functions J_o, J_1 give the magnitude and sign dependence on the rf amplitude which was observed experimentally. The sinusoidal dependence on α may explain the current dependence as the d.c. supercurrent (eq. (5.21)) is also modulated by the rf voltage and depends on the phase α as:

$$\langle j_s \rangle_{d.c.} \simeq -j_J\ J_o(v)\ \sin\alpha + C(\nabla\phi)_{d.c.}\{1 + J_o(v)\ \cos\alpha\} \qquad (D.13)$$

Also since an external magnetic field modulates $\langle j_s \rangle_{d.c.}$, $V_{d.c.}$ is hence similarly modulated. Hence a superconducting voltage probe placed asymmetrically inside the bridge will sense a d.c. potential. This may be the voltage observed experimentally. Our measurement with normal probes also indicated that the chemical potential μ has similar behavior.

REFERENCES

E. Abrahams and T. Tsuneto, Phys. Rev. 152, 416 (1966)

P. W. Anderson and A. H. Dayem, Phys. Rev. Lett. 13, 195 (1964)

P. W. Anderson and Y. B. Kim, Rev. Mod. Phys. 36, 39 (1964)

P. W. Anderson, N. R. Werthamer and J. M. Luttinger, Phys. Rev. 138, A1157 (1965)

A. F. Andreev, Sov. Phys. JETP 19, 1228 (1964)

A. F. Andreev, Sov. Phys. JETP 22, 455 (1966)

L. G. Aslamazov and A. I. Larkin, Sov. Phys. JETP Lett. 9, 87 (1969)

J. Bardeen, L. N. Cooper and J. R. Schrieffer, Phys. Rev. 108, 1175 (1957)

J. Bardeen, Phys. Rev. Lett. 1, 399 (1958)

J. Bardeen and J. L. Johnson, Phys. Rev. B 5, 72 (1972)

K. H. Benneman and J. W. Garland in AIP Conference Proceedings #4, Superconductivity in d and f Band Metals (D. H. Douglass, ed.) p. 103 (1972)

J. M. Blatt, Theory of Superconductivity, Academic Press, New York (1964)

Chemical Rubber Company, Handbook of Chemistry and Physics, 52d Ed. (1971-72)

J. Clarke, Proc. Roy. Soc., Ser. A, 308, 447 (1969)

J. Clarke, Phys. Rev. Lett. 28, 1363 (1972)

L. N. Cooper, Phys. Rev. 104, 1189 (1956)

A. H. Dayem and J. J. Wiegand, Phys. Rev. 155, 419 (1967)

S. Decker, Private Communication, 1973

P. G. deGennes, Superconductivity of Metals and Alloys, Benjamin, New York (1966)

D. H. Douglass Jr. and L. M. Falicov, Prog. Low Temp. Phys. IV (C. J. Gorter ed.), North Holland, Amsterdam (1964)

G. M. Eliashberg, Sov. Phys. JETP Lett. 11, 114 (1970)

H. J. Fink, Phys. Lett. 42A, 465 (1973)

P. E. Friebertshauser, H. A. Notarys and J. E. Mercereau, Bull. Am. Phys. Soc. 13, 1670 (1968)

H. Frölich , Phys. Rev. 79, 845 (1950)

D. M. Ginsberg, Phys. Rev. Lett. 8, 204 (1962)

V. L. Ginzburg and L. D. Landau, Sov. Phys. JETP 20, 1064 (1950)

L. P. Gor'kov and G. M. Eliashberg, Sov. Phys. JETP 27, 328 (1968)

M. H. Halloran, J. H. Condon, J. E. Graebner, J. E. Kungler and F.S.L. Hsu, Phys. Rev. B 1, 366 (1970)

J. J. Hauser and H. C. Theuerer, Rev. Mod. Phys. 36, 80 (1964)

T. K. Hunt, Phys. Lett. 22, 42 (1966)

T. K. Hunt and J. E. Mercereau, Phys. Rev. Lett. 18, 551 (1967)

B. D. Josephson, Phys. Lett. 1, 251 (1962)

B. D. Josephson, Adv. Phys. 14, 419 (1968)

H. Kamerlingh-Onnes, Leiden Comm. 122b, 124c (1911)

R. K. Kirschman and J. E. Mercereau, Phys. Lett. 35A, 177 (1971)

R. K. Kirschman, PhD Thesis, California Institute of Technology, 1972

R. K. Kirschman, J. Low Temp. Phys. 11, 235 (1973)

C. Kittel, Introduction to Solid State Physics (3rd Ed.) John Wiley & Sons, Inc., New York (1968)

I. O. Kulik, Sov. Phys. JETP 30, 944 (1970)

J. S. Langer and V. Ambegaokar, Phys. Rev. 164, 498 (1967)

J. L. Levine and S. Y. Hsieh, Phys. Rev. Lett. 20, 994 (1968)

F. London, Superfluids, Vol. 1, New York, John Wiley & Sons (1950)

E. A. Lynton, Superconductivity, Methuen & Company (1969)

L. F. Mattheiss, Phys. Rev. B 1, 373 (1970)

D. C. Mattis and J. Bardeen, Phys. Rev. 111, 412 (1958)

W. Meissner and R. Ochsenfeld, Naturwiss 21, 787 (1933)

J. E. Mercereau, Tunneling Phenomena in Solids (Burstein, ed.), p. 461, (1967)

J. E. Mercereau, Proc. Intern. Conf. Detection and Emission of Electromagnetic Radiation with Josephson Junctions, Perros Guirec, France, Sept. 1973.

J. Meyer and G. V. Minnigerode, Phys. Lett. 38A, 529 (1972)

H. A. Notarys and J. E. Mercereau, Physica 55, 424 (1971)

H. A. Notarys, M. L. Yu and J. E. Mercereau (NYM), Phys. Rev. Lett. 30, 743 (1973); also Bull. Am. Phys. Soc. 18, 463 (1973)

H. A. Notarys and J. E. Mercereau, J. App. Phys. 44, 1821 (1973)

C. S. Owens and D. J. Scalapino, Phys. Rev. Lett. 28, 1559 (1972)

D. W. Palmer and S. K. Decker, Rev. Sci. Inst. (to be published, 1973)

D. W. Palmer, Private Communication, 1973

R. D. Parks (Ed.), Superconductivity, Vol. 2, p. 1006, Marcel Dekker, New York (1969)

A. B. Pippard, Proc. Roy. Soc. A216, 547 (1953)

A. B. Pippard, J. G. Shepherd and D. A. Tindall, Proc. Roy. Soc. A324, 17 (1971)

W. H. Parker and W. D. Williams, Phys. Rev. Lett. 29, 924 (1972)

W. H. Parker, Private Communication, 1973

G. Rickayzen, Theory of Superconductivity, Interscience Publishers (1965)

T. J. Rieger, D. J. Scalapino and J. E. Mercereau (RSM1), Phys. Rev. Lett. 27, 1787 (1971)

T. J. Rieger, D. J. Scalapino and J. E. Mercereau (RSM2), Phys. Rev. B 6, 1734 (1972)

J. R. Schrieffer and D. M. Ginsberg, Phys. Rev. Lett. 8, 207 (1962)

S. Shapiro, Phys. Rev. Lett. 11, 80 (1963)

L. Y. L. Shen, Phys. Rev. Lett. 24, 1104 (1970)

W. J. Skocpol, M. R. Beasley and M. Tinkham, Intern. Conf. Detection and Emission of Electromagnetic Radiation with Josephson Junctions, Perros Guirec, France, Sept. 1973; also, Bull. Am. Phys. Soc. 18, 302 (1973)

L. Solymar, Superconductive Tunneling and Applications, Wiley-Interscience (1972)

M. Strongin, A.I.P. Conference Proceedings No. 4 (D. H. Douglas, Ed.) (1972)

L. R. Testardi, Phys. Rev. B 4, 2189 (1971)

R. S. Thompson and C. R. Hu, Phys. Rev. Lett. 27, 1352 (1971)

M. Tinkham, Phys. Rev. B 6, 1747 (1972)

M. Tinkham and J. Clarke, Phys. Rev. Lett. 28, 1366 (1972)

M. Tinkham, Preprint (1973)

J. R. Tucker and B. I. Halperin, Phys. Rev. B 3, 3768 (1971)

J. Wilks, The Properties of Liquid and Solid Helium, Clarendon Press, London (1967)

A.F.G. Wyatt, V. M. Dmitriev, S. W. Moore and F. W. Sheard, Phys. Rev. Lett. 16, 1166 (1966)

L. Young, Anodic Oxide Films, Academic Press, London (1961)

M. L. Yu and J. E. Mercereau, Phys. Rev. Lett. 28, 1117 (1972); also, M. L. Yu, H. A. Notarys and J. E. Mercereau, Bull. Am. Phys. Soc. 17, 46 (1972)

M. L. Yu and J. E. Mercereau, Proc. 13th Intern. Conf. on Low Temp. Phys., Boulder, 1972

M. L. Yu and J. E. Mercereau, Bull. Am. Phys. Soc. 17, 1196 (1972)

J. M. Ziman, Electrons and Phonons, Oxford Univ. Press, London (1958)

J. E. Zimmerman and A. H. Silver, Phys. Lett. 10, 47 (1964); also, Phys. Rev. 141, 367 (1966)